2016-01-01

Commercialization Of Cobalt Promoted Molybdenum Disulfide Hydrodesulfurization Unsupported Catalyst

Juan Hilario Leal
University of Texas at El Paso, jhleal@yahoo.com

COMMERCIALIZATION OF COBALT PROMOTED MOLYBDENUM DISULFIDE HYDRODESULFURIZATION UNSUPPORTED CATALYST

JUAN HILARIO LEAL

Doctoral Program in Materials Science and Engineering

APPROVED:

Russell R. Chianelli, Ph.D., Chair

Devesh Misra, Ph.D.

Felicia Manciu, Ph.D.

Binata Joddar, Ph.D.

Charles Ambler, Ph.D.
Dean of the Graduate School

Dedication

I dedicate this to my family and especially my daughter, Caroline. The people of El Paso, including UTEP faculty and friends have made this a memorable experience. Thank you to all my friends, which I will not name, but you know who you are. I would not have made it without your support.

COMMERCIALIZATION OF COBALT PROMOTED MOLYBDENUM DISULFIDE HYDRODESULFURIZATION UNSUPPORTED CATALYST

by

JUAN HILARIO LEAL, M.S., B.S.

DISSERTATION

Presented to the Faculty of the Graduate School of

The University of Texas at El Paso

in Partial Fulfillment

of the Requirements

for the Degree of

DOCTOR OF PHILOSOPHY

Material Science and Engineering

THE UNIVERSITY OF TEXAS AT EL PASO

May 2016

ACKNOWLEDGEMENTS

I would like to take this opportunity to thank everyone who has helped me. A big thanks to my committee members, Dr. Chianelli, Dr. Misra, Dr. Manciu, F., and Dr. Joddar for participating in my dissertation process. I want to acknowledge Porocel for their support as well as the family at EPCC. I acknowledge the work of Dr. Brenda Torres and the aid of Jaime Manuel Valencia for his help. Stephen Halliday and Dr. Ian Manson were part of this research team and their input was greatly appreciated and at times instrumental with regards to experiment design. Dr. Jason Parsons for his work on the EDS and surface area analysis as well for his encouragement.is also to be acknowledged. I also acknowledge Dr. Miguel Yacaman and his researchers, for they did some fine work on the STEM images. Victor Gonzalez of Dr. Botez' crystallography lab is acknowledged for his XRD work.

ABSTRACT

Catalysis is a key player in the petroleum refining process. Our focus is primarily on the improvement of a commercial HDS (HydroDeSulfurization) hydrotreating catalyst. The commercial catalyst sold today is cobalt promoted molybdenum supported on γ-alumina. Our aim is to work with Porocel Industries LLC to produce an unsupported, cobalt promoted, molybdenum disulfide catalyst by improving on previous work conducted by Dr. Brenda Torres. The catalysts (B3&B5) developed by Dr. Torres were reported to be highly active on real feedstocks and were produced via hydrothermal process. Oxidic Mo, and H_2S were used to make an ammonium tetrathiomolybdate precursor that was added to a Co salt, which underwent decomposition in the hydrothermal reactor. The ultimate goal for Porocel is to commercialize the material and in pursuance of the hydrothermal process would have to be optimized for industry scale up. In order not to infringe on current catalyst manufacturing process patents, the process was carefully adapted to a novel synthesis method, ultimately resulting in lower temperatures, less time, lower pressure and full sulfidation using elemental sulfur in lieu of H_2S. The synthesized catalyst was characterized with powder X-ray diffraction, SEM, STEM, EDS, and BET surface area analysis. Catalytic testing was conducted using a Parr reactor setup to model the hydrodesulfurization of a petroleum feedstock. The sulfur-containing molecule used in the model was DBT (DiBenzoThiophene) and its conversion to either biphenyl or cyclohexylbenzene was observed via GCMS analysis.

TABLE OF CONTENTS

LIST OF TABLES

LIST OF FIGURES

CHAPTER 1: BACKGROUND AND SIGNIFICANCE

Environmental pundits the world over have long been warning of the dangers of using fossil fuels as our chief source of energy. Fossil fuels include coal, natural gas and oil. Dangers that impact health directly or increasing complications through environmental fouling mechanisms are cause for concern [1]. Coal is the most abundant fossil fuel on the planet and as a result, is widely used. Approximately 7.4 million metric tons of coal is consumed each day throughout the world [2]. Coming in second is the petroleum industry with about 91 million barrels consumed daily worldwide [3].

Although coal is the most abundant fossil fuel to date and responsible for most of the negative environmental effects, we will turn our focus onto the petroleum industry and the current environmental challenges it faces.

Petroleum is a complex yellow to black mixture of gaseous, liquid and solid hydrocarbons found naturally beneath the earth's surface [4-5]. Petroleum can be classified into three subcategories—natural gas, crude oil and tar. Petroleum use can be traced back to early recorded civilization (ca. 4000 B.C.) [6]. Asphalt was used in the construction of the walls and towers of Babylon [6]. The ancient Greeks have left archaeological evidence of their use of tar and asphalt for waterproofing waterborne vessels as well as pottery. The Greeks weaponized petroleum by making an incendiary device termed "Greek fire" which was integral to the success of naval battles of the Byzantine era [6]. The word "petroleum" has Greek and Latin origins as well. The word "petros" is Greek for rock and "oleum" is Latin for oil. The importance of petroleum is realized today, probably more so than ever before. Our future generations have tough challenges ahead with the ever-looming threat of depleting resources.

1.0 Crude Oil

Although the composition of crude may vary, its major components are carbon (93%-97%), hydrogen (10%-14%), nitrogen (0.1%-2%), oxygen (0.1%-1.5%), and sulfur (0.5%-6%) as well as trace metals [7]. Hydrocarbons in crude oil are classified into paraffins, cycloparaffins, and aromatics. Paraffins are saturated hydrocarbons, which are either branched or normal and are without ring structure (C_nH_{2n+2}). Cycloparaffins (napthenes) are saturated hydrocarbons containing at least one ring (C_nH_{2n}). Aromatics are hydrocarbon ring structures with alternating double bonds such as benzene (C_nH_{2n-6}).

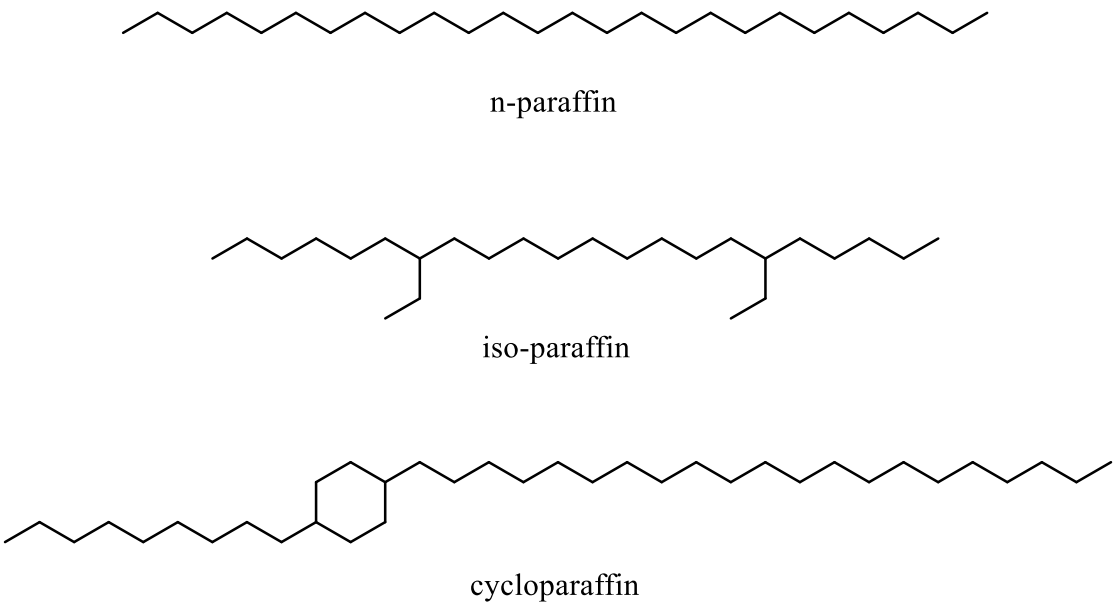

Figure 1: Paraffin structure

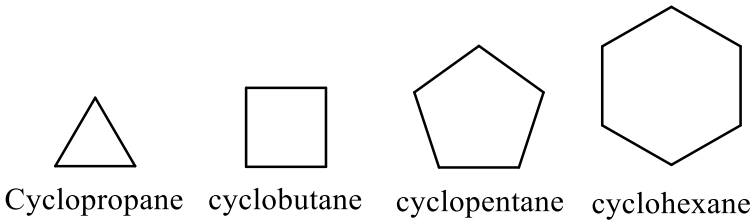

Figure 2: Cycloparaffin structures

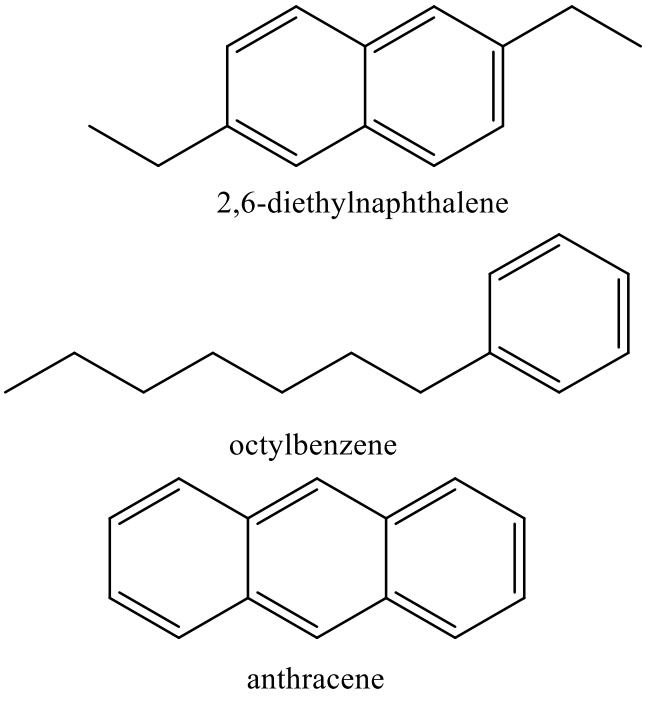

Figure 3: Aromatic structures

Crude oil is classified mostly by the location of its origin and by its relative weight or its viscosity (heavy, intermediate, and heavy). Heavy crude is highly viscous and does not easily flow through pipes or wells under normal conditions. The American Petroleum Institute classifies heavy crude as having an API gravity value of less than 22.3 [8]. API gravity is inversely related to density so the higher the value the lower the density. A value of anything less than 10 will sink

in water and is termed extra heavy crude. Intermediate crude has API gravity values from 22.3 and 31.1. Values above 31.1 are designated as light crude. Since the API gravity values are related to density, it can be used to estimate the volume or amount of barrels produced from a metric ton of assigned gravity. Unfortunately, the world's supply of light crude is severely depleted so the industry has turned to refine mostly heavy crude and bitumen [9].

Most heavy crude is rich in bitumen and is mostly found in the tar sands of Canada and Venezuela [10]. Bitumen is not to be confused with tar, which is made through the distillation of coal. Bitumen is naturally forming and referred to as pitch, resin or asphaltum. Bitumen is heavy in asphaltenes which are large polycyclic aromatic hydrocarbons used to make roads. Canada tar sands known as the Athabasca tar sands are some of the largest known bitumen deposits [11].

Crude oil can be further classified into two subcategories based on its sulfur content. Sweet crude is oil containing less than 0.5% sulfur and commands up to $15 dollars U.S. per barrel over sour crude [12]. The justifications for a premium price are primarily because the sweet crude is easier to refine and less corrosive resulting in less damage to transport vessels and refineries.

The exploration and use of oil continued throughout the world and in 1853, kerosene was successfully extracted from petroleum [13]. By 1857, with the invention of a clean burning lamp kerosene quickly replaced whale oil and the market for refined petroleum was established by demand [14]. Once the kerosene was extracted, there was no use for the other components of the oil so they were either dumped on site or burned off.

At the turn of the 20th century with the recent advances in the internal combustion engine and the newly formed auto industry, the need for refined petroleum was increasing. For the first two decades of the century, the need for gasoline was there, but the refining technology was not able to keep up. Small distillation setups to fraction off the gasoline would only produce about 20% gasoline from a given amount of petroleum [15].

1.1 Oil Refining

Two chemical engineers at Standard Oil of Indiana presented a solution to the inherent inefficiency of the current refining process. William Burton and Robert Humphreys initially failed at an attempt to extract more gasoline using catalysts [16]. Burton however had the idea to add pressure to the heating process during distillation and was able to cleave larger molecules into smaller ones, thus cracking kerosene into gasoline. This method is known as the Burton process, which is thermal cracking and is still used today to produce diesel. Thermal cracking improved the gasoline yield from 20 to 25% from a given amount of crude oil. Oil refining can thusly be divided into three steps.

1.1.0 FRACTIONATION

Technically speaking the first step is desalting. Desalting prevents corrosion of the refinery equipment by removing water from the crude. After desalting, separation is the first step of fuel refinement and is achieved through distillation. Crude oil is pumped in and heated in a large furnace and hydrocarbons are fractioned off by boiling point. It is not uncommon for the furnaces to operate at temperatures up to 900°C depending on the composition of the crude [17]. In atmospheric distillation, light fractions flash into vapor and condense as they rise up the tower that is around 120 feet high. Fractionation can be achieved through atmospheric or vacuum distillation. In vacuum distillation, separation occurs at lower temperatures and this helps to prevent undesired cracking. Unseen in figure 4, the tower has plates/trays or surfaces to allow the hydrocarbons to condense and the fractions are collected elsewhere or sent to other treatment units. Crude material that is not drawn off is too heavy for atmospheric distillation and vacuum is needed to further distill them. From the atmospheric tower, the residuals are transferred to a vacuum distillation tower for separation of gas oils, lubricants and the really heavy stuff will eventually be collected or sent to a coker, visbreaker or deasphalter.

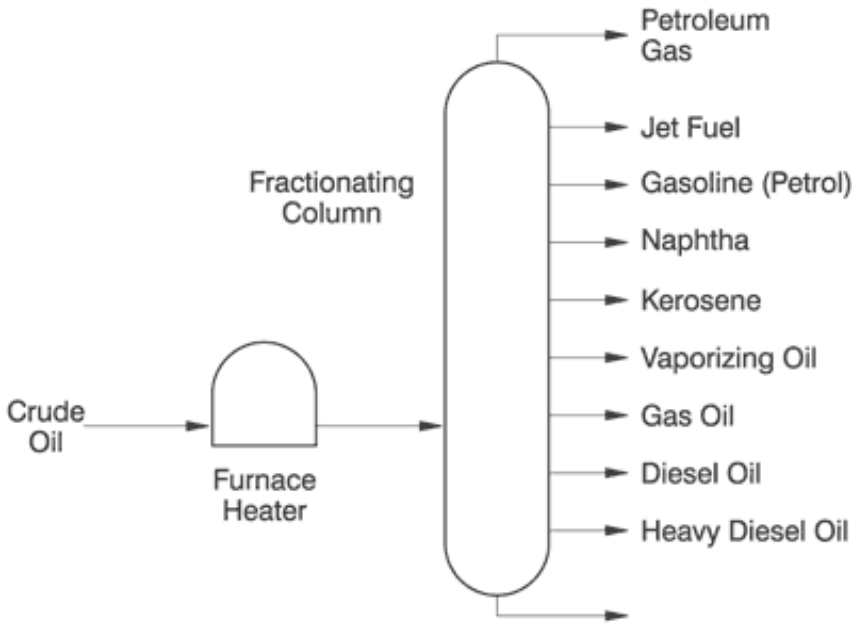

Figure 4: Diagram of refinery distillation [18]

1.1.1 CONVERSION

The conversion step is broken down into three main processes.

- Decomposition
- Unification
- Alteration

In decomposition, larger molecules are "cracked" into smaller molecules either by thermal or catalytic cracking techniques. Other decomposition techniques are coking, hydrocracking, steam cracking, visbreaking, and hydrogen steam reformation. In unification, the opposite occurs and smaller molecules are combined to make larger products via alkylation, grease compounding or polymerization. In alkylation smaller byproducts are chemically combined to make larger products. The alteration process is where catalytic reformation occurs to branch straight chains of hydrocarbons or to isomerize them into higher quality products (higher octane).

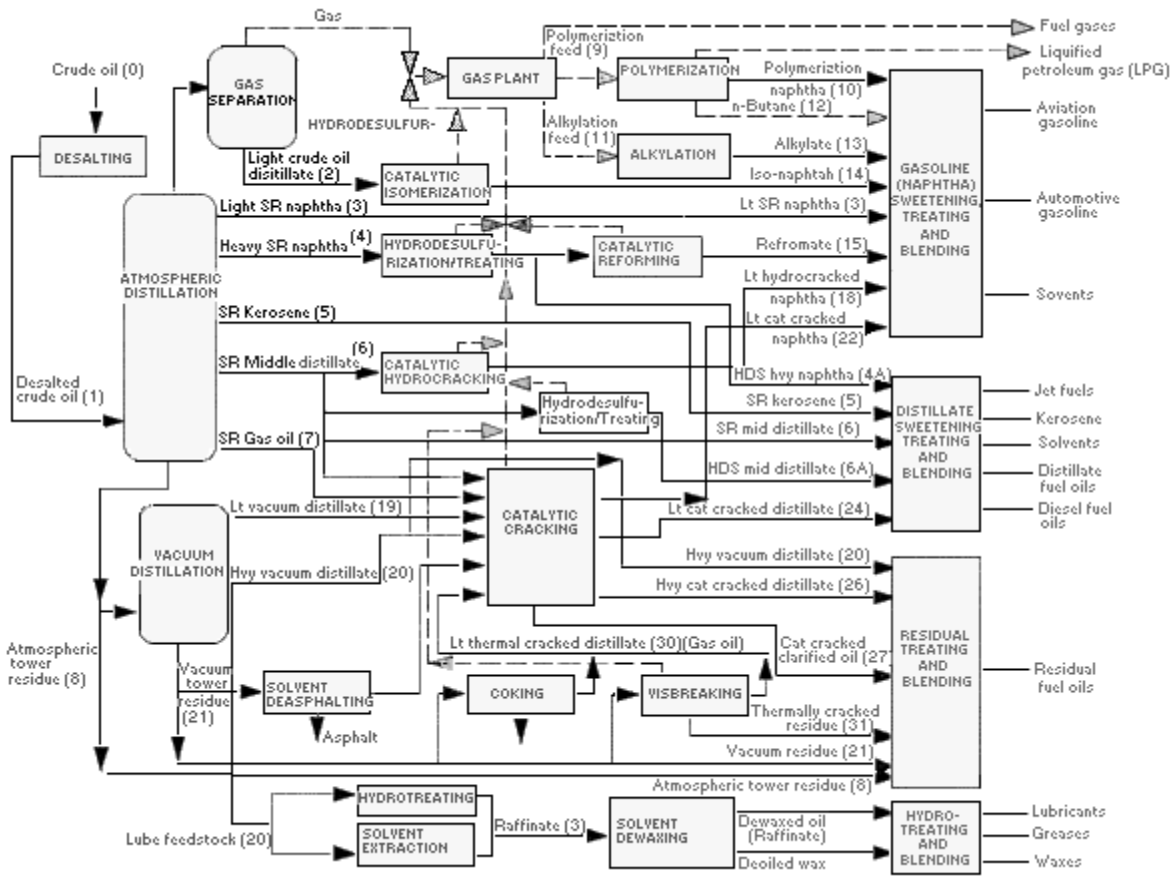

Figure 5: Diagram outlining refinery processes [19]

1.1.2 TREATMENT

The final step in crude oil refinement has many processes. These processes remove acidic contaminants, solvents, impurities, heteroatoms (N, S, O), water and H_2S. Hydrodesulfurization (HDS) and hydrotreating (HDT) remove sulfur, nitrogen and aromatics in order to meet the global trend for cleaner fuels.

CHAPTER 2: INTRODUCTION

2.0 Hydrodesulfurization

HDS removes sulfur compounds (thiols, thiophenes, thiophanes, polysulfides, organic sulfides, mercaptans) from distilled petroleum feed stocks. The treatment utilizes high pressures (150-3000 psig) with hydrogen gas flows of 250-2000 SCF/bbl and anywhere from 250°C-450°C to produce hydrogen sulfide and hydrocarbons [20]. Pressures and temperatures are dependent on the design of the reactor, but mostly on the composition of the crude oil. Sulfur compounds are removed mainly for environmental reasons. Sulfur containing compounds are acid rain precursors and they diminish the activity of reforming catalysts as well. If not removed at the refinery they can ruin engine components via acidic corrosion. Precious metal catalysts (platinum, rhodium, and palladium) in catalytic converters on vehicles become poisoned as well by sulfur compounds [21]. The upper range pressures and temperatures during hydrodesulfurization are required for the most stubborn sulfur containing compounds. These compounds are thiophenes and are extensively studied to improve the current processes. More specifically, benzothiophenes (BT) and dibenzothiophenes (DBT) are the molecules mostly under study and are illustrated in Table 1, below.

Reactivity is dependent on the chemical structure of the molecule and the immediate region surrounding the sulfur atom. Shape plays a role as steric hindrance can prove to make the desulfurization challenging if the sulfur has limited contact to the catalyst surface. Molecules that are easily processed are thiols (mercaptans), sulfides, and disulfides. Conversely, HDS is not as effective on aromatic thiophenes or their derivatives [22]. The doubly substituted 4,6 dimethyl Dibenzothiophene can be seen in Table 1 where the methyl groups would provide enough steric hindrance to be problematic to the conversion of the sulfur to hydrogen sulfide. Researchers in

HDS have used these compounds in the lab to model conditions in the refinery to test catalytic activity of various materials [23].

Table 1: Sulfur containing compounds in petroleum

COMPOUND CLASS	STRUCTURE
Thiols (mercaptans)	RSH
Sulfides	RSR′
Disulfides	RSSR′
Thiophene	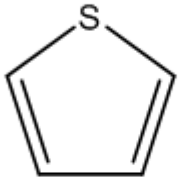
Dibenzothiophene (DBT)	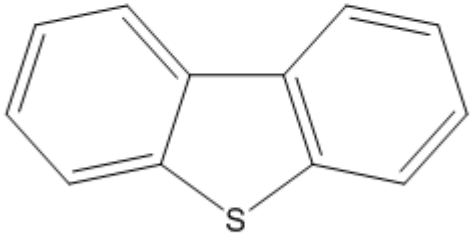
4,6 Dimethyl Dibenzothiophene	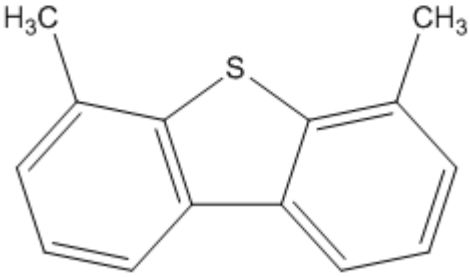

The catalysts used in hydrodesulfurization are transition metal sulfides (TMS) comprised of metals such as cobalt, molybdenum, tungsten, or nickel. The industry favorite combination happens to be CoMoS which is bimetallic, cobalt promoted molybdenum disulfide. These

catalysts tend to be supported on γ-alumina for increased surface area, dispersion as well as to spare the amount of cobalt and molybdenum required [24]. The alumina has shown to promote excellent dispersion exposing an increased number of edge sites of MoS_2 where the cobalt should reside for the best activity (Co-Mo-S). There is said to be a strong interaction between the MoS_2 and the support (support synergism) [25][26][27].

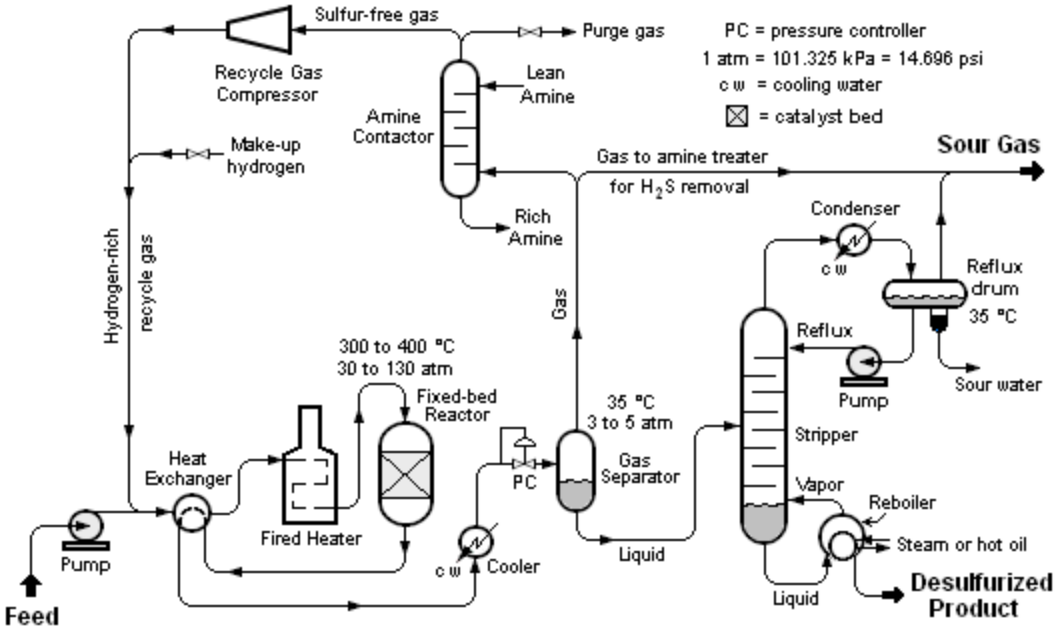

Figure 6: Flow diagram of HDS unit [28]

Figure 6 shows a diagram outlining the fate of feedstock introduced into an HDS unit. The previously condensed feed stock is preheated with the aid of a steam heat exchanger and mixed with gas containing a high concentration of hydrogen. After preheating, the liquid is vaporized in a fired heater and the vapors are introduced into a fixed bed reactor where the catalyst resides. After the conversion the sour gas has to be sweetened (H_2S removal) and is sent to an amine unit for sour gas removal. Most of the gas that makes it past the amine unit is rich in hydrogen and is recycled to the initial heat exchanger to be mixed with fresh incoming feed. The condensate after the fixed bed reactor is refluxed and routed through a stripper distillation tower ultimately

producing the desulfurized product. H_2S is further processed to produce either sulfuric acid or elemental sulfur depending on the treatment.

2.1 HYDRODESULFURIZATION OF DBT: PREDICTOR OF LIVE FEED ACTIVITY

One way to effectively screen catalysts for activity and selectivity is to model the refinery HDS unit conditions. The hydrodesulfurization of DBT in a solvent on a benchtop has demonstrated to be a good predictor of catalytic activity in real live feeds [29][30][31]. It is important to understand that the conditions for these lab scale tests are very different from those in a refinery. For the sake of simplifying the analysis, only one solvent and one sulfur containing compound are used (DBT). The model reaction is a liquid phase reaction while the refinery reaction takes place in gas phase. With that being established, the model reaction is the method used by researchers to investigate pathways or mechanisms by analyzing the products formed during the reaction.

Desulfurization of DBT proceeds through two pathways [32][33][34][35].

- Direct desulfurization (DDS)
    - C-S bond scission resulting in biphenyl (BP)
- Hydrogenation (HYD)
    - Hydrogenation of a ring resulting in cyclohexylbenzene

Figure 7 shows the hydrogenation pathway (HYD) begins with the protonation of the aromatic rings of dibenzothiophene (DBT). Tetrahydrodibenzothiophene (THDBT) is an intermediate formed from the HYD pathway and further hydrogenation results in C-S bond rupture producing cyclohexylbenzene (CHB). In direct desulfurization, the C-S scission occurs immediately

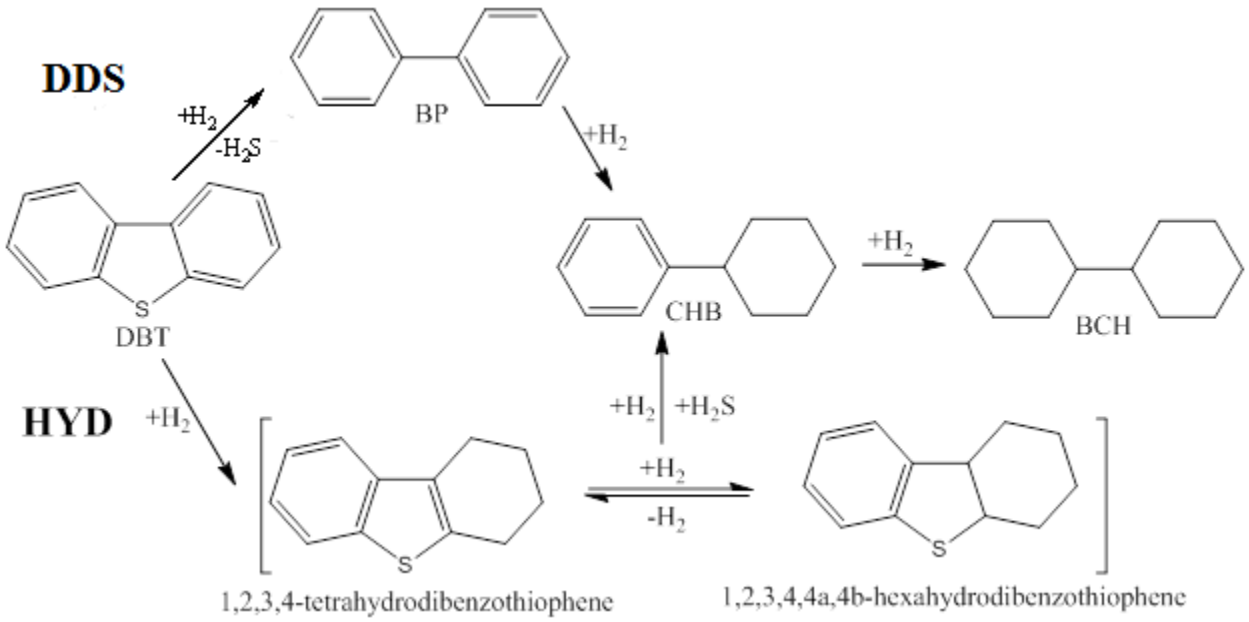

Figure 7: Desulfurization pathways of DBT

resulting in biphenyl (BP). Hydrogenation of BP results in CHB—this is where both pathways intersect. Selectivity (HYD/DDS) can be investigated with a ratio of concentrations of CHB/BP during analysis of the aliquots pulled from the reaction chamber (steady state).

2.2 Hydrodesulfurization Catalysts

Transition metal sulfides (TMS) are a good fit for the conditions of the refinery because they are resistant to catalyst fouling/poisoning unlike their metallic counterparts. Sulfur tends to poison expensive noble metal catalysts, but TMS catalysts thrive in a sour environment and only decrease in activity after a carbon has covered the active sites (hard carbon). Tungsten and molybdenum sulfides are gentle on hydrocarbons (minimal cracking) while allowing for deep hydrodesulphurization at high levels of sulfur in sour feeds. Nickel is used as well for hydrogenation in upgrading feedstock. TMS catalysts are the chief catalysts for hydrodesulfurization and hydrodenitrogenation (nitrogen removal) in refineries.

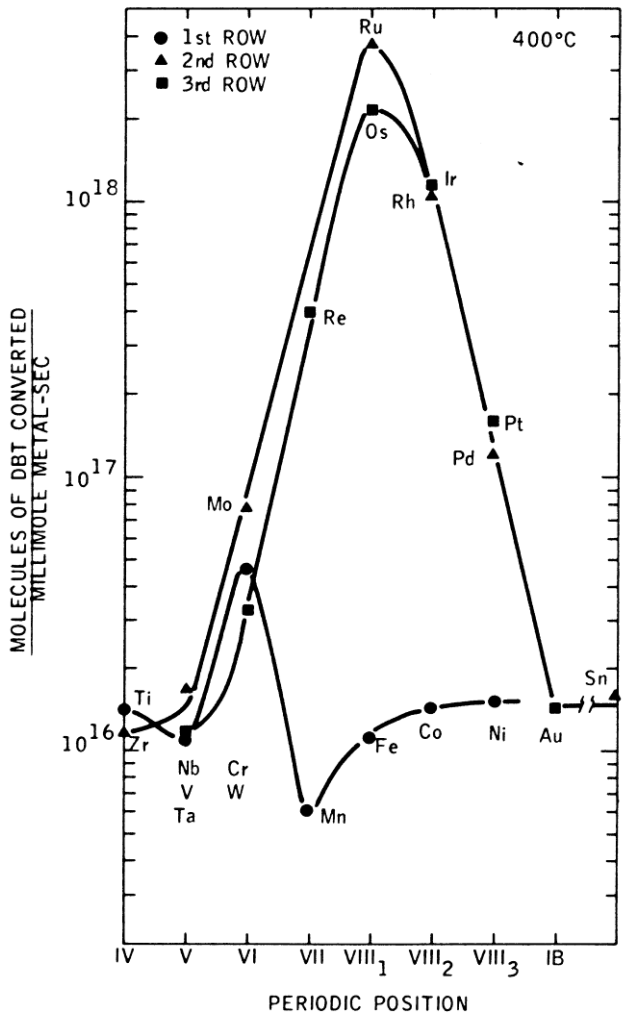

Figure 8: Conversion of DBT over transition metal sulfides at 400°C [36]

Figure 8 shows the volcano plot developed by Pecoraro and Chianelli which correlates periodic position of the transition metal to DBT conversion based on the Sabatier Principle [36]. The Sabatier Principle explains that binding energy of a substrate plays a large role in conversion rate. If the interaction is too weak then the substrate will not bind—no reaction. If the binding is strong enough to prevent dissociation—the reaction dies. Interestingly enough, if one simply followed the Sabatier Principle, MnS should be the most active of the series due to its favorable heat of formation. This however, was not the case—experimentally MnS was reported to be the

least active. Later, the metal sulfur bond (M-S) was explored and plotted in a volcano plot by Ledoux et al. resulting in the figure below (figure 9).

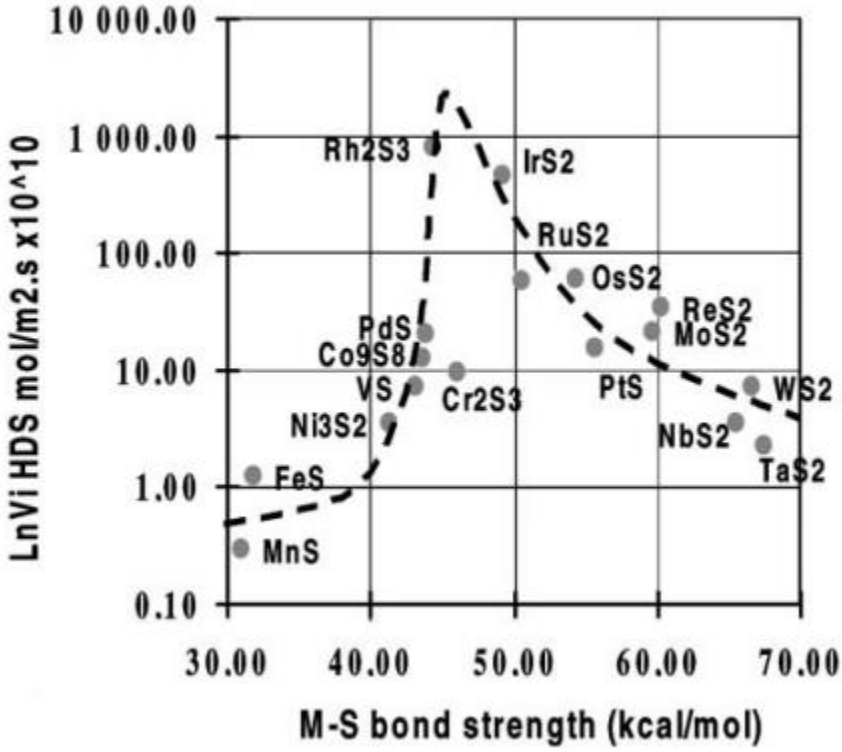

Figure 9: Ledoux et al. HDS activity vs. metal–sulfur bond strength [36]

Rhodium and Iridium have intermediate bond strength; not too strong and not too weak. It is suggested that the Co_9S_8 phase of the CoMoS catalyst weakens the M-S bond in MoS_2 just enough to increase or promote the activity. In other words, decorating MoS_2 with the optimal amount of Co_9S_8 would theoretically move its positon on the volcano plot (figure 9) to a position on the X-axis closest to Rhodium and Iridium.

2.2.0 CoMoS Catalyst

Extensive research has been conducted into improving industry catalysts, especially Cobalt promoted Molybdenum disulfide (CoMoS). The MoS_2 portion of CoMoS is a 2D material with

symmetry group: hexagonal P63/mmc3, wherein the layers or slabs of S-Mo-S are weakly held together by Van der Waals interactions. The slabs are comprised of a hexagonal plane of Mo atoms (prismatic coordinated to S) in between two hexagonal planes of Sulfur atoms (Figure 10).

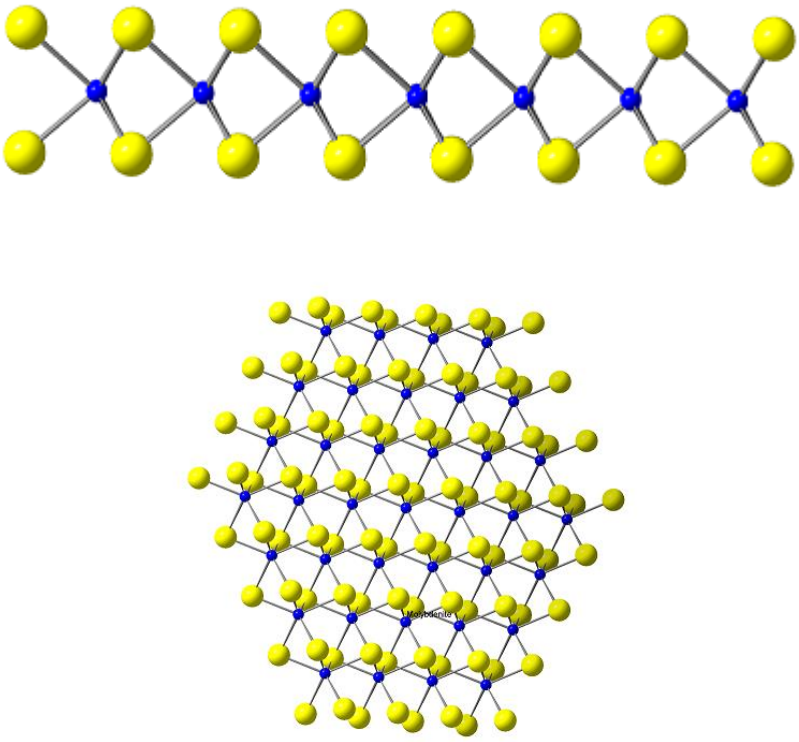

Figure 10: Molybdenite structure (yellow=S, blue=Mo)

The CoMoS catalyst maintains this MoS_2 like structure. The edge surfaces of the catalysts are said to be the active sites on the slab. Chianelli et al. explains a connection between the height of stacked MoS_2 planes and selectivity with his Rim-Edge Model [37] (Figure 11).

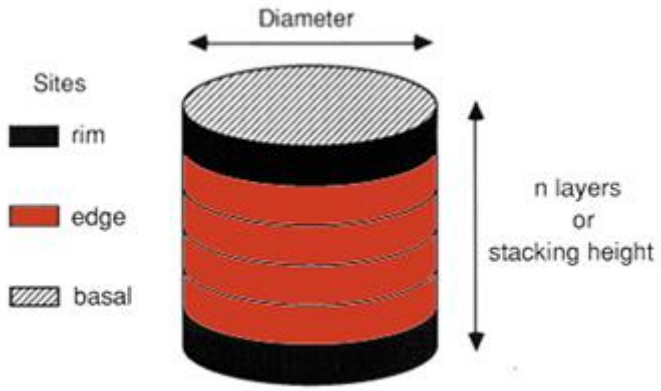

Figure 11: Rim Edge Model [30]

According to the Rim Edge Theory, the edges of the outermost stacking layers (rim=black) are responsible for DDS and HYD. The edges of the intermediate planes are active in DDS only. The basal planes consist of fully coordinated sulfur atoms rendering its activity negligible. Selectivity (HYD or DDS) is ultimately determined by the ratio of rim to edge sites in this theory.

It has been established and is widely accepted that introducing elements such as Cobalt to MoS_2 increases the disorder and gives rise to a highly active catalyst [38-39]. Cobalt is said to be a promoter because it works synergistically with MoS_2. As discussed previously with the volcano plots, the synergy can be explained by heat of formation (binding energy) of substrate to catalyst vacancy. The intermediate heat of formation resulting from Cobalt promoted MoS_2 is optimal for significant adsorption of the substrate (sulfur containing organic compound) and subsequent release of H_2S. From an atomic electronic standpoint, it is thought that donations of electrons from Co to Mo would weaken the M-S bond by filling the 4d sub orbitals [40]. Topsoe et al., using Mossbauer Spectroscopy and high resolution electron microscopy, determined that the position of the Cobalt was mostly on the edge of the molybdenite (MoS_2) crystals [41]. XPS studies have also shown that it is possible for Cobalt to migrate from the interior to the outer edges of the crystallites during reaction conditions. On a crystallite of MoS_2, there are Sulfur edges and Molybdenum edges. Cobalt generally tends to reside on the Sulfur edge of the crystallite and the disorder

provides for more vacancies [42][43][44]. It's also understood amongst researchers that the active phase of the Cobalt Sulfide is Co_9S_8, but its dispersion and placement on the molybdenum sulfide crystals is of high importance.

Certain changes in morphology or structure may occur during hydrodesulfurization so it is noteworthy to investigate changes in surface area and crystal phase transformations. The stable form of the catalyst has been debated throughout the literature. Chianelli et al. synchrotron analysis of a spent catalyst shows a carbide phase suggesting the stable phase of a highly active catalyst to consist of a carbide surface [45]. Most of the unsupported and supported CoMoS catalysts studied in literature have not been stabilized under catalytic conditions. Recent research shows that the catalyst de-stacks and is mostly single layers in catalytic environments [30]. Figure 12 illustrates the de-stacking that leads to the stabilized single layers.

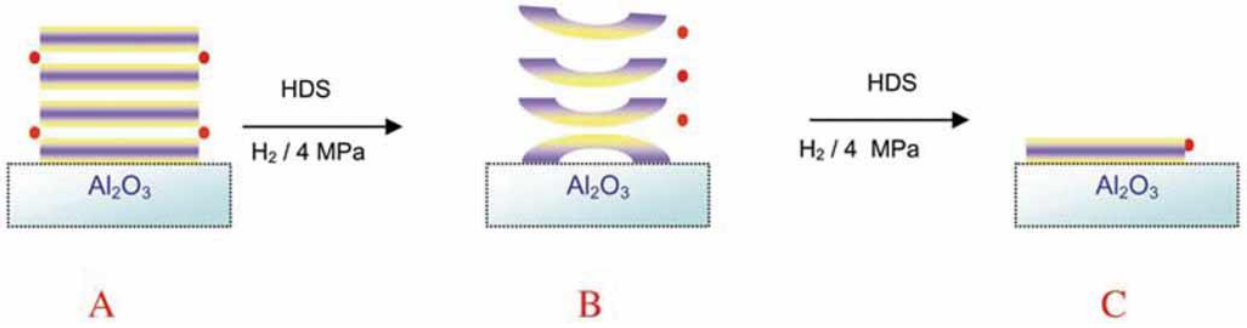

Figure 12: De-stacking during HDS process, A) sulfided precursor, B) hydrogen activated catalyst, C) stabilized single layer catalyst. [30]

The surface chemistry of the active phase during hydrotreating conditions is of great interest and has been under debate. Berhault et al. examined several fresh catalysts, catalysts made with carbon compounds in situ (DBT) as well as Mo_2C. CoMoS can be prepared by either decomposing a precursor hydrothermally or in a tube furnace. The type of chemical environment during decomposition (catalyst synthesis) is responsible for the surface structure and chemistry of

the final product. In a tube furnace, the precursor can be decomposed in inert atmosphere, hydrogen, H_2S/H_2 with argon balance or in situ (hydrotreating conditions) with sulfur containing organic compounds. It was observed that MoS_2 prepared by decomposing ammonium tetrathiomolybdate (ATTM) hydrothermally in a DBT and decalin mix (hydrotreating conditions) produces a carbide like structure on the surface.

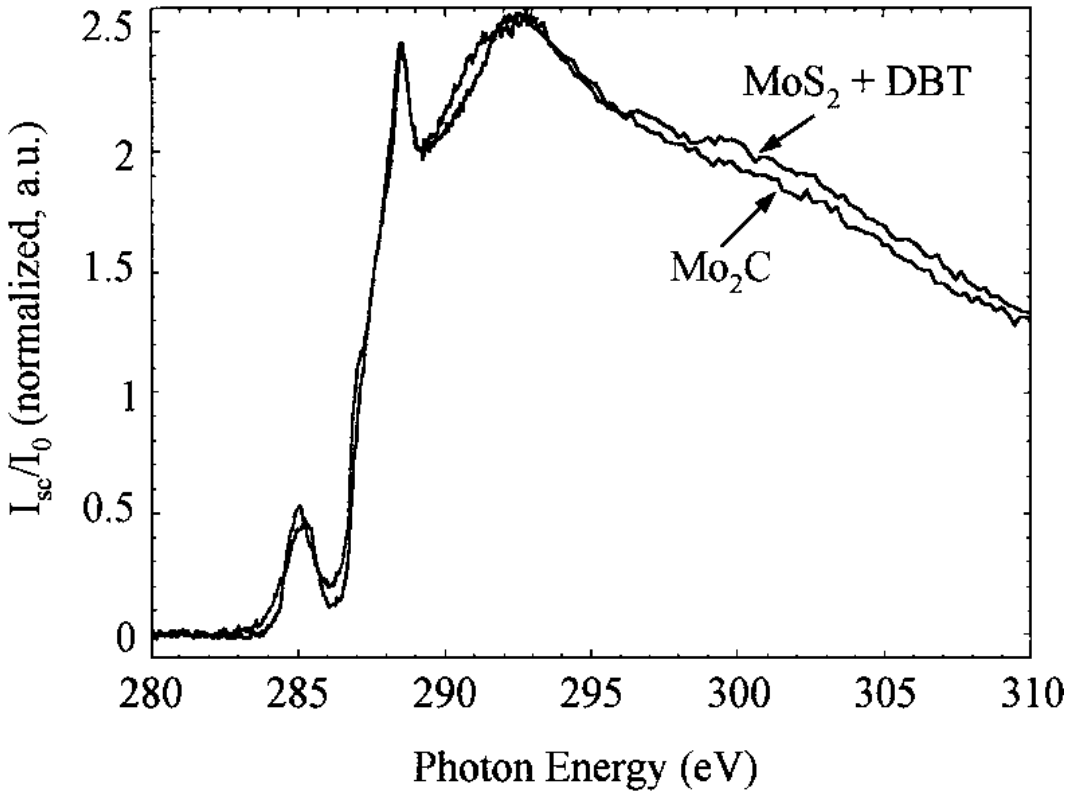

Figure 13: NEXAFS analysis of molybdenum carbide and MoS_2 synthesized by decomposition of ATTM in DBT/decalin mix [45]

Near Edge X-ray Absorption Fine Structure (NEXAFS) analysis showed there to be no difference between the surfaces of MoS_2 and Mo_2C (figure 13). "Carbon capping" (carburization of catalyst surface) of the catalyst during synthesis was also observed to produce higher surface area, porosity and prevent stacking of the MoS_2 slabs. Furthermore, Berhault's results were complimented by a density functional theory study conducted by Wen [46].

2.2.1 Methods of CoMoS Synthesis

2.2.1.0 Pore Volume Impregnation Method

Ammonium heptamolybdate is dissolved in a water and ammonia solution and kept at a pH above 8. The solution is then used to impregnate a support, carbon, or γ-alumina via pore volume impregnation procedure. This involves adding the solution dropwise while stirring the solution until the liquid has been absorbed by the support. The support is then dried and calcined above 400°C for over four hours in air. This yields MoO_3/support. This takes time in a tube furnace to allow proper heating and cooling. The support is passivated at room temperature with an inert gas for an hour. The impregnated support is then impregnated with a solution of a Cobalt salt such as $Co(NO_3)_2$ with the same drop wise method. The resultant is dried and calcined to obtain the oxide version of a supported catalyst. The catalyst would then require an activation step—sulfidation. Sulfidation takes place at the refinery at times under heat and H_2S/H_2 stream.

2.2.1.1 Wet impregnation Method

Wet impregnation begins with the preparation of ammonium heptamolybdate (AHM), $Co(NO_3)_2$ and citric acid. The support is added to the solution in a beaker. The solution is stirred anywhere between 5-24 hours. An excess of impregnation solution is used and filtered off later. The materials are then dried and calcined. At this point it, the impregnated support is characterized to ensure proper metal loading. This method is repeated at times to achieve the desired metal loading. The amount of Cobalt to Molybdenum varies between a 1:1 or 1:3 ratio, respectively.

2.2.1.2 Temperature Controlled Decomposition

An ammonium tetrathiomolybdate (ATTM) precursor is made from an ammonium heptamolybdate (AHM), water/ammonia solution by bubbling H_2S through it under heat while stirring. The resultant is mixed with the desired amount of cobalt II nitrate and is filtered and placed in a tube furnace under a flow of hydrogen in argon balance to 450°C for four hours. The catalyst is passivated with inert gas before opening the tube. When the catalyst is removed, it is fully sulfided and active.

2.3 DR. BRENDA TORRES (MRTI) AND POROCEL

Dr. Brenda Torres of Materials Research and Technology Institute (MRTI) at the University of Texas at El Paso provided the basis and fundamentals for this work. The fine work of Dr. Torres, under the guidance of Dr. Russell Chianelli, resulted in several hydrodesulfurization catalysts of high surface area and high activity. In 2012, her research caught the attention of Porocel Industries LLC and gave rise to a research grant with the promise of commercialization of Dr. Torres' technology. Porocel's area of business is sales in adsorbents and activated alumina as well as catalyst regeneration/rejuvenation. Porocel purchases spent catalyst from refineries and either rejuvenates them or regenerates them. Rejuvenation and regeneration processes recover up to 85% of original catalytic activity. Porocel was hoping to commercialize an unsupported CoMoS catalyst developed by Dr. Torres termed B5. In order to do so, patent protected synthesis methods from current commercial CoMoS manufacturers would have to be avoided. One synthesis method includes the decomposition of certain salts to obtain binary metal oxide which can then be impregnated (wet chemistry) onto the surface of a high surface area support to aid dispersion and increase surface area—the oxidic metals are then sulfide under a stream of H_2S in a tubular furnace. Another method is to produce a slurry of metal oxides with ammonium sulfide and pull vacuum during thermal decomposition [47]. Dr. Torres' synthesis method involved a hydrothermal decomposition of ATTM with a cobaltous salt which was unlike the current methods used by industry. Two years later, after several catalytic tests conducted in a lab in Ensenada, Baja California Mexico, along with some live feed results from Singapore, Porocel was ready to move forward with the industrial scale up portion of the project. Porocel was also shopping around for facilities that housed large hydrothermal reactors used for zeolite manufacturing and began evaluating the cost effectiveness of Dr. Torres' methods.

2.3.0 Brief Description of Dr. Torres' Hydrothermal synthesis Methods

Dr. Torres uses a two-step method wherein a sulfur containing precursor is first obtained and is decomposed hydrothermally in the second step. In the first step, ammonium tetra-

thiomolybdate (ATTM) was synthesized using the following method: Ammonium heptamolybdate (AHM) was dissolved in water with ammonium hydroxide. The solution was then introduced to a stream (bubbling through solution) of H_2S for two hours resulting in the precipitation of ATTM crystals [47]. The ATTM, $(NH_4)_2MoS_4$, was then added to an aqueous solution of Cobalt II Chloride, $CoCl_2$ under moderate stirring conditions to produce a black precipitate which is subsequently vacuum filtered [47].

Figure 14: Parr High Pressure Reactor Model 4540 [47]

The second step (hydrothermal decomposition) was carried out in a high pressure Parr Model 4550 quartz lined reactor (figure 14). The mass ratio of bimetallic precursor to diluent (water) was 1:10 respectively and the volume of the reactor was 600 mL [47]. During all of these decompositions, it is important to note that no more than 10% volume of the reactor was liquid—over 90% was empty head space which was purged and filled with N_2 gas before being sealed. The decomposition temperature reported was 300°C which produced pressures upwards of 1500psi. The duration of decomposition was two hours and the reactor was allowed to cool down

to room temperature, which took another four hours before depressurizing the vessel. The catalyst was recovered, washed and filtered with isopropyl alcohol (IPA).

2.4 Changes to the Hydrothermal Method for Industrial Scale Up

Porocel project managers expressed several concerns with the current method and made several requests. The pressure produced in the reactor during decomposition was considered high and the two step process did not appeal to the company as they felt it could be shortened into one step. One of the major setbacks was their reluctance to use H_2S in their facilities due to regulations and operating/safety concerns. Their facilities in the U.S. weren't outfitted at the time to handle H_2S gas for synthesis of the precursor—their facility in Canada (run by Dr. Ian Manson) was the site for the initial 10X scale up was not in regulation to handle H_2S gas either. MRTI initially overcame this challenge by synthesizing large batches of ATTM and shipping them overnight to Dr. Manson in Canada on dry ice in nitrogen gas until Porocel requested that an alternative, H_2S free, pathway be used instead. Porocel also wanted to maximize the volume of the hydrothermal reactor to reduce the overall cost of production. Studies were conducted to lower the time and temperature of the current process, but proved unsuccessful due mainly to the physical properties of water (vapor pressure).

The following lists the challenges during the scale up of the CoMoS catalyst:

1. Eliminate use of H_2S
2. Lower pressure to under 500psi
3. Reduce time (two step to one step/as well as decomposition time)
4. Maximize volume of the hydrothermal reactor
5. Use industrial grade MoO_3 and $Co(NO_3)_2$ as precursors in lieu of expensive high purity research grade material

2.4.0 Reduction in Pressure

In order to address Porocel's concerns, several experiments were designed to systematically approach each challenge beginning with the reduction in decomposition pressure. By immediately switching to either AHM, MoO_3 and $Co(NO_3)_2 \cdot 6H_2O$ provided by Porocel we could meet yet another objective. Once this was achieved with good catalytic results, we would move on to optimizing the temperature and decomposition time. Initial experiments were carried out by decomposing ATTM in n-decane with $Co(NO_3)_2 \bullet 6H_2O$ as shown in Table 2. An acceptable activity of CoMoS catalyst relative to %DBT removal in the catalytic test is greater than 80% conversion of DBT at five hours. These experiments produced material that was not very active but we did learn that it was possible even under these chemically unfavorable conditions that elemental sulfur could be used instead of H_2S.

Table 2: Preliminary studies using n-decane as a diluent to reduce decomposition pressure

Mo Source	Co Source	Sulfur Source	Mol Ratio	Diluent 50mL	Time hr	Temp °C	Pressure psi	H_2 pressure psi	EDA mL	NaOH mL	% DBT remaining after five hours	XRD Phases present
ATTM	$Co(NO_3)_2{\cdot}6H_2O$	ATM	1:1 Co:Mo	decane	2	350	700	40	0	0	50	MoS_2
ATTM	$Co(NO_3)_2{\cdot}6H_2O$	ATM	1:1 Co:Mo	decane	2	350	700	80	0	0	50	MoS_2, Co_9S_8
ATTM	$Co(NO_3)_2{\cdot}6H_2O$	ATM	1:1 Co:Mo	decane	2	350	700	160	0	0	50	MoS_2, Co_9S_8
ATTM	$Co(NO_3)_2{\cdot}6H_2O$	ATM	1:1 Co:Mo	decane	2	350	400	0	15	0	100	MoS_2, Co_9S_8
ATTM	$Co(NO_3)_2{\cdot}6H_2O$	ATM	1:1 Co:Mo	decane	1	350	700	300	0	0	50	MoS_2, Co_9S_8
ATTM	$Co(NO_3)_2{\cdot}6H_2O$	ATM	1:1 Co:Mo	decane	2	350	700	300	0	0	50	MoS_2, Co_9S_9, Co, Mo
ATTM	$Co(NO_3)_2{\cdot}6H_2O$	ATM	1:1 Co:Mo	decane	2	300	400	300	0	0	50	MoS_2, Co_9S_8
ATTM	$Co(NO_3)_2{\cdot}6H_2O$	ATM	1:1 Co:Mo	decane	2	350	700	0	0	0	50	MoS_2
ATTM	$Co(NO_3)_2{\cdot}6H_2O$	ATM	1:1 Co:Mo	decane	2	350	400	0	15	0	100	MoS_2, Co_9S_8
ATTM	$Co(NO_3)_2{\cdot}6H_2O$	ATM	1:1 Co:Mo	decane	1	350	700	0	0	0	50	amorphous
ATTM	$Co(NO_3)_2{\cdot}6H_2O$	ATM	1:1 Co:Mo	decane	2	300	400	0	0	0	50	amorphous
MoO_3	$Co(NO_3)_2{\cdot}6H_2O$	Sulfur Z 12g	1:1 Co:Mo	decane	2	300	1400	0	5	10	100	MoS_2, Co_9S_8 MoO_2
MoO_3	$Co(NO_3)_2$	Sulfur Z 12g	1:1 Co:Mo	decane	2	300	<300	0	5	10	100	MoS_2, Co_9S_8 MoO_2
MoO_3	$Co(NO_3)_3$	Sulfur Z 12g	1:1 Co:Mo	decane	2	300	<300	0	10	0	100	MoS_2, Co_9S_8 MoO_2

2.4.1 Elimination of H_2S Via Sulfur^0 Ionization

Incorporation of sulfur zero (elemental sulfur) would reduce the synthesis to one step as well as avoid the use of H_2S. The structure of elemental Sulfur is cyclic, in either a six or eight member ring, the latter being the most common. The first experiments that were conducted to bypass the use of H_2S using sulfur zero were unsuccessful primarily because the sulfur rings were too stable and not willing to react under the initial chemical conditions. A quick literature search revealed ethylene diamine to be a powerful ionizer. Putnam compares ethylene diamine (EDA) to liquid ammonia [48] and a study by Davis et al. investigated the interactions of octatomic sulfur (S_8) with EDA and suggested that ring opening occurs to produce polysulfanes (H_2S_n) [49].

2.4.2Diluent/Solvent selection

Decane lowered the pressures, but was not a suitable replacement for water due to its non-polar nature—the precursors did not dissolve or interact well even under higher temperatures (350°C) or added hydrogen pressure. Diethylene glycol (DEG) was the next logical replacement for water for the following:

- High boiling point (245°C)
- Greater dispersion and miscibility of Sulfur
- EDA does not react and is soluble in DEG
- Lower heat capacity than water
- Low vapor pressure

After the adoption of DEG, the new process was termed solvothermal in lieu of hydrothermal.

CHAPTER 3: METHODOLOGY

3.0 Synthesis

3.0.0 SOLVOTHERMAL SYNTHESIS OF COMOS

Solvothermal synthesis of CoMoS was carried out in a 300mL Parr autoclave reactor without a glass liner. All chemicals were obtained from Porocel Industries LLC with the exception of diethylene glycol and ethylene diamine, which was provided by Alfa Aesar. The purity of the DEG and EDA were above 95%. No glass liner was used upon the request of Porocel in order to keep conditions during the scale up as close as possible between the small reactor and the larger one in Canada. A 3:1 mol ratio of Mo to Co was maintained throughout all experiments. The ratio of Sulfur zero to Mo was 3.5:1. EDA (4mL) was added to the 300mL Parr reactor and sulfur zero (1g sulfur) in a 7:1 mol ratio (EDA:Mo) was stirred into the EDA in the vessel until the Sulfur was dissolved resulting in a dark green color. 1.25g of MoO_3 was added along with 0.85g of $Co(NO_3)_2 \bullet 6H_2O$. DEG (12.5mL) was added as a diluent and the reactor was sealed. The autoclave was placed in a heating mantle at 200°C for 2 hours. The autoclave was allowed to cool down without assistance to room temperature before venting. The catalyst was washed with methanol and toluene in preparation for characterization and catalytic testing. This method was the preferred over others because it gave rise to the most active catalyst. Instructions were sent to Dr. Ian Manson in Canada for scale up and the catalysts were returned for characterization and catalytic testing. Four catalysts (U1, U2, U3, U4) synthesized in the lab are reported in this paper with few variations. U1 was made via the process aforementioned. U2 was made with a slight change—EDA was added onto sulfur instead of Sulfur onto EDA. Caution should be exercised in this step, as the reaction was rather violent, exothermic and resulted in ammonia vapor and vigorous effervescence. The resulting solution of EDA/Sulfur color was a deep red color. U3 was prepared with 10 times the amount of materials in the same reactor under the same conditions as U2, to evaluate the effects of reducing reactor headspace and maximizing reactor loading volume. U4

was prepared by pouring all materials simultaneously into the reactor at the same time (moderate effervescence).

A catalyst prepared by Porocel in their Canadian facility will also be included and will be referred to as P1. P1 was made in a 6L reactor with no glass liner. The same procedure as U3 outlined above was used (with 20X the material used in the 300mL reactor) and special care was taken to match the cooling profile of the 300mL reactor.

3.1 Catalytic Testing for Rate determination

3.1.0 Catalytic Testing (DBT Model Reaction)

Catalytic activity was evaluated for U-series catalysts (U1-U4), P1 (Porocel) and a commercial alumina supported catalyst sent to us by Porocel from the catalyst manufacturer Haldor Topsoe, (TK-578 BRIM). The catalytic test was a model reaction that follows the conversion of DBT through hydrodesulfurization in decalin in a Parr reactor under constant stirring. This technique has been used worldwide amongst researchers to model the conditions of petroleum feedstock. Reaction rate constants (k) can be determined as well as the order of the reaction by manipulating the data graphically that is obtained from GCMS analysis of the aliquots. The HDS of DBT were carried out in a 300mL Monel Parr reactor model 4520 with a quartz liner and equipped with mechanical overhead stirring to assist in catalyst dispersion. A quartz liner was loaded with 0.5g of catalyst with 3.5g of DBT in 75 mL of decahydronaphthalene. The quartz liner was placed in the Monel Parr reactor and sealed. The reactor head space was purged three times with hydrogen gas before pressurizing the vessel to 160psi. The reactor was heated up to 350°C at a rate of 8°C/min while stirring at 400RPM. Time 0 for the reaction was at the exact time the temperature controller reached 350°C. Aliquots (0.75mL) were taken through a dip tube every 30 minutes beginning at time 0. The total time for the catalytic test was 300 minutes.

3.1.1 Gas Chromatography Mass Spectroscopy

Qualitative and Quantitative analysis was achieved with the aid of a Hewlett Packard GCMS system. The Hewlett Packard (HP) 5890 gas chromatographer plus was equipped with an auto sampler and HP-5ms capillary column 20m in length, 0.18mm inner diameter with a (5%-Phenyl)-methylpolysiloxane film 0.18μm thick. The flow rate for the Helium carrier gas was 2mL with an inlet temperature of 220°C. The splitless injection volume was 1μL with the auto sampler fast injection option. Oven parameters or heating profile was 70°C initial then ramped up to 185°C at a rate of 35°C/min and held for three minutes followed by a final ramp to 200°C at 15°C/min. The GC was connected to a 5972 Electronic Ionization HP 5972 mass spectrometer outfitted with a DeTech 2300 Electron Multiplier mounted on a 2373 optics frame. The temperature of the mass transfer line was 240°C. The system was run with Chemstation software.

3.2 Characterization

3.2.0 Scanning Electron Microscopy (SEM)

Micrographs were taken with a Zeiss Evo LS scanning electron microscope (SEM). Samples were fixed onto stages with conducting carbon double side adhesive. Samples were sputter coated with palladium. Sputter coating was done with a Denton vacuum sputter coater and the duration was 35 seconds at 45 millivolts. The technique provides a coating that is approximately <10 angstroms thick. Parameters such as spot size were adjusted as needed and various magnifications were taken.

3.2.1 Scanning Transmission Electron Microscopy (STEM)

STEM images were acquired at The University of Texas at San Antonio with Dr. Miguel Yacaman's group using a JEOL JEM-ARM200F microscope with spherical aberration (Cs) correction. Operating accelerating voltage was between 80 and 120kV, both bright and dark field images were obtained simultaneously with in-line (bright-field) and high-angle annular dark-field

(HAADF) detectors, respectively. The samples were prepared and mounted by drop-casting with methanol onto copper grids.

3.2.2 Powder X-Ray Diffraction Analysis (XRD)

Some preliminary analyses were conducted using a Rigaku Miniflex diffractometer with a scintillation counter. Other scans were obtained with a Bruker D8 Discover with a Lynxeye XE 1-D detector or a PANalytical Empyrean with a PIXcel3D detector. The source was always Cu-Kα radiation with a corresponding wavelength of 1.541 nm. A step rate of 0.01°, with a count time of 1s, and a scan from 20-60° in 2θ was used. The analyses were performed to compare literature patterns to the patterns of synthesized material.

3.2.3 Surface Area Analysis (BET)

Nitrogen adsorption BET surface area analyses were conducted using a Quantachrome NOVA 2200e surface area and pore size analyzer. Prior to analysis, all samples were degassed at room temperature for 15 minutes, and sample tubes were backfilled with Helium gas.

3.2.4 Energy Dispersive Spectroscopy (EDS) for Elemental Analysis

Elemental analysis and elemental mapping was conducted using an EDAX system with an Octane Silicon Drift Detector (SDD). Accelerating voltage was 30kV in order to observe the Kα transitions in Co and S while viewing the Lα transitions for Mo. Dead time was 40% with 2000cps.

3.3 Kinetics Approach to Activity

3.3.0 Kinetics and Reaction Order

Kinetic plots were produced based on the results of the DBT catalytic testing to compare activity between the U-series catalysts, P1 catalyst and the TK-578 BRIM catalyst. A catalyst lowers the energy of activation for a particular reaction by supplying an alternate pathway [2]. The kinetic of the reactions were determined by plotting the integrated area of the DBT peak in the chromatogram as a function of time. Samples were taken every 30 minutes during the reaction for five hours with time zero is marked when the reactor reaches 350°C. The rate constant (k) was

then determined graphically as the negative slope of the best-fit line. The determination of the reaction order can be obtained by graphical function. A zero order reaction produces a linear correlation of points when plotting concentration of substrate over time. When plotting concentration of DBT over time produces a non-linear decay plot such as the one below (Figure 15), then the reaction is not zero order and could be first or second. The next approach would be to take the natural log of the concentration and re-plotting the data with the goal of achieving linear correlation between data points. Taking the natural log of the concentration of DBT over time will yield a straight line for first order reactions such as Figure 16. In this case, the relationship is linear and the rate constant (k) is the negative slope of the line. All catalysts evaluated here unto, exhibited first order kinetics with some interesting features in the in U-series catalysts. Chapter 4 reaveals rates for the catalysts including surface area measurements.

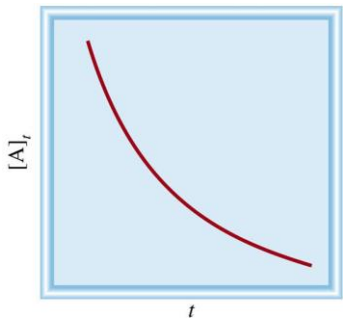

Figure 15: Example of First order plot of concentration over time

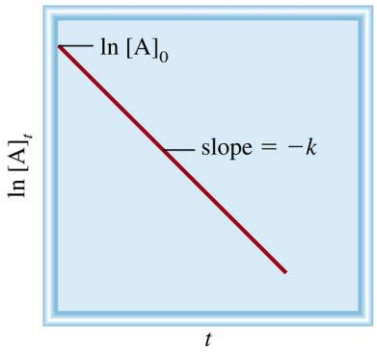

Figure 16: Example of First order plot with the natural log of concentration over time

3.3.1 CALCULATIONS FOR A FAIR RATE COMPARISON

Surface area measurements will enable us to determine the rate of DBT conversion per area of catalyst. The rate units for a first order reaction are 1/s, we also know the amount of catalyst used which was 3.5g and the amount of catalyst (.5g). The surface are will be determined experimentally and has the units of m^2/g. Calculating moles of DBT using molar mass of 184g/mol can be divided by the rate to give moles of DBT per second. The moles per second can then be divided by the surface area of the mass of catalyst used for the test. The result is rate of moles converted per second by area of the catalyst ($mol/m^2 \cdot s$).

CHAPTER 4: RESULTS AND DISCUSSION

4.0 XRD of Starting Materials

4.0.0 Molybdenum Trioxide XRD Pattern

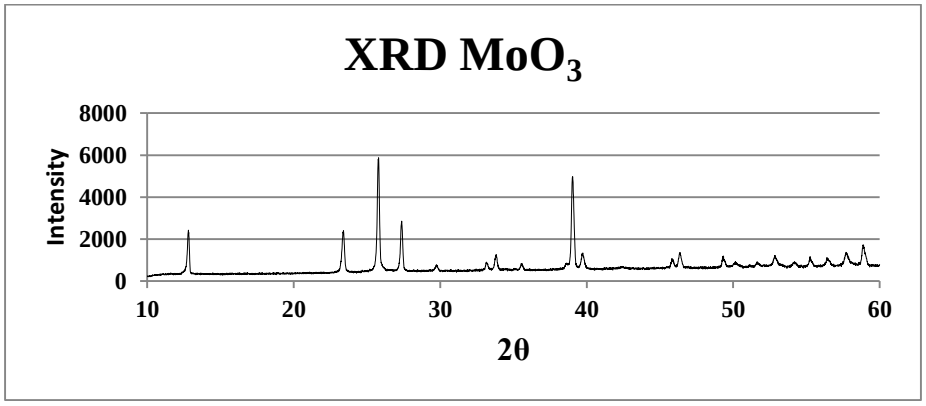

Figure 17: XRD Pattern of MoO_3

4.0.1 $Co(NO_3)_2$ XRD Pattern

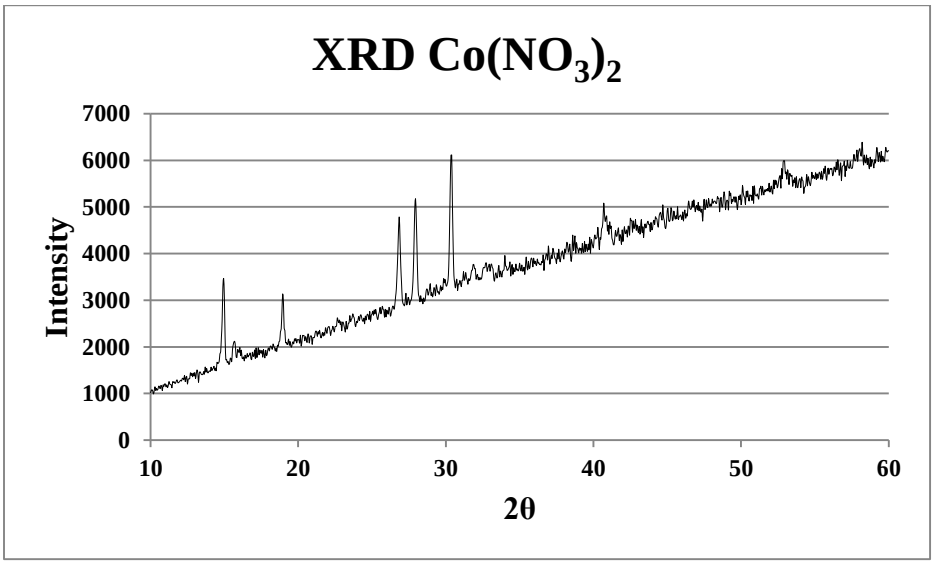

Figure 18: XRD of Cobalt II Nitrate

4.0.2 SULFUR^0 XRD PATTERN

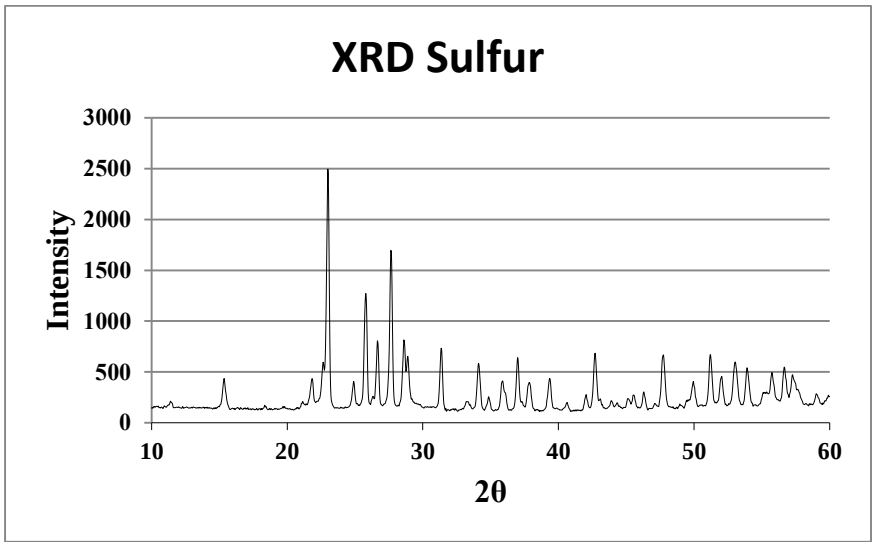

Figure 19: XRD of Sulfur starting material

4.1 XRD Results of Catalysts with Discussion

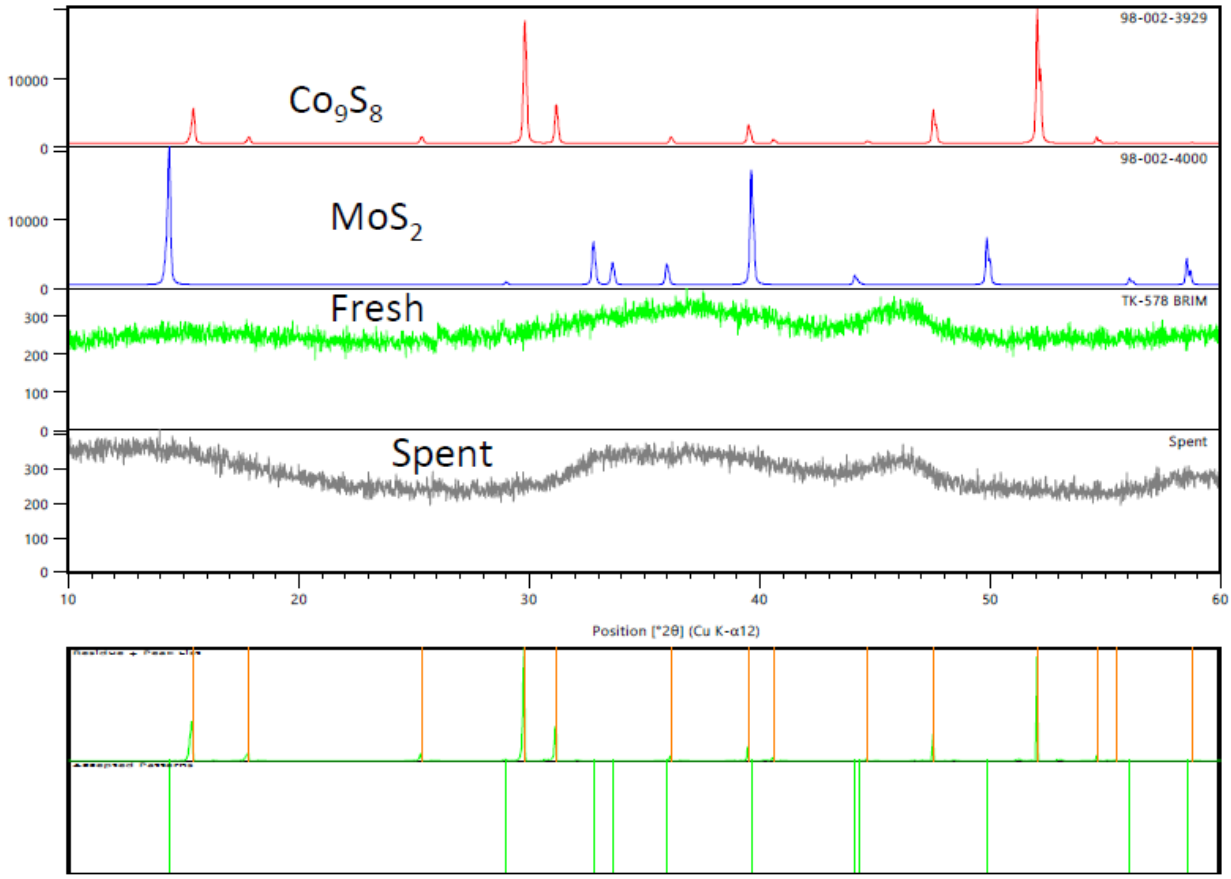

Figure 20: XRD of Fresh and Spent TK-578 BRIM

4.1.0 XRD OF TK-578 BRIM CATALYST

Figure 20 is the XRD of the fresh and spent TK-578 BRIM Catalyst. There are no apparent phases of cobalt or molybdenum sulfide—the catalyst is amorphous before DBT testing and remains amorphous after.

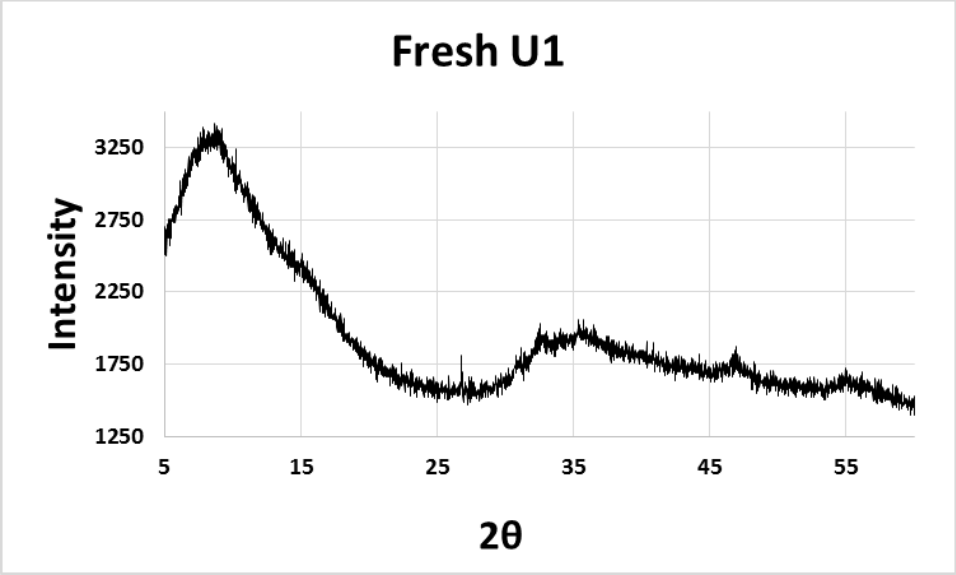

Figure 21: Fresh U1 catalyst

4.1.1 XRD OF U1 CATALYST

Fresh catalysts are catalysts that have not been subjected to a DBT conversion test for catalytic activity. The spent catalysts are the same catalyst that has been subjected to a catalytic test and has been recovered, filtered with methanol and air-dried. Depending on the stability of the catalyst it is possible to undergo phase, morphological or surface chemistry transformation under the rigorous conditions of the reaction. It is not uncommon to see an entirely different diffraction pattern after a DBT test; however, it could be the result of insufficient time or temperature during synthesis. All catalysts were either amorphous or poorly crystalline. This is the nature of catalyst characterization. Industry catalysts are amorphous and the Porocel project engineers were having trouble using X-Ray diffraction for QA/QC and characterization. Porocel had a Bruker D2 diffractometer at their Little Rock facility that was rarely used for just that reason.

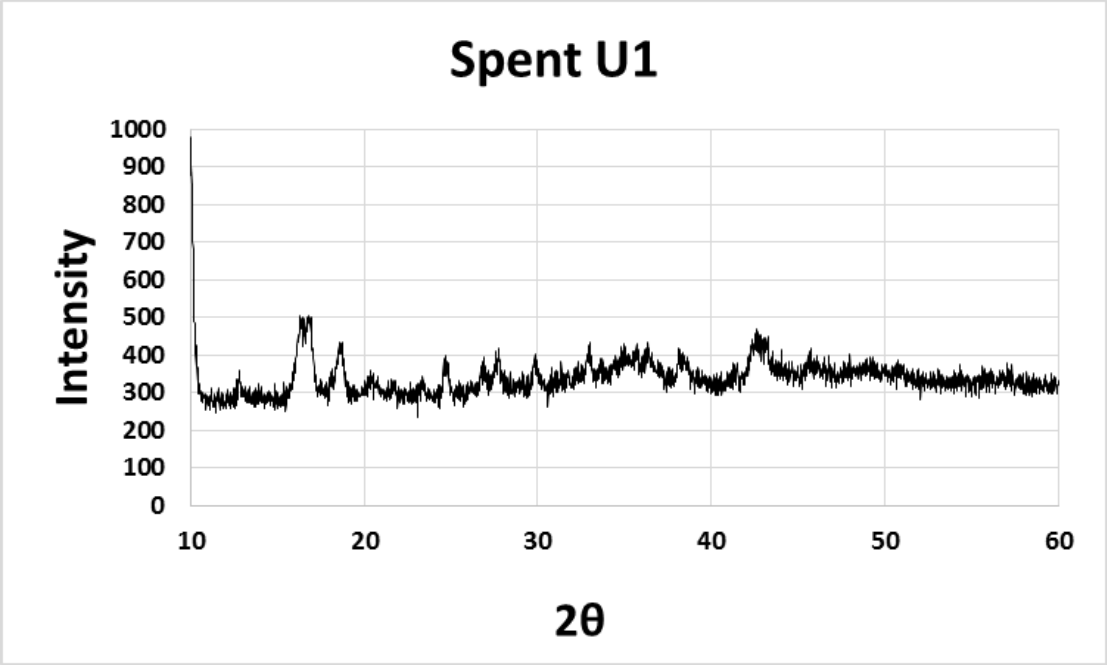

Figure 22: Spent U1 catalyst

Fresh U1 in figure 17 is poorly crystalline and the relative high counts would suggest that there is a phase present between 5 and 15 two theta. Crystalline MoS_2 has a (002) reflection for and is at 2θ =14.4º (6.14 Å). It is noted that the presence of a strong (002) 2θ peak is indicative of the stacking of planes (periodicity in c-axis). In the case of fresh U1, the peak is undetected. No reflections at the 2θ =14.4º would suggest monolayer MoS2, i.e. single stacks.

It is possible for intercalation to be responsible for a shift of this peak to a lower 2θ value. This would depend on the distance between the planes, as the planes separate in distance (exfoliation) the reflections shift to lower diffraction angles. An additional 4 Å to the original spacing of 6.14 Å would give rise to a reflection at a lower diffraction angle approximately at 2θ= 10º.

Spent U1 is amorphous and has few fluctuations rising from the noise below 20°=2θ. The position of those two pseudo peaks is 17 and 19° respectively and they are not part of the starting material or product indexed peaks.

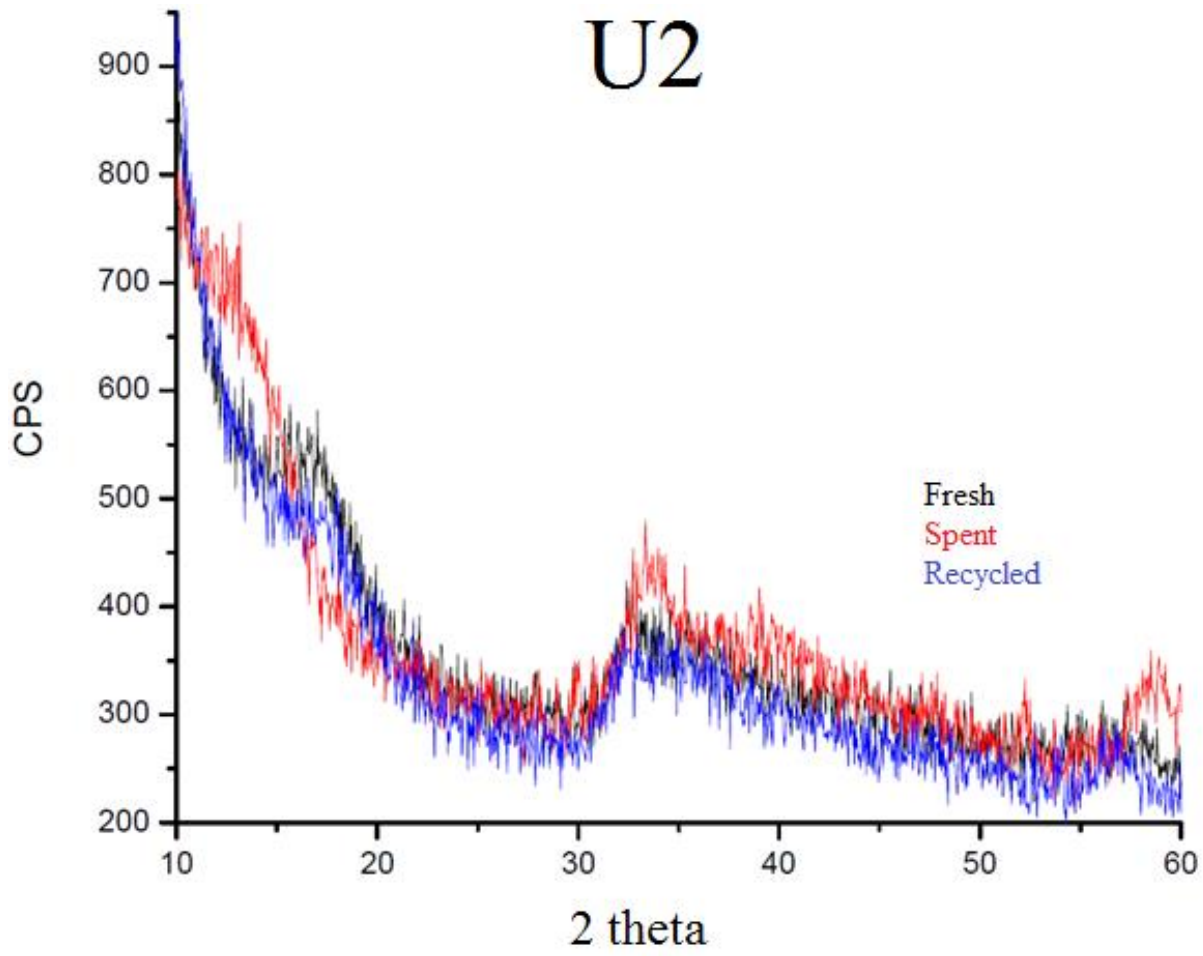

Figure 23: XRD pattern of Fresh and spent U2 catalyst

4.1.2 XRD OF U2 CATALYST

Figure 19 shows the fresh, spent and rewashed fresh U2 catalyst. The catalyst was re-washed and filtered to ensure the reason diffraction was so difficult was not due to solvent trapped in or on the catalyst, but due to its amorphous nature. There was not much change to the diffraction pattern, which is a testimony to the catalysts stability under hydrotreating conditions. The differences in U1 and U2 synthesis were minor and not much was expected to change, but it is noted that stability has increased with the change of addition of reagents. In U1, sulfur was added to EDA, where in U2, EDA was added to sulfur. It is important to note that the addition of sulfur to EDA did not effervesce as much and the color was closer to an emerald green in lieu

of a dark red. The dissolution of sulfur also took longer—it took up to 3 times as long, 15 minutes.

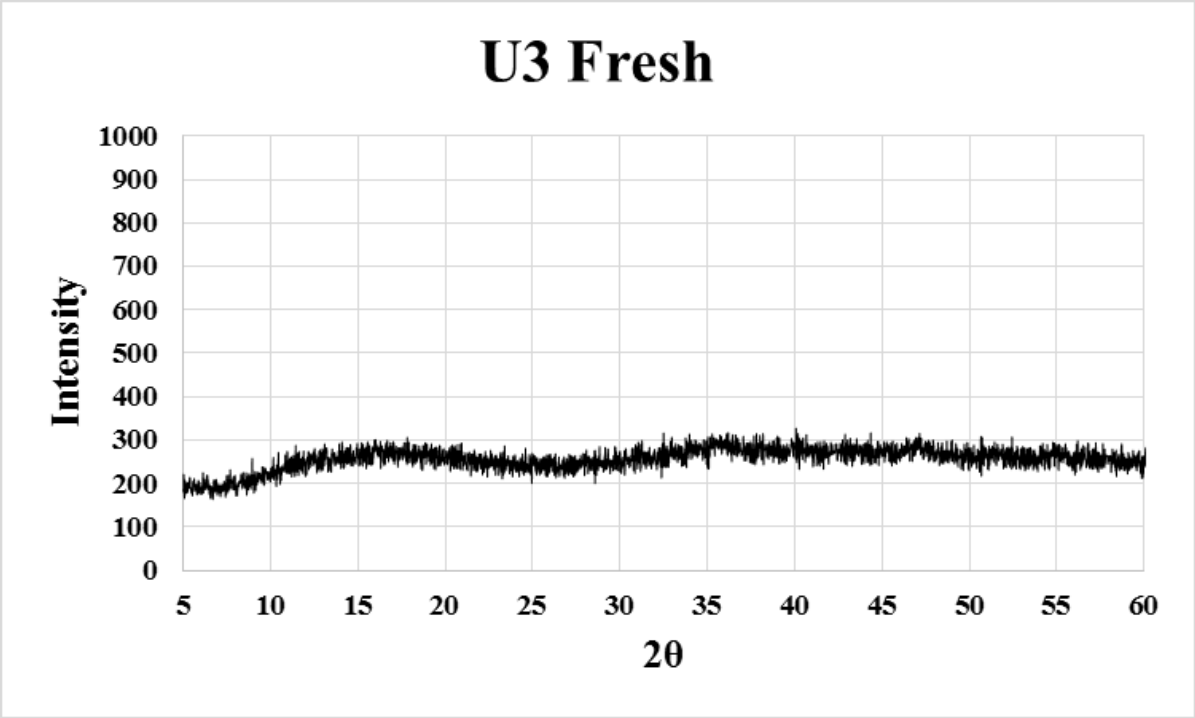

Figure 24: XRD Pattern of Fresh U3 catalyst

4.1.3 XRD OF U3 CATALYST

U3 was synthesized under the same condition as U2 with the only change being an increase in the load volume of materials in the reactor. U3 fresh was amorphous with no reflections to either a molybdenum or cobalt sulfide phase.

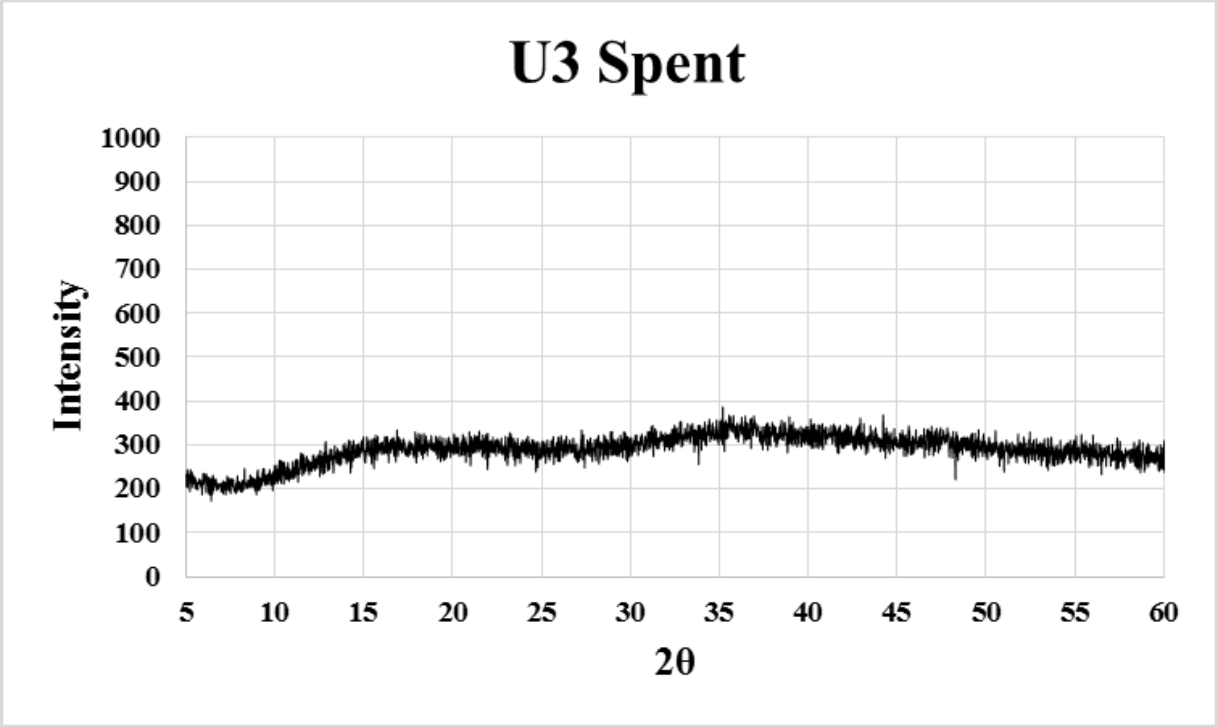

Figure 25: XRD Pattern of Spent U3 catalyst

The diffraction pattern obtained with U3 spent shown in figure 21 does not show much change from the fresh version of the catalyst. The catalyst seems to have been stabilized in situ during thermal decomposition and synthesis under solvothermal conditions.

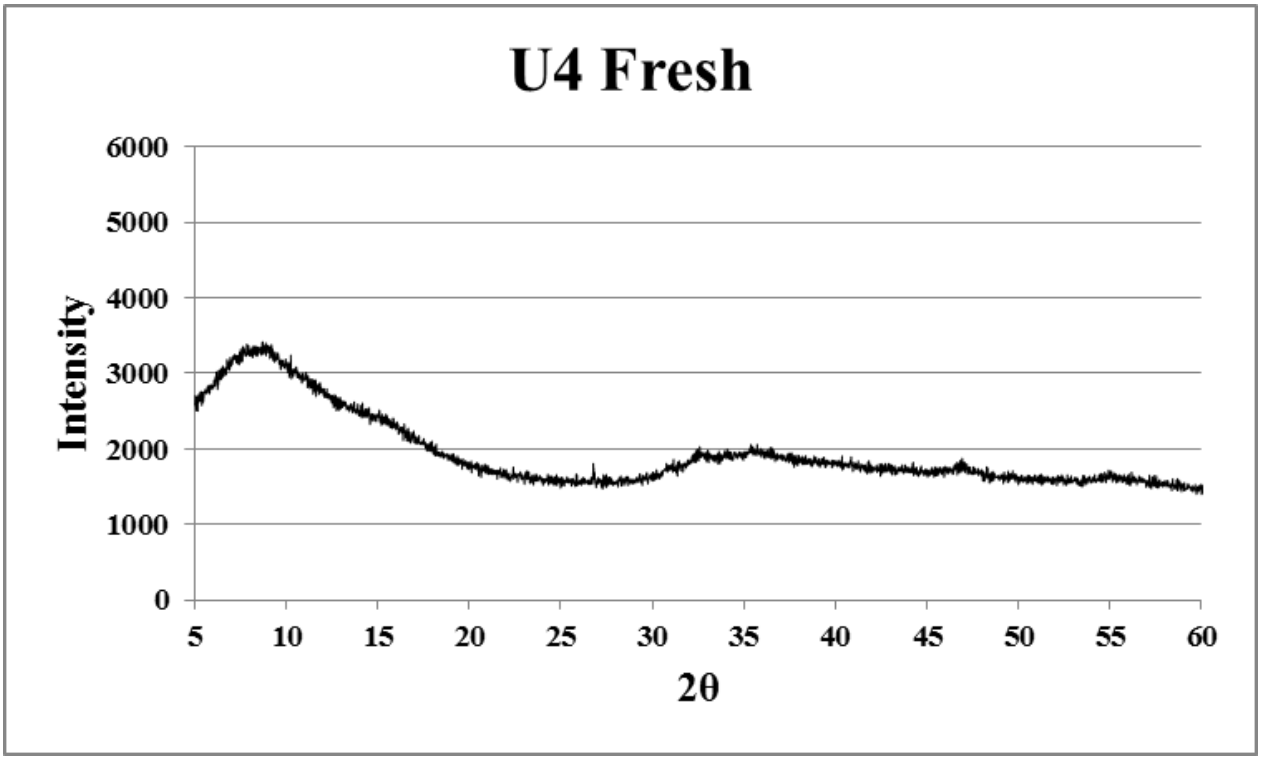

Figure 26: XRD Pattern of Fresh U4 catalyst

4.1.4 XRD OF U4 CATALYST

Fresh U4 shows a higher intensity due to the stronger source of the PANalytical Empyrean as opposed to the Rigaku Miniflex that the spent U4 was obtained with. It is interesting to note, the broad slope between 5 and 15 two theta look similar to the patterns in U1. This was repeated several times with the same results, and it was determined that the order of the addition of the reagents, sulfur and EDA was important and had an effect in catalyst preparation.

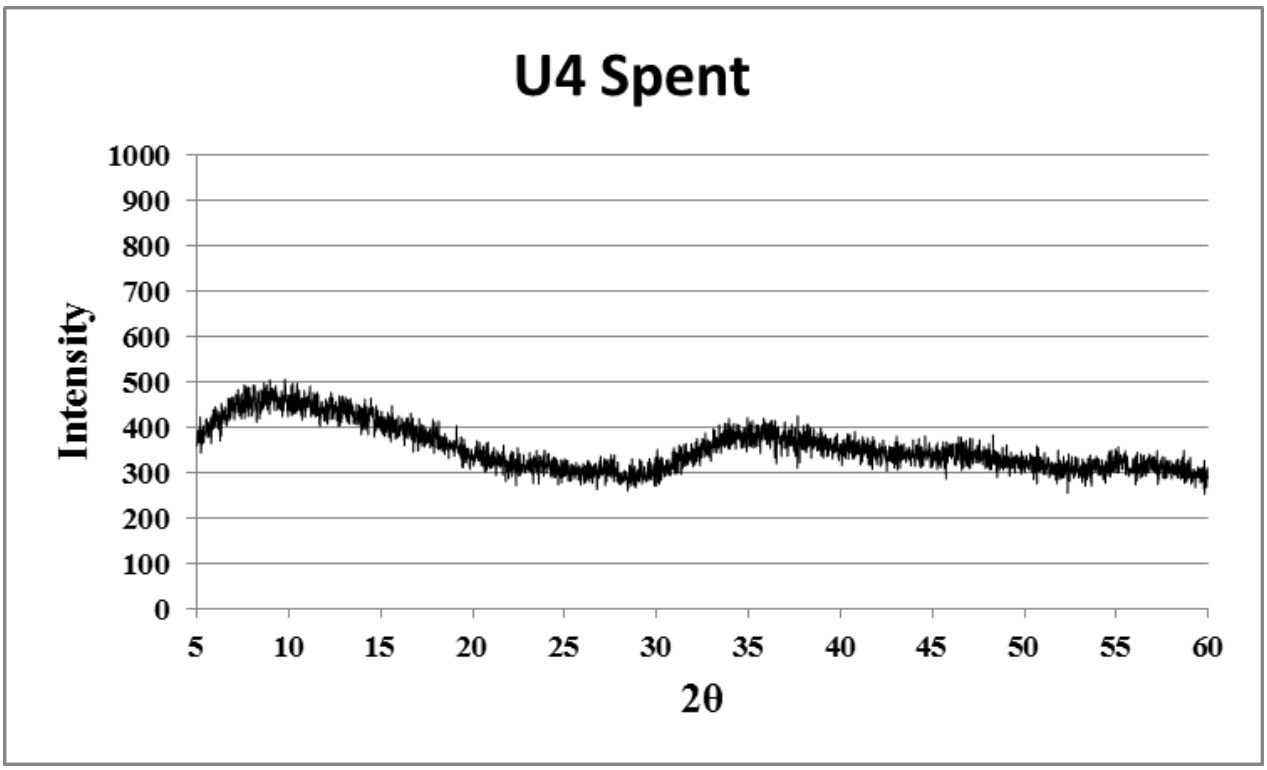

Figure 27: XRD Pattern of Spent U4 catalyst

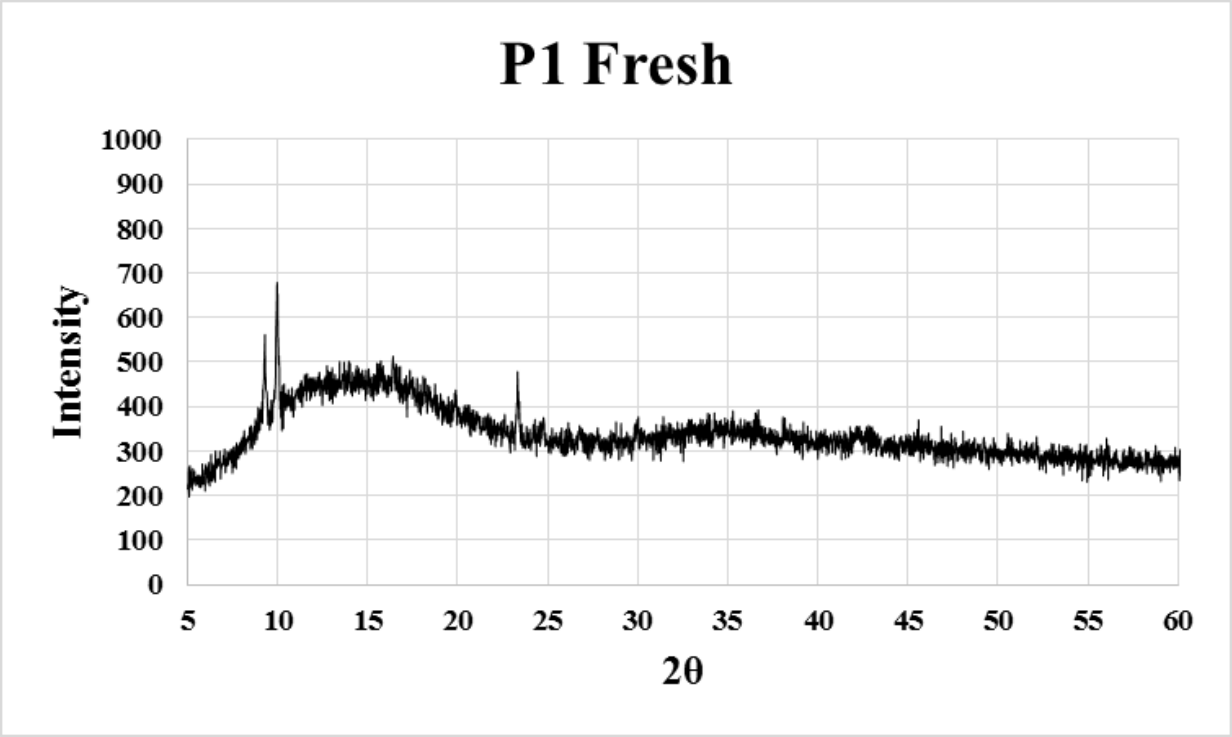

Figure 28: XRD Pattern of Fresh P1 catalyst

4.1.5 XRD OF P1 CATALYST

Porocel produced many samples in their facility in Canada, but none were as close to the ones produced at UTEP save this one (P1). Many of Porocel produced catalysts would show molybdenum oxide peaks (MoO_2), but this one showed MoO_3 split peaks at 10 two theta. These are and indicator of incomplete sulfidation, either due to localized heating issues, or it would suggest that the scale up is not linear in nature. That perhaps a concentration of materials relative to the volume of the reactors should be approached. Elemental analysis would aid is in further determining an approach to this problem.

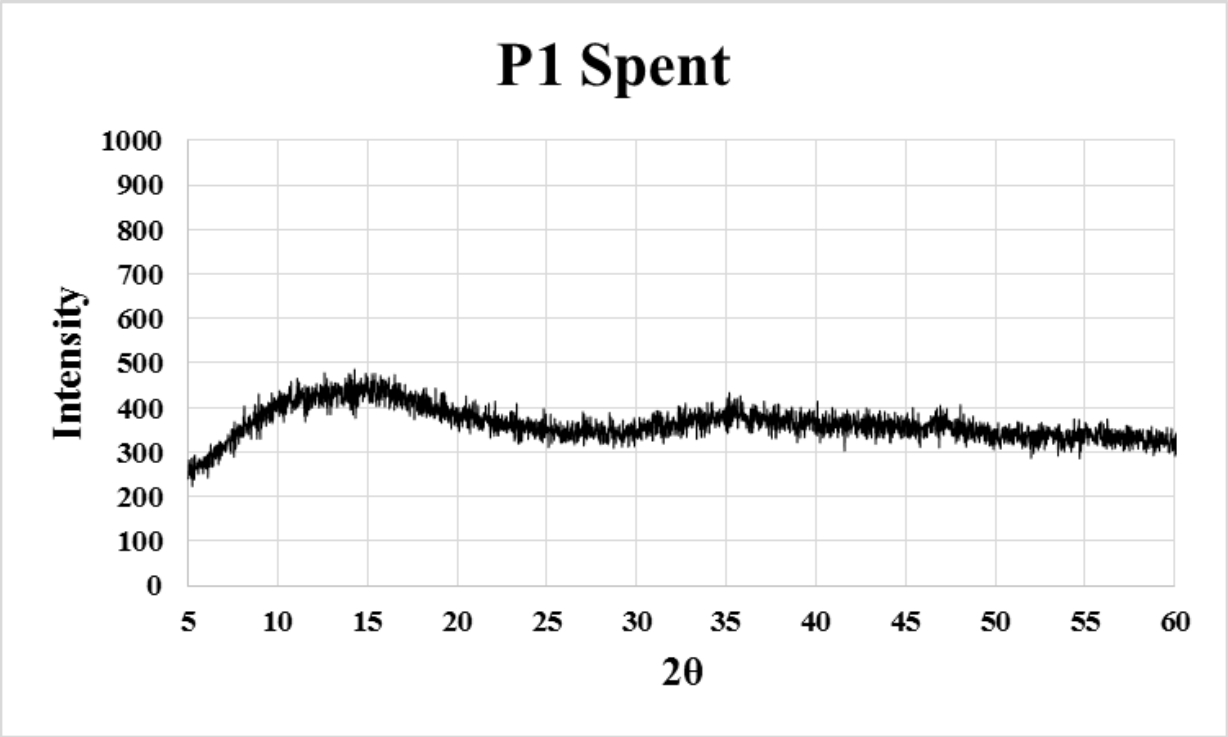

Figure 29: XRD Pattern of Spent P1 catalyst

Figure 25 shows spent P1 and that it was stabilized and fully sulfided during the catalytic testing. The small peaks at approximately 10 two theta have vanished, suggesting that any further sulfidation could be done in situ at the refineries in the first few hours or days of HDS conditions in a live feed containing sulfur.

4.2 Surface Area Analysis (BET Nitrogen adsorption)

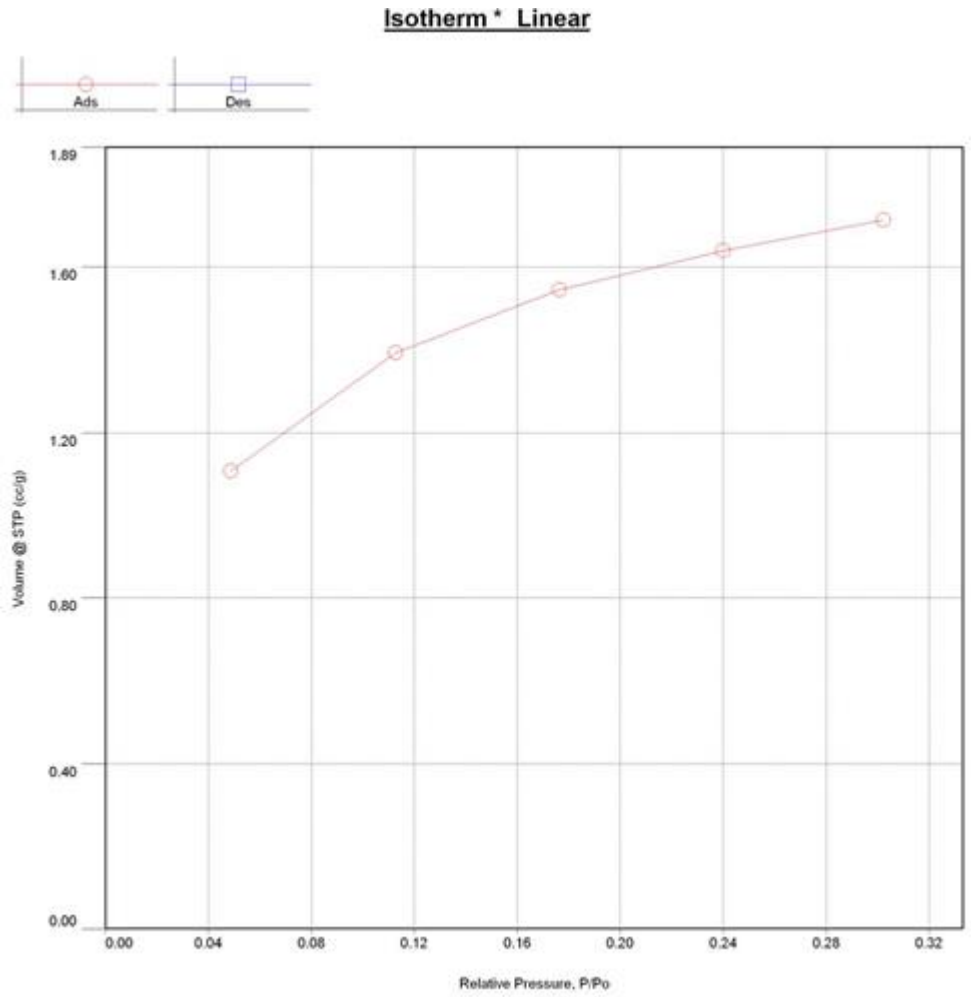

Figure 30: Isotherm for U1 Fresh catalyst

Figure 29 shows nitrogen adsorption for U1 fresh catalyst and the surface area was calculated to be 5.362 m^2/g. The correlation coefficient, r, was 0.997.

Table 3: Surface Area of catalysts fresh and spent

Catalyst Surface Area m^2/g		
	Fresh	**Spent**
U1	5	10
U2	8	14
U3	5	30
U4	3	8
P1	6	8
TK-578 BRIM	150	150

Surface area of the catalysts were obtained through BET nitrogen adsorption. All values are tabulated above in Table 3. TK-578 BRIM data was obtained from Porocel. U3 shows the largest increase in surface area after the DBT testing with a final area of $30m^2/g$. The surface are is comparable to other values in literature with a few exception of reported high surface area [51][53].

4.3 SEM Images

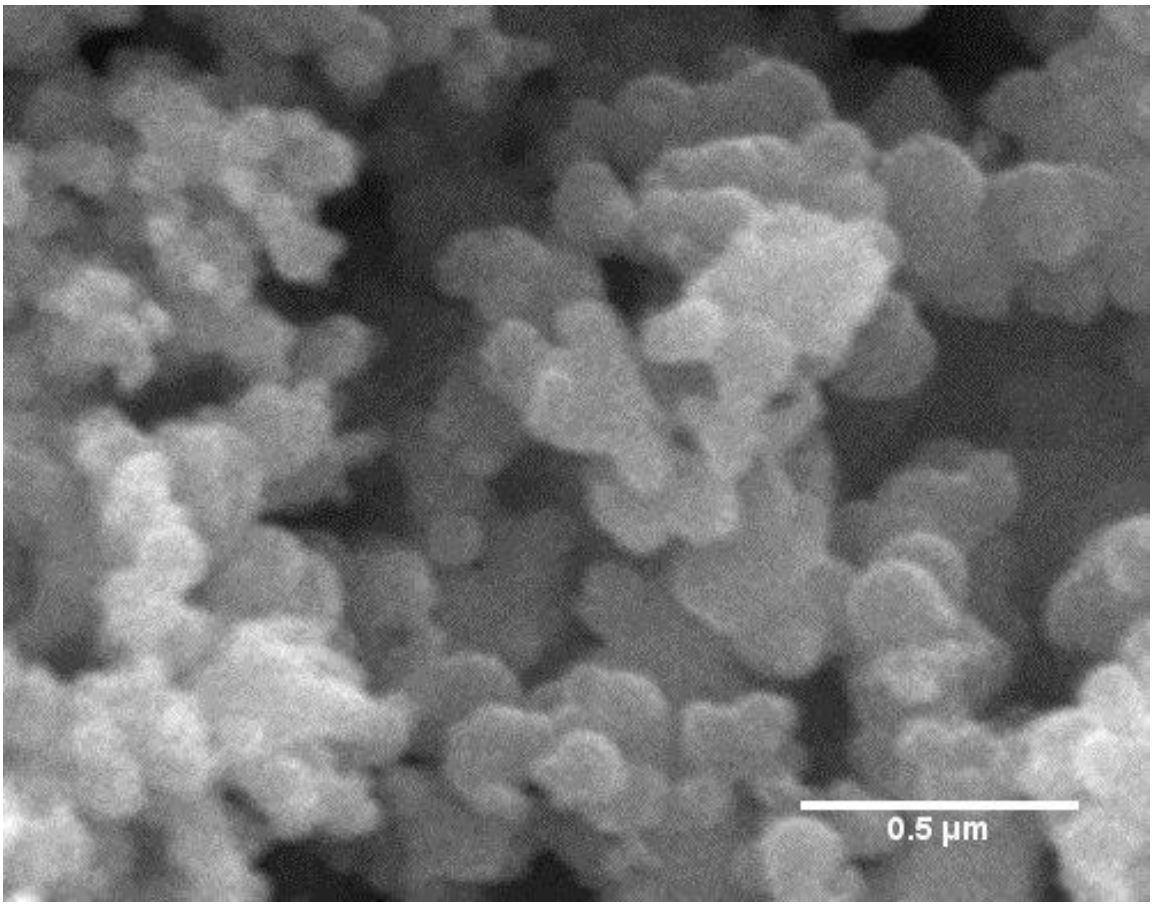

Figure 31: SEM image of fresh U1 catalyst

Fresh U1 (figure 36) catalyst exhibited morphology of spherical particles with an average diameter of 0.15µm. The particles appeared to be agglomerated—note that no treatment other than grinding was used before the images were taken. This morphology is very common in hydrothermal/solvothermal synthesis of unsupported catalysts.

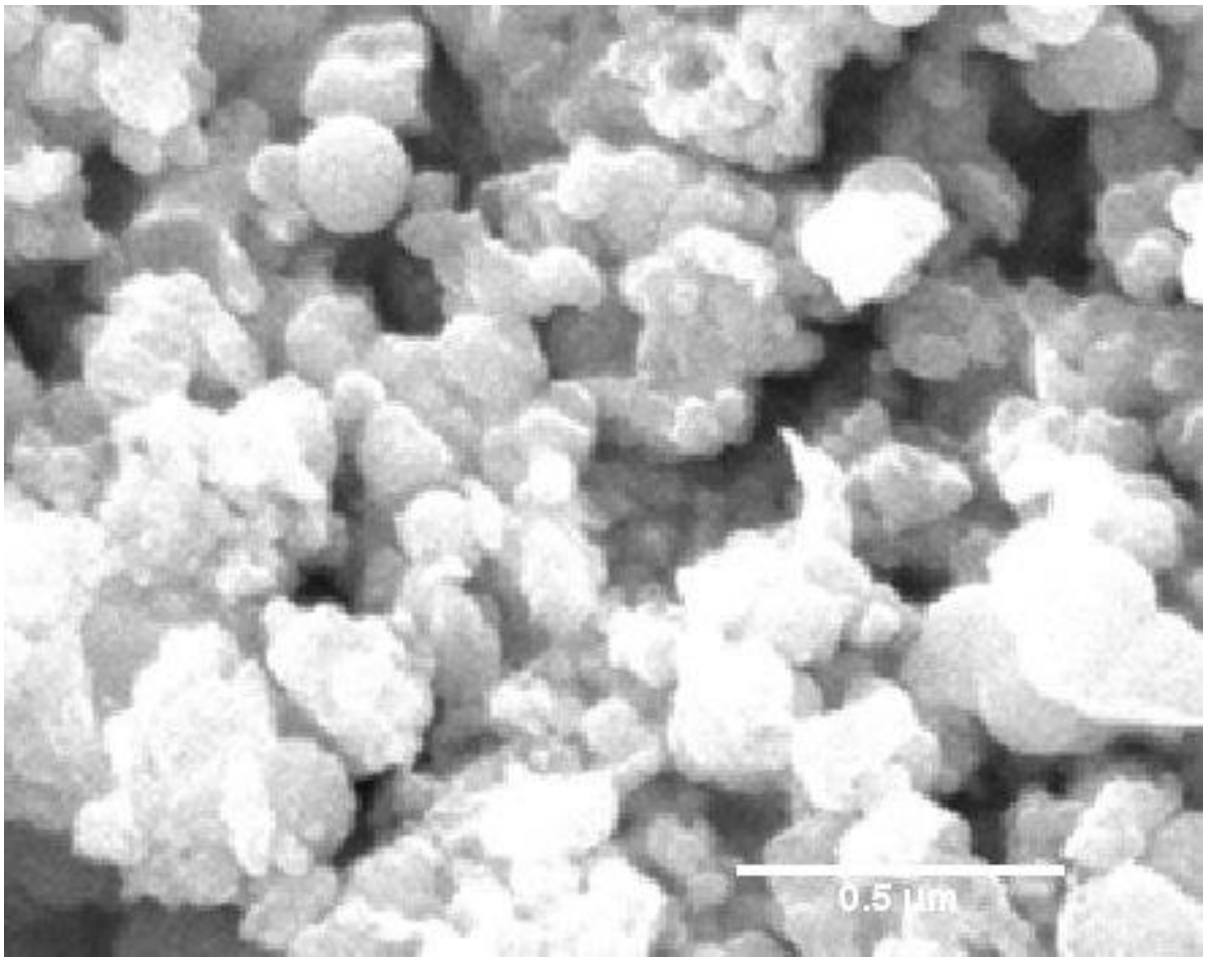

Figure 32: SEM image of U2 fresh catalyst

The particles of U2 (figure37) were spherical but were agglomerated more than U1. The average particle size for this catalyst was also a little higher at 0.25µm. Some of the spheres were a part of larger geometric slabs and can be seen in the lower left area of the micrograph.

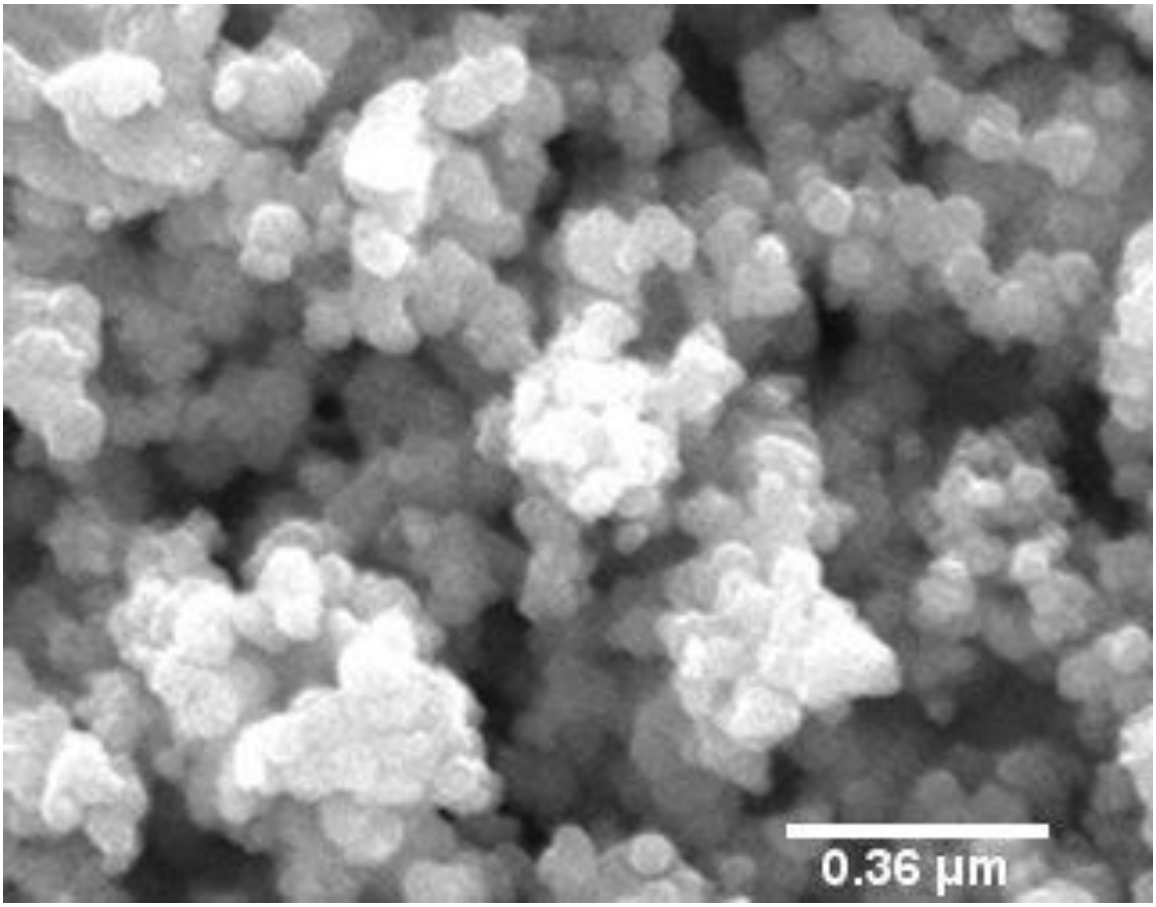

Figure 33: SEM image of U3 fresh catalyst

Figure 38 was taken at 50KX and shows particles less than 0.10µm in diameter in the fresh U3 catalyst. There were no large slabs as in the case of U2. The particles were also not as aggregated as U1, or U2. This morphology could account for the larger surface area compared to the other U-series catalysts. It is important to note that U3 was the catalyst prepared with complete dissolution of sulfur by pouring EDA onto the sulfur and stirring to properly produce the sulfane molecules, which prove to be the enhanced chemical state for sulfur in these reactions.

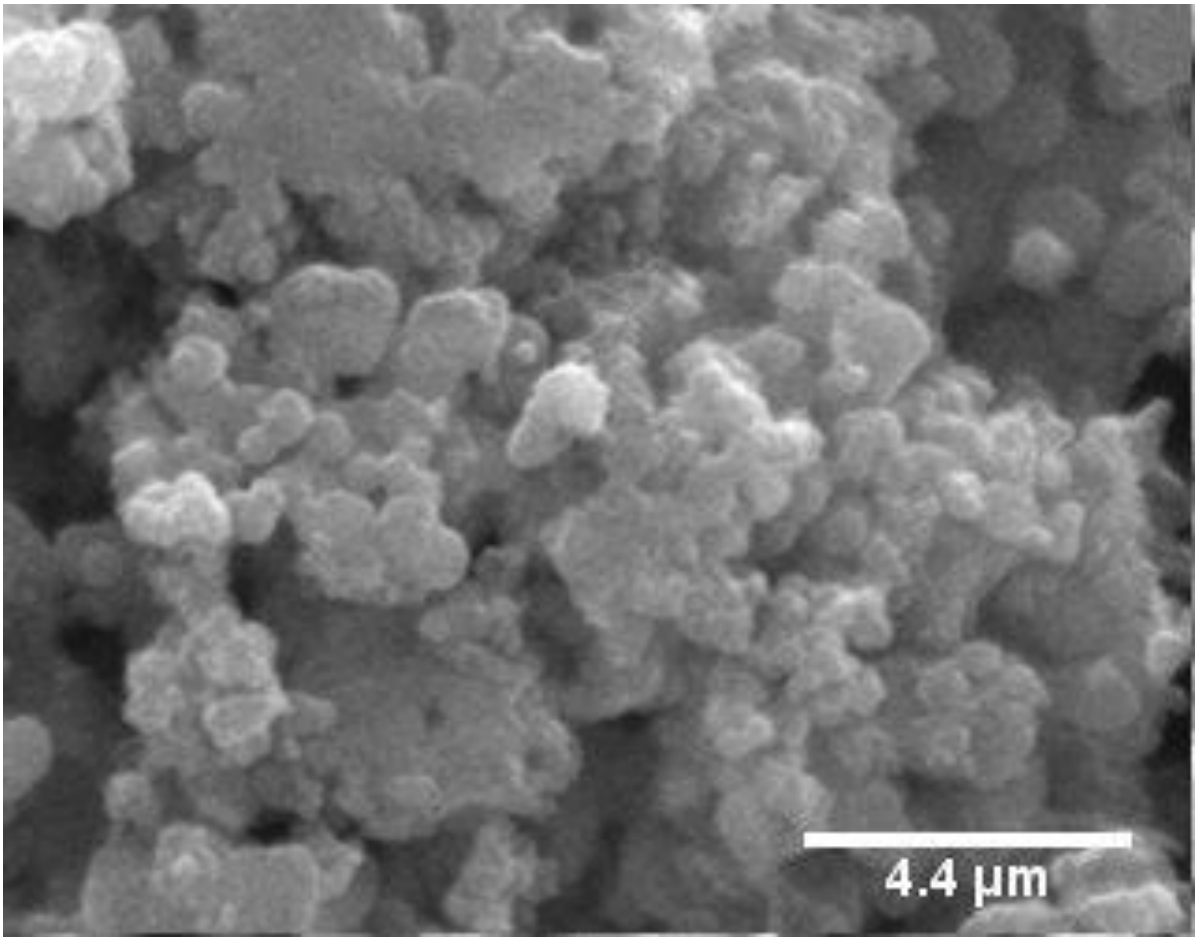

Figure 34: SEM of U4 fresh catalyst

U4 morphology is a mixture of large bulk catalyst slabs decorated with spheres ranging from 0.8µm and 1.5µm. The flakes have appeared before with this synthesis method and might be due to the lack of initial sulfur zero ionization. In the U4 synthesis method, all reagents were mixed together and placed in the reactor. The trends suggest that the ionization of sulfur through EDA is crucial for the proper sulfidation of the molybdenum. Sulfur zero alone will not allow for full sulfidation of the molybdenum oxide without EDA treatment.

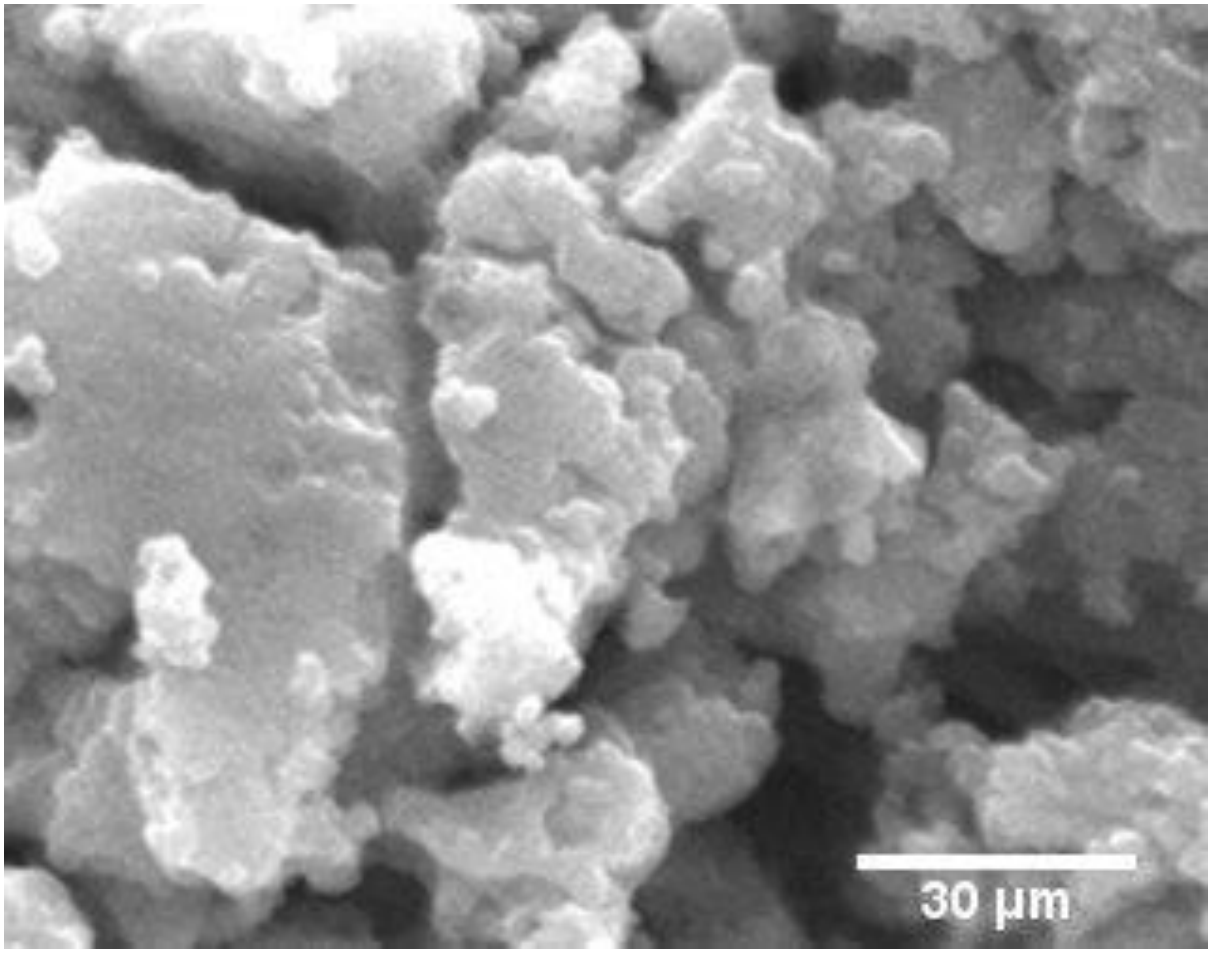

Figure 35: SEM of P1 fresh catalyst

P1 in figure 43, was synthesized with the same method as U3, however the spherical particles are not visible and the catalyst morphology has been replaced with large slabs of catalyst. This would account for the poor surface area and limited increase in surface area during the catalytic testing. In the case of U4 the increase in surface area could be attributed to the spheres separating from the bulk slabs, where in this case there are no such spheres that could free themselves from the bulk.

4.4 STEM Images

4.4.0 STEM Images of Fresh U3

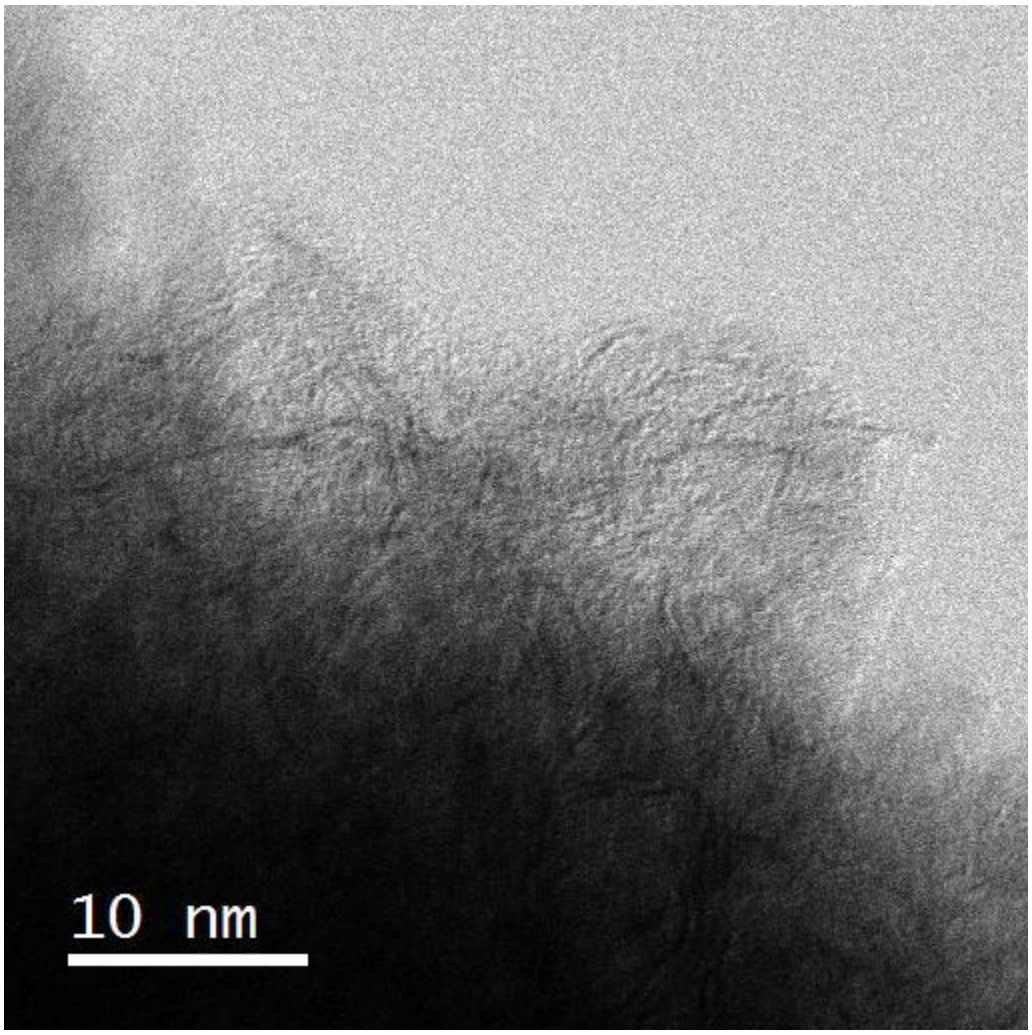

Figure 36: Bright field STEM image of edge of sphere of fresh U3

The image in figure 36 is of U3 fresh and shows single layers almost no stacking at the edge of the spheres. This would suggest that there are more rims than edges in the catalyst. The XRD pattern corroborates the lack of stacking with the absent (002) diffraction reflection. If this is the case, according to Chianelli's Rim/Edge theory, the catalyst is active in DDS as well as HYD.

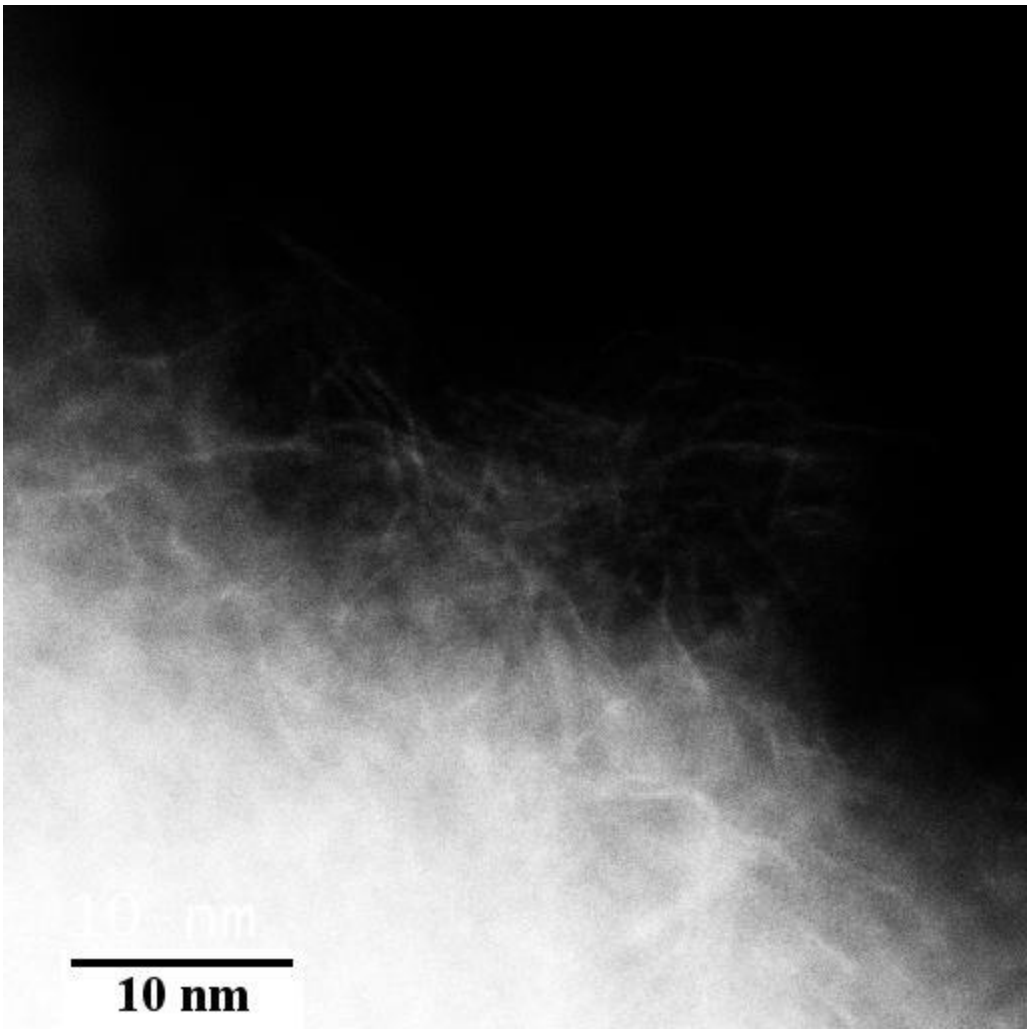

Figure 37: Dark field STEM image of edge of sphere of fresh U3

Dark field image of catalyst edge (figure 36) shows a rag structure with no visible stacking. The structure is analogous to wrinkled fine sheets of fabric or paper. Dr. Russell Chianelli of MRTI coined the term rag structure.

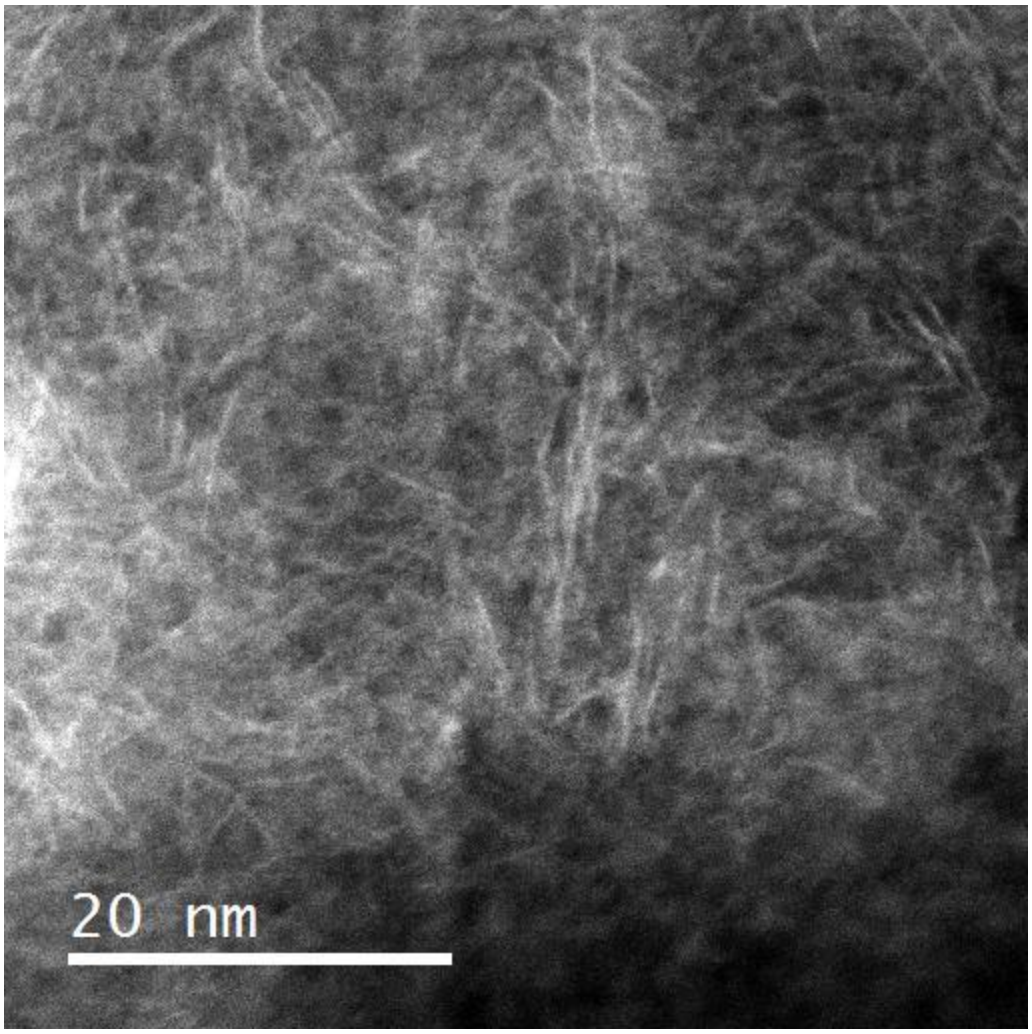

Figure 38: Darkfield STEM image of center of sphere of U3 fresh catalyst

Figure 38 is a dark field image of the center of the same sphere from figure 42. This image shows the rag structure and no observable order or stacking of the material.

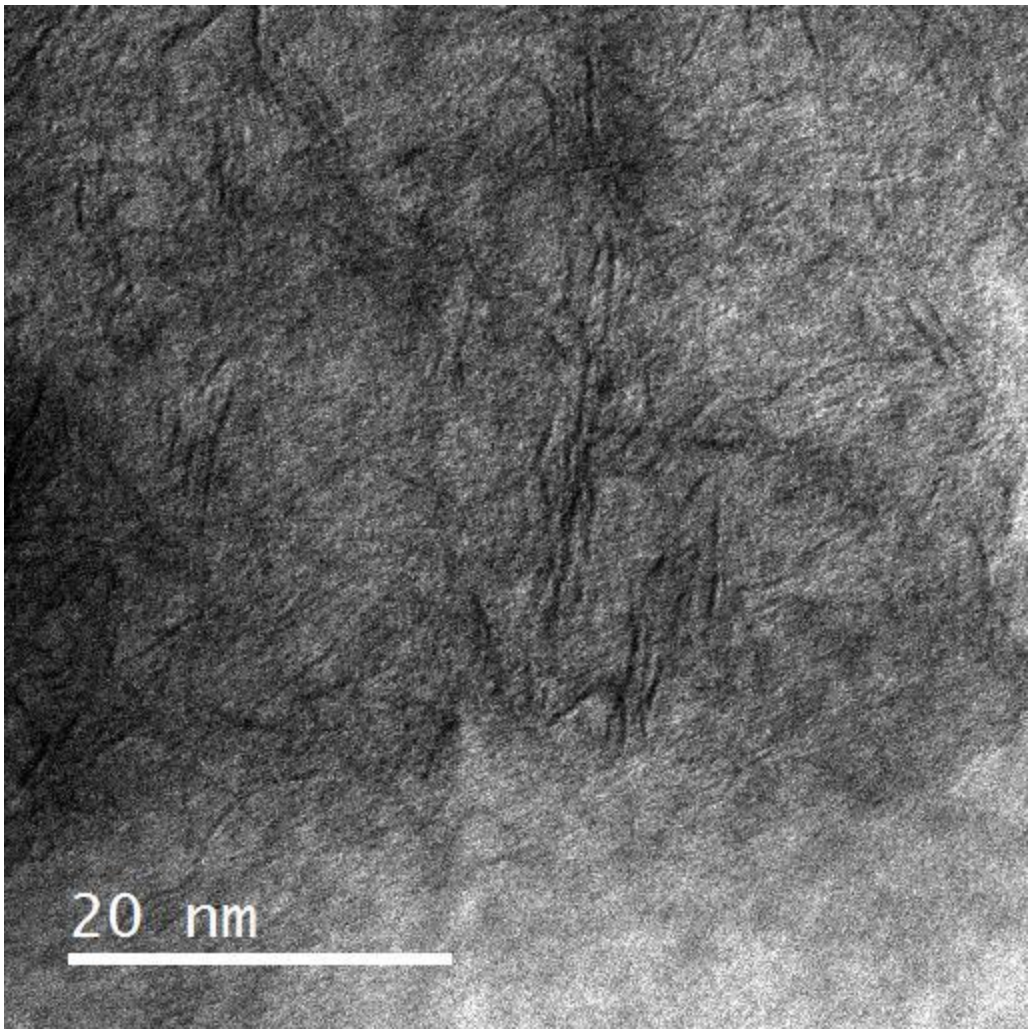

Figure 39: Bright field STEM image of center of sphere of U3 fresh catalyst

Figure 39 is a bright field image of figure 43 and the higher contrast allows us to see mostly single stacks with the exception of the darker lines, which might be double stacks or simply the orientation of the material in 3D. The center of the sphere is denser and the STEM has trouble resolving an image with a surface of varying distance (peaks and valleys). The surface of the spherical particles is not smooth and by morphology alone, one would suggest the material to be of high surfaces area. However the surface area for this material was measured to be very low.

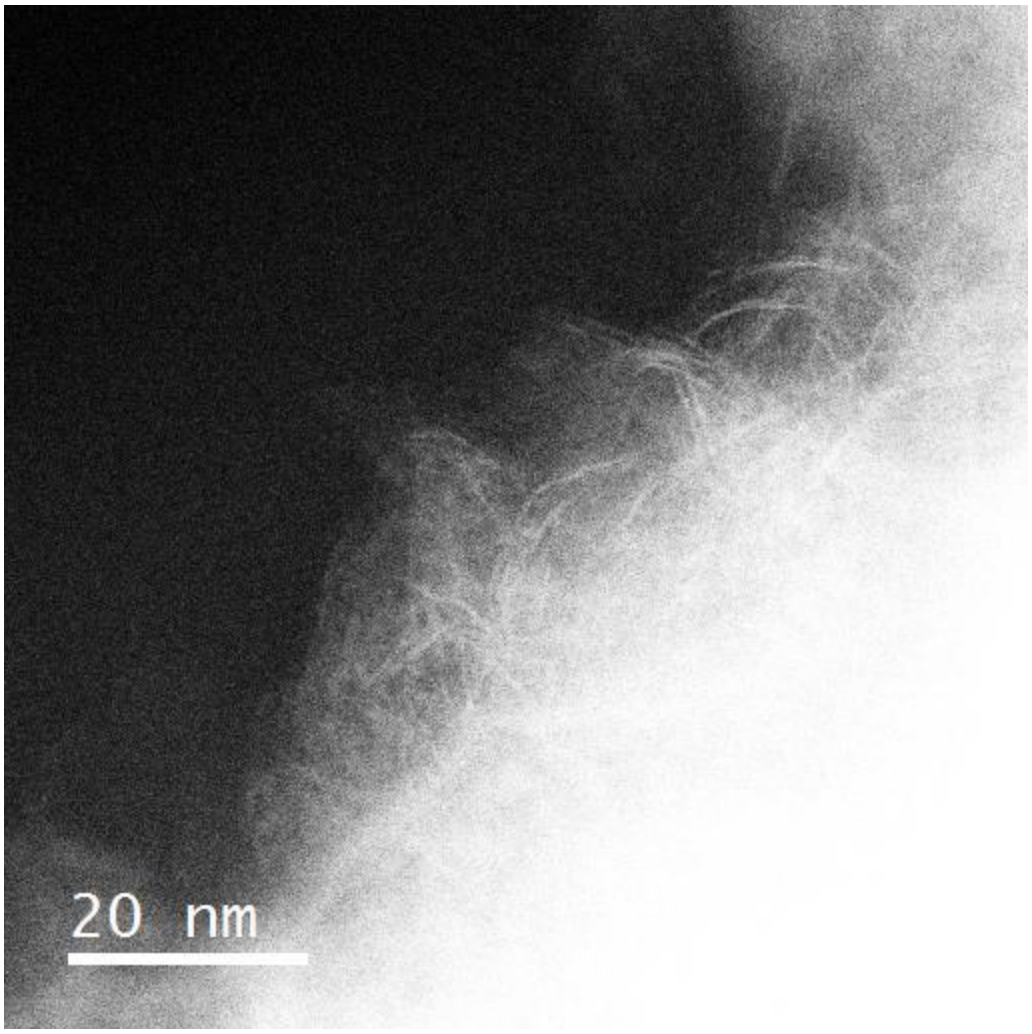

Figure 40: Dark field STEM image of edge of sphere in U3 fresh catalyst

Once again the edge (figure 40) of the particles can be best seen here to display an irregular surface proving difficult for the STEM to resolve at such high magnifications between relative near and far material.

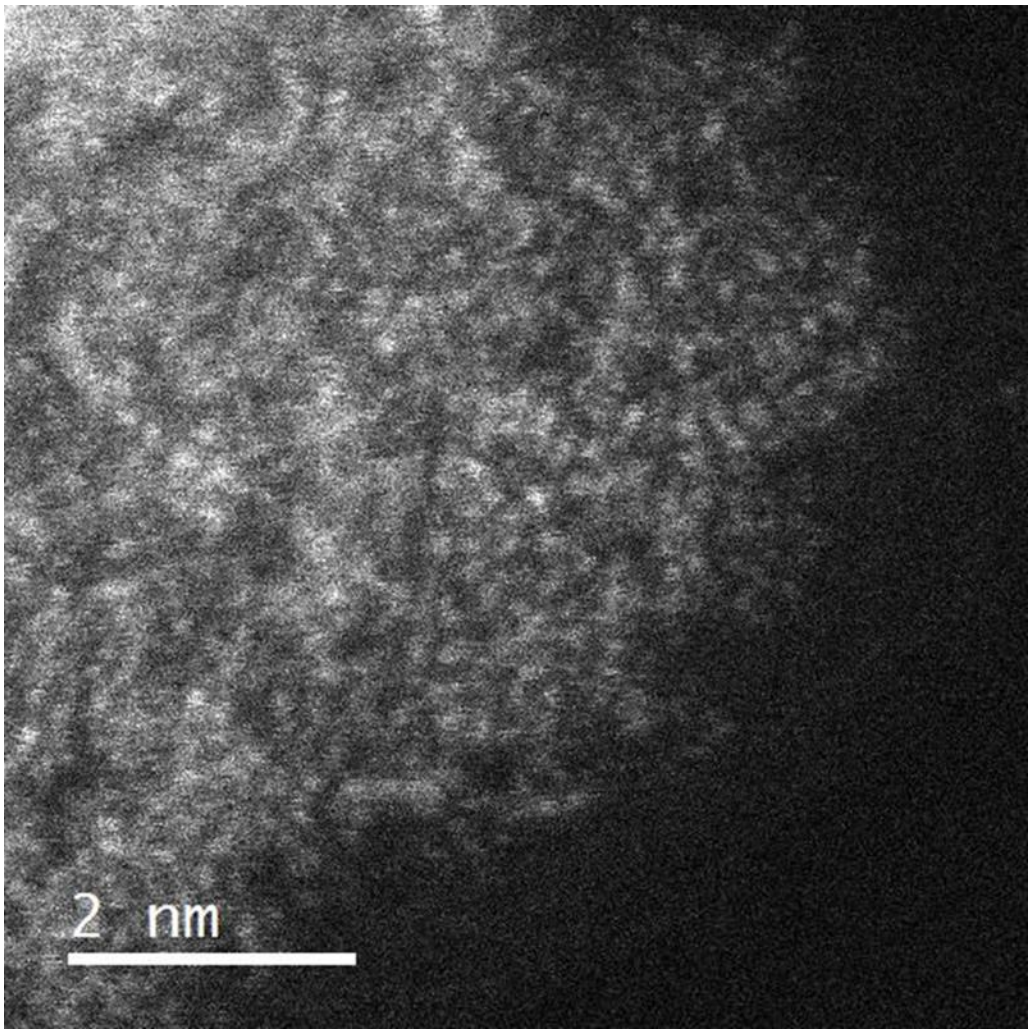

Figure 41: Dark field STEM image of fresh P1 catalyst

STEM images were difficult to obtain with the Porocel (P1) fresh catalyst. Figure 41 shows the edge of a slab of P1 and the dendritic wire like features that were visible in U3 are not present. Moreover, the bright field image did not show any recognizable features. This was the best STEM image we were able to attain. This sample was synthesized, washed, filtered and dried in Canada. The difficulty in obtaining images could be attributed to remaining carbonaceous impurities or crystallized solvent from the synthesis on the surface. No contaminants however, were observed in XRD or EDS analysis.

4.4.1 STEM IMAGES OF SPENT U3 AND P1

STEM images in both bright and dark field were obtained for U3 spent only. At the time of STEM analysis, the catalytic testing of P1 had not yet been conducted.

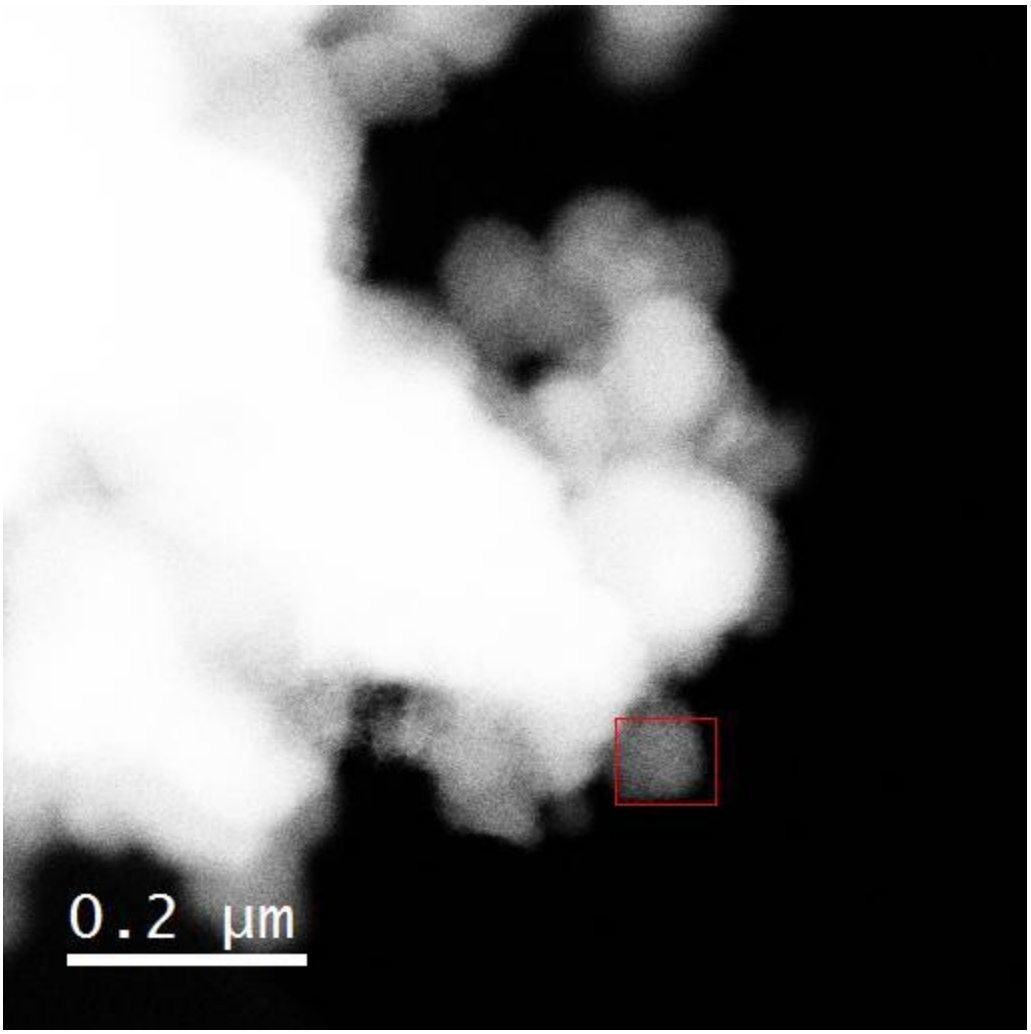

Figure 42: Dark field image of spent U3 catalyst focused a sphere (point of interest)

Images of the spent U3 catalyst were taken to see if any observable morphological change took place. The surface area was evaluated to have increased six fold—it was of interest to attempt

to correlate the morphology to surface area increase. A sphere was chosen as the point of study and is illustrated in figure 42.

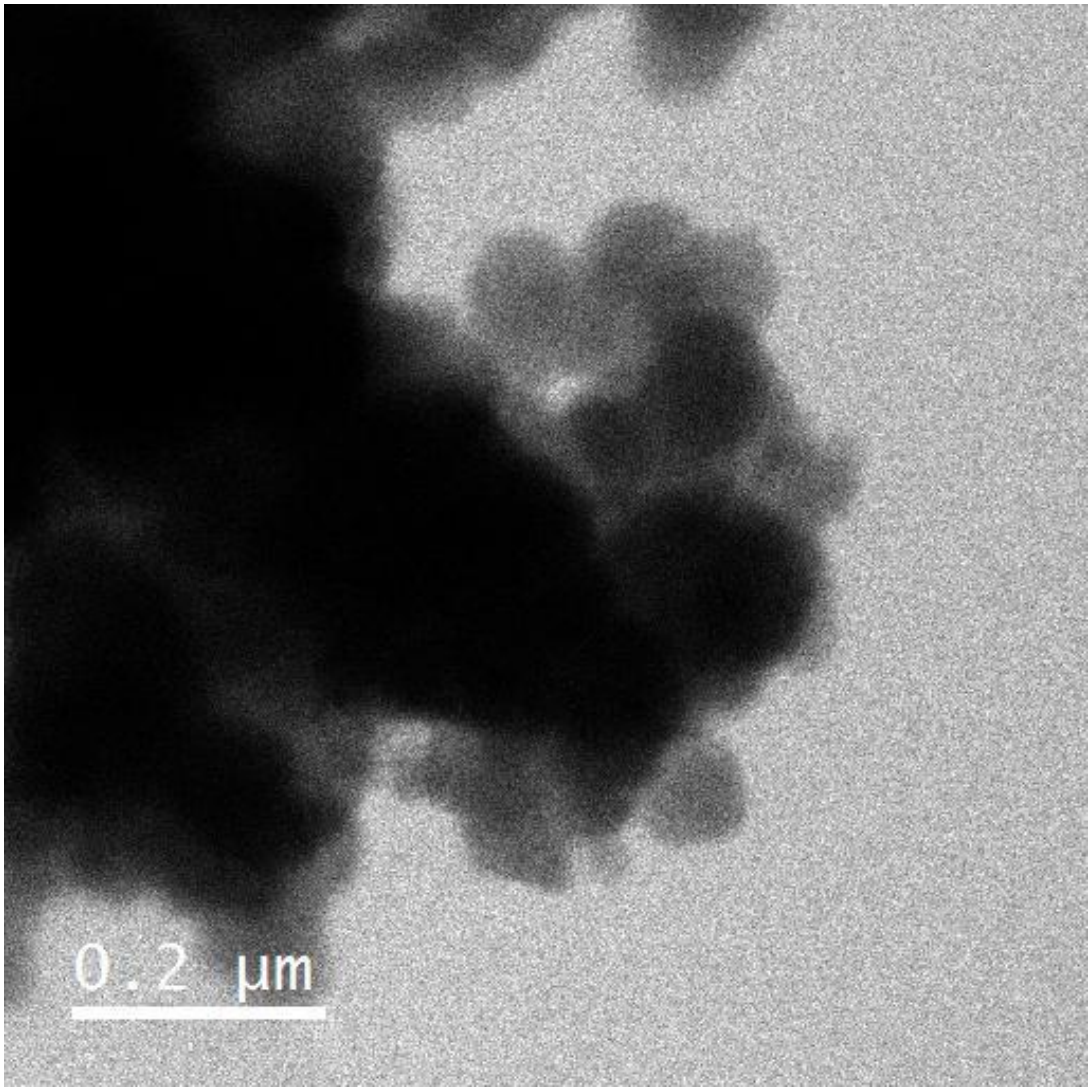

Figure 43: Bright field image of spent U3 catalyst focused a sphere (point of interest)

Figure 47 shows the same sphere as figure 42 with dark field perspective. The next focus was to investigate the edge of that sphere.

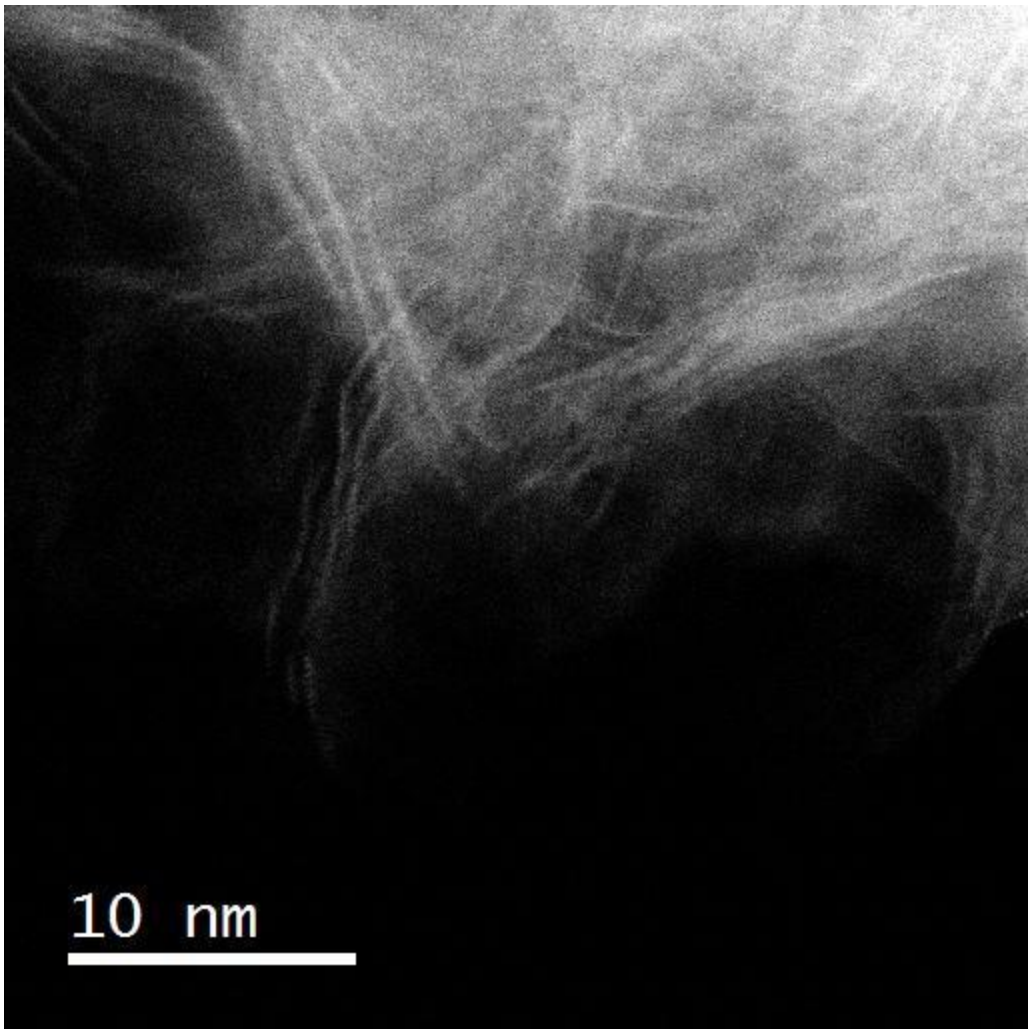

Figure 44: Dark field STEM image of U3 spent catalyst at the edge of point of interest (sphere)

There is little observable difference in the dark field STEM image (figure 44) of spent and fresh U3 (figure 45) on the edges of the spheres. There appears to be no stacking in the bright field images, nor does there appear to be an observable morphological change to account for the increase in surface area reported by the BET results.

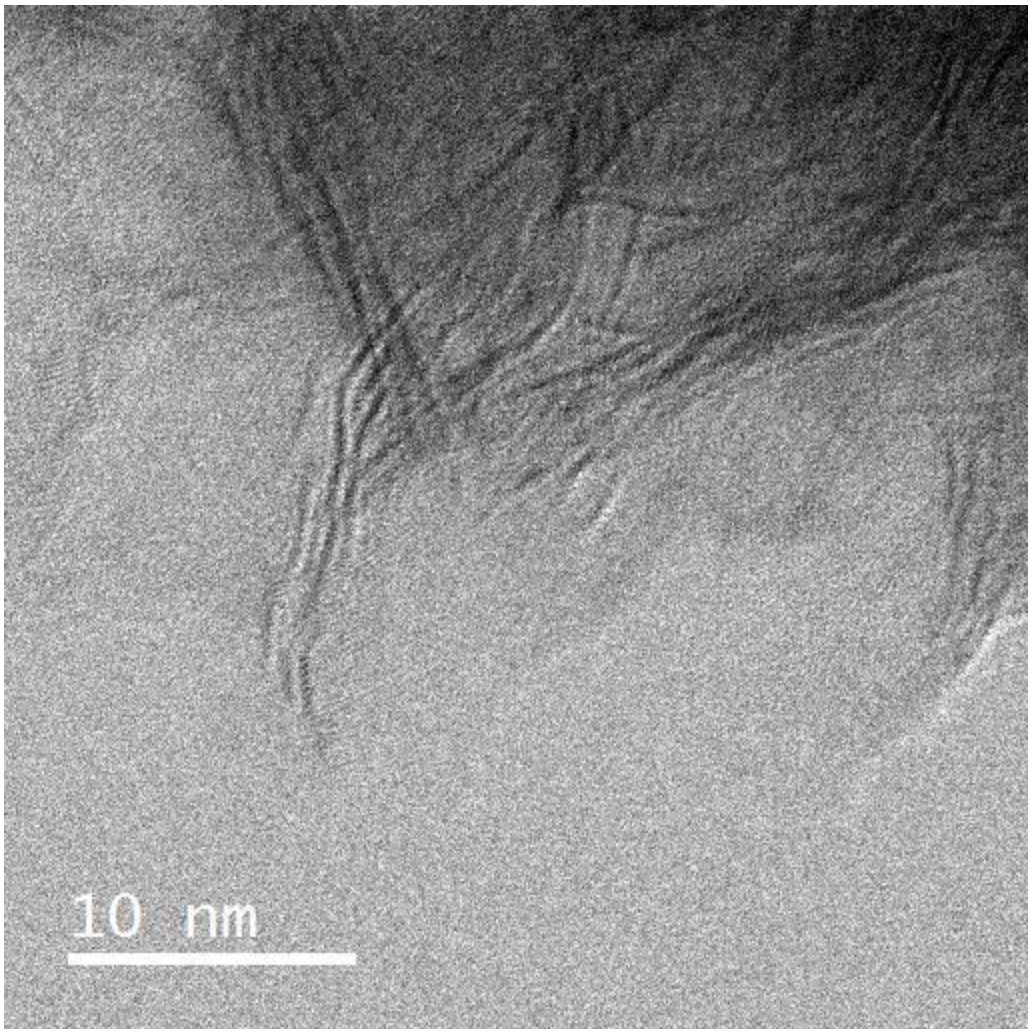

Figure 45: Bright field STEM image of U3 spent catalyst at the edge of point of interest (sphere)

The bright field image of figure 44 (figure 45) shows more contrast on the wire like structures at the edge of the sphere. Darker object in bright field are denser or comprised of more material than the surrounding material. It is difficult to ascertain whether this is attributed to stacking or simply orientation of the sheet like material.

4.5 Energy Dispersive Spectroscopy (EDS Mapping) Elemental Analysis

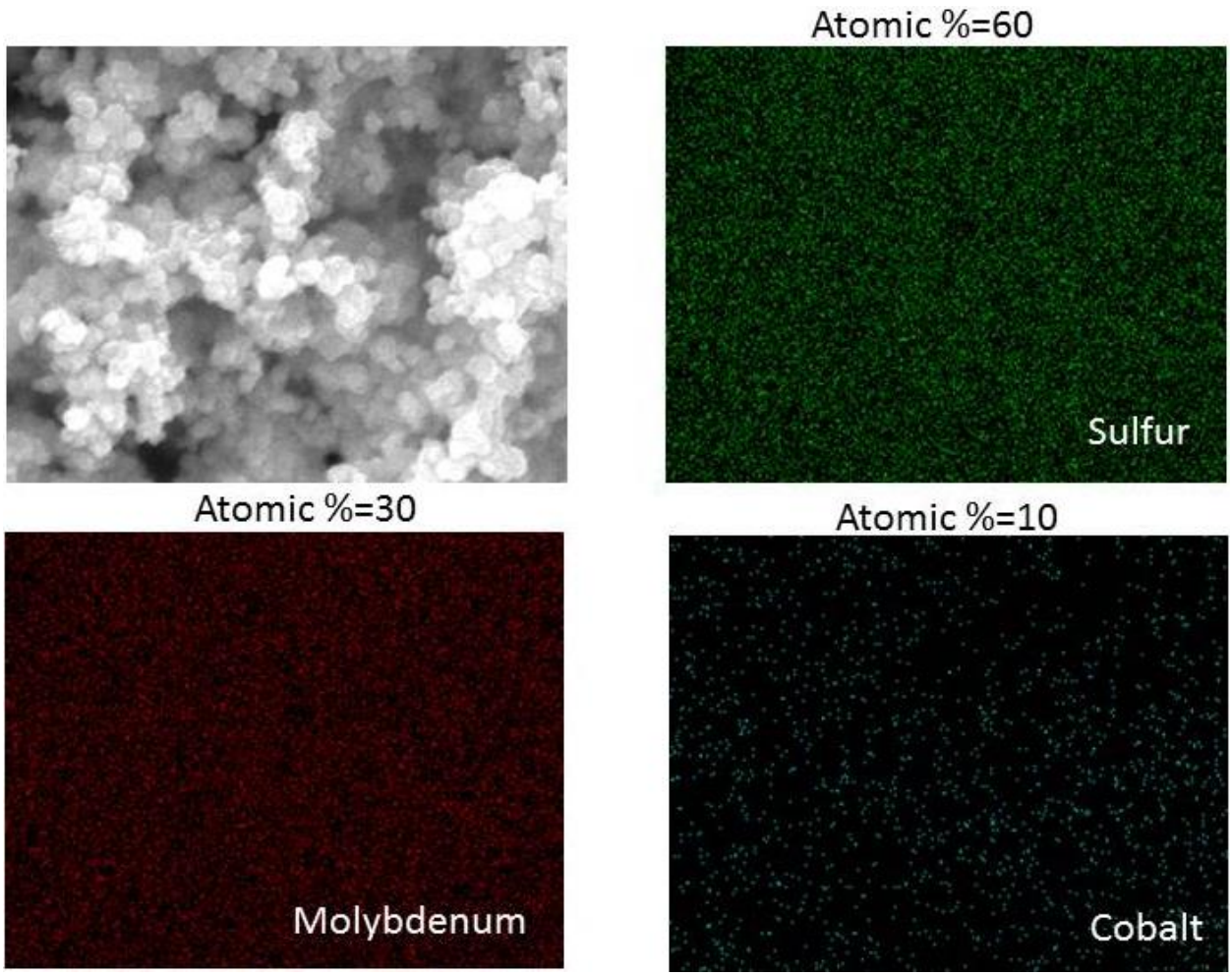

Figure 46: EDS mapping of U3 spent

EDS mapping shows good dispersion of metals and sulfur. Mapping and atomic ratios for U3 and P1 are shown in Figures 46 and 47, respectively. The green dots are represented by sulfur, red by Mo, and blue by Co. The mapping for all other catalysts is attached in the appendix and a table is listed here with their mole ratios.

Table 4: Metal loading ratios as represented by EDS

Sample	Mo:Co	S:M
U1	3:1	3:2
U2	3:1	3:2
U3	3:1	3:2
U4	3:1	3:2
P1	5:1	5:3
TK-578 BRIM	5:2	1:1

Table 4 is tabulated data for the EDS measurements outlining metal loadings. Samples U1-U4 all exhibited the same Mo:Co ratio which corroborates with the synthesis method where 3 mol of Mo to 1 mol of Co were used. The only difference was the catalyst produced by Porocel. There was an observable loss in Co, possibly due to heating uniformity issues in the larger reactor. Because of the drop of Co amount the Sulfur amount went up from a 3:2 to 5:3 S to metal ratio. The Tk-578 BRIM was noted as having a different loading but is in accordance with range of metal loading. The have more cobalt, so more sulfur is taken up by the Co_9S_8 phase in thusly reducing their sulfur to metal ratio.

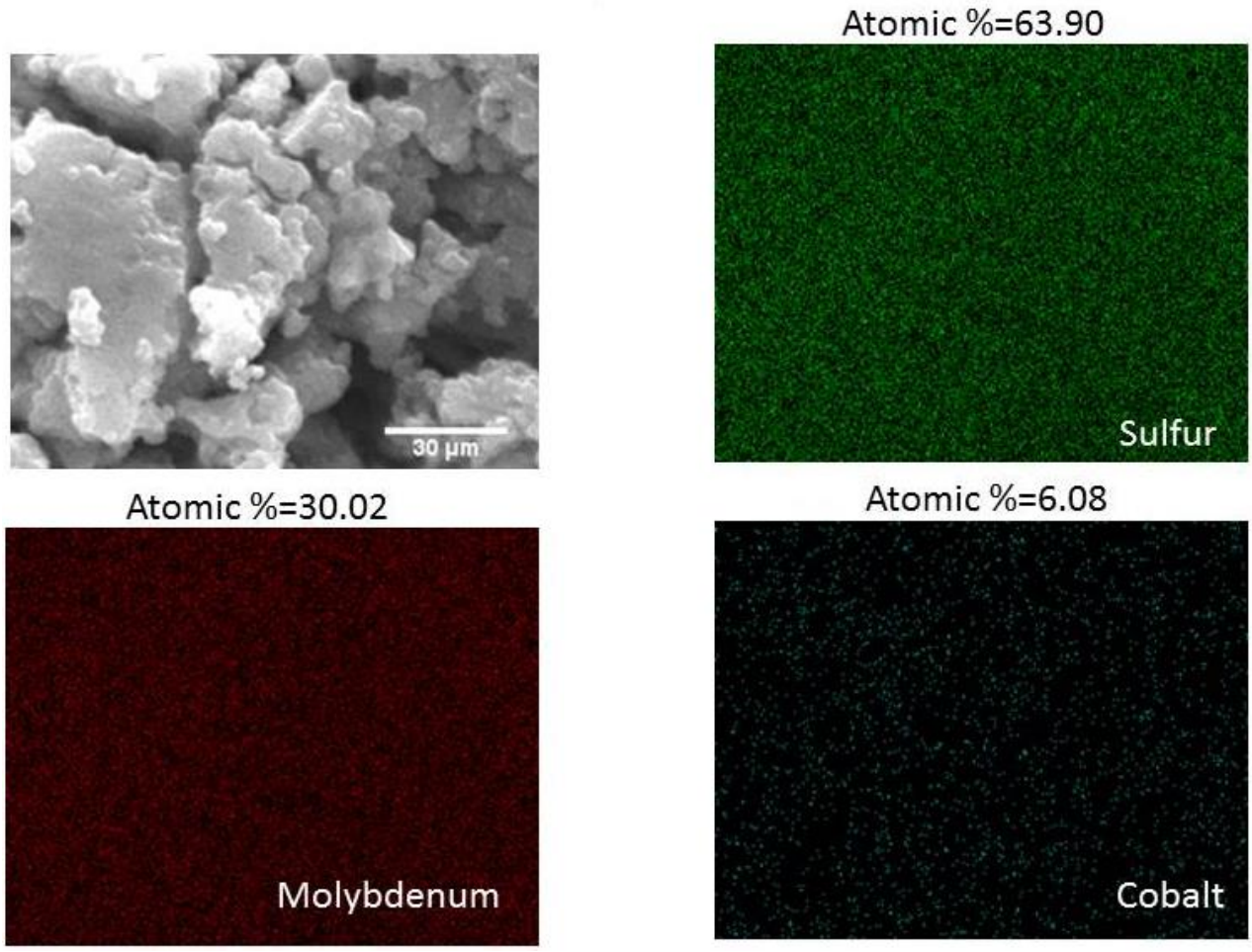

Figure 47: EDS mapping of P1

EDS mapping of P1 shows very good dispersion amongst the sulfur and metals in Figure 46. Even though the super structure was not spheres but consisted of large plates or slabs, the metals and sulfur were very well dispersed. This is one of the advantages of solvothermal synthesis. This is not always the case with impregnation techniques as pH and stirring of the materials has to be optimal for correct loading and at times the procedure has to be reproduced wasting time and money.

4.6 GCMS Analysis of DBT Test

Chromatograms taken for every sample pulled at 30 minutes during the test are the basis for our activity measurements. The area underneath the curve of the peak for DBT is directly correlated to DBT concentration. The rate of the disappearance of DBT was tracked and plotted over time for rate determination. Below in Figure 48 a chromatogram taken at t=0 was taken during the testing of TK-578 BRIM. The retention time is annotated as well as the abbreviated form of chemical responsible for the signal.

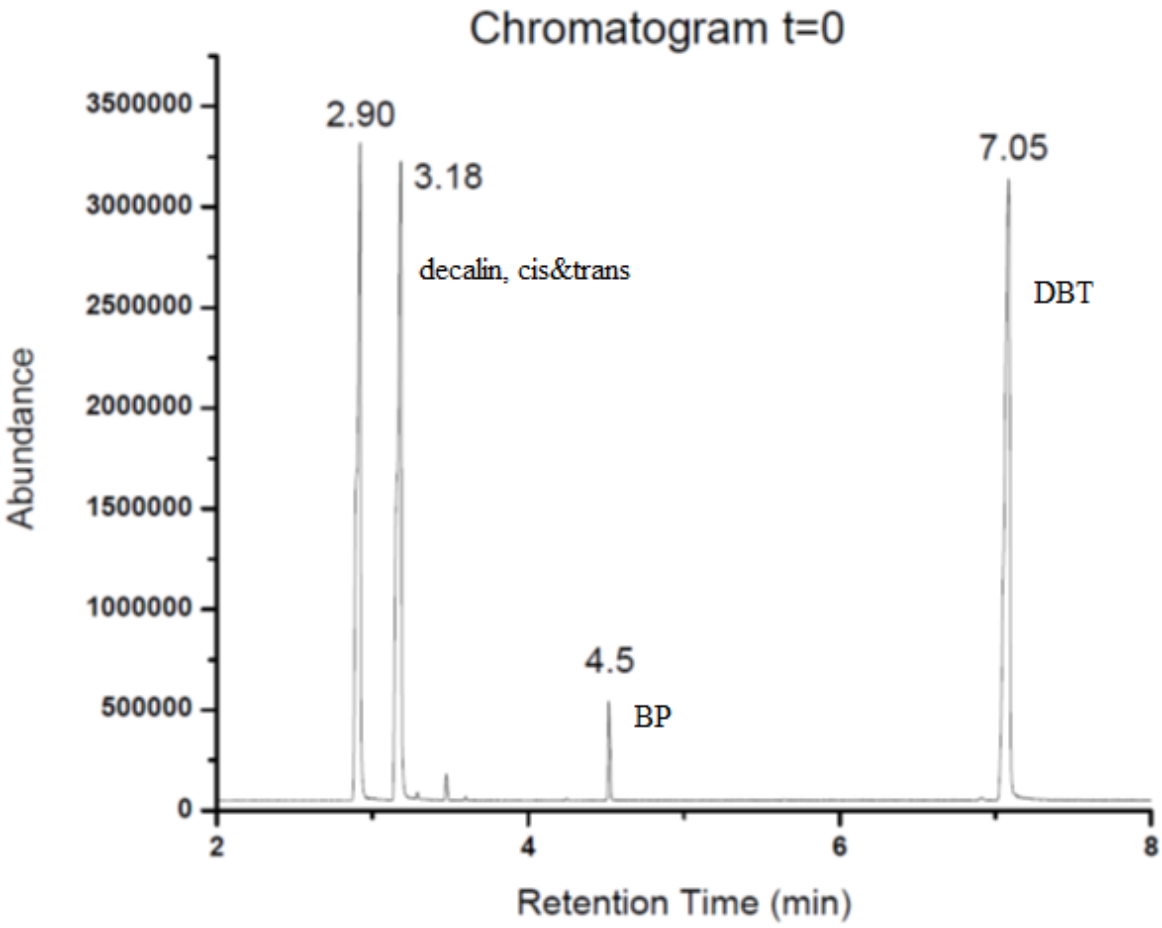

Figure 48: Chromatogram of DBT test at t=0

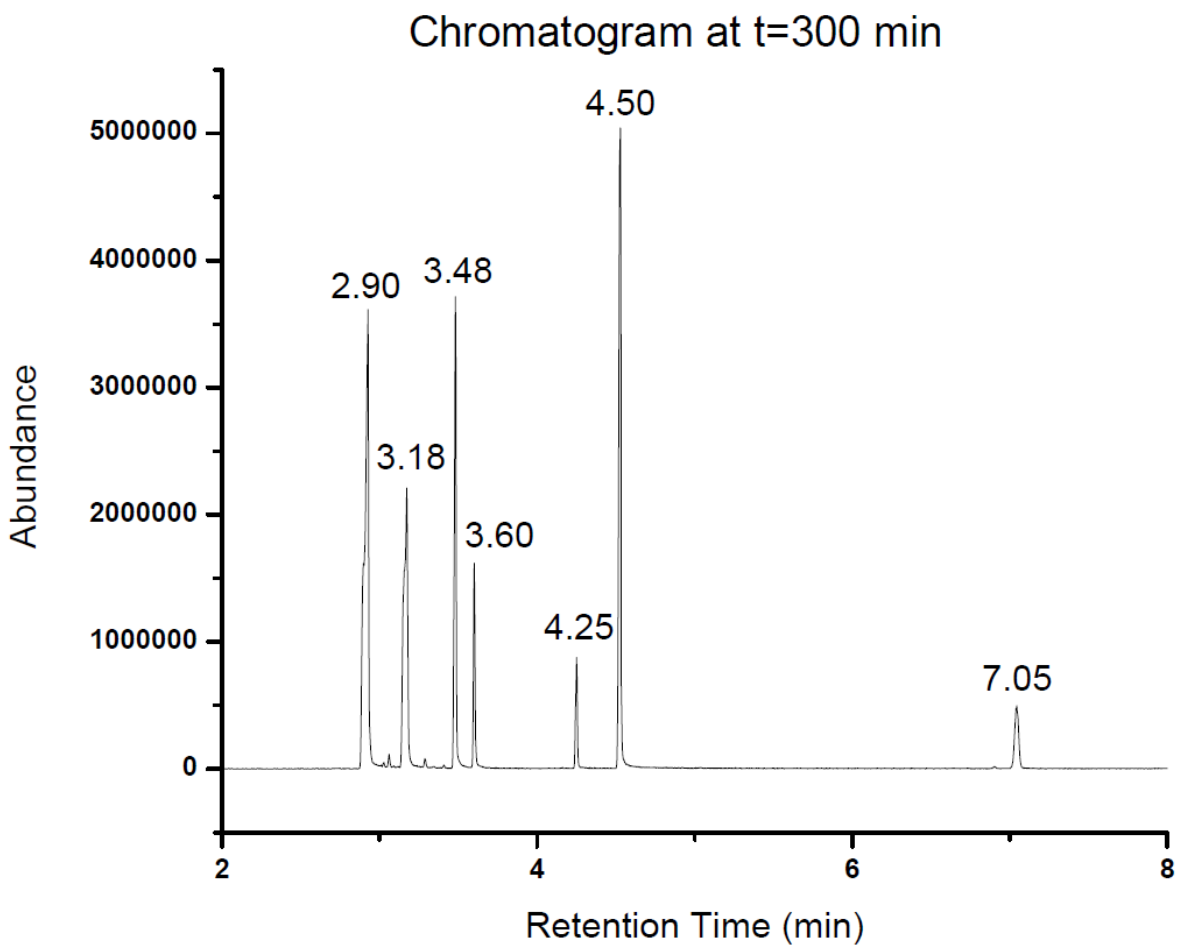

Figure 49: Chromatogram of DBT test at t=300

The chromatogram above in Figure 49 is representative of a typical catalytic run at 300 minutes (the end of testing). The retention times are annotated and the molecules responsible for each signal is tabulated in Table 5. The table has the word product, however that is a misnomer. The only real products are cyclohexylbenzene and biphenyl.

Table 5: Table showing products to their respective peaks on figure 48

Product	Min
Cis-Decalin	2.90
Trans-Decalin	3.18
1,2,3,4-Tetra-hydronaphthalene	3.48
Naphthalene	3.60
Cyclohexylbenzene	4.25
Biphenyl	4.50
Dibenzothiophene	7.05

The mass spectras for all these peaks are in the appendix. The only one listed here is the DBT mass spectra shown in Figure 50. The mass spectra shows the mass peak of DBT at 185 along with the rest of the fragmentation pattern above 100m/z. The mass spectras were evaluated with the NIST 2008 database and were matches with 99% accuracy. In the testing of U3, there was not enough peak or area after 250 minutes to integrate so the last point obtained was at 210 minutes.

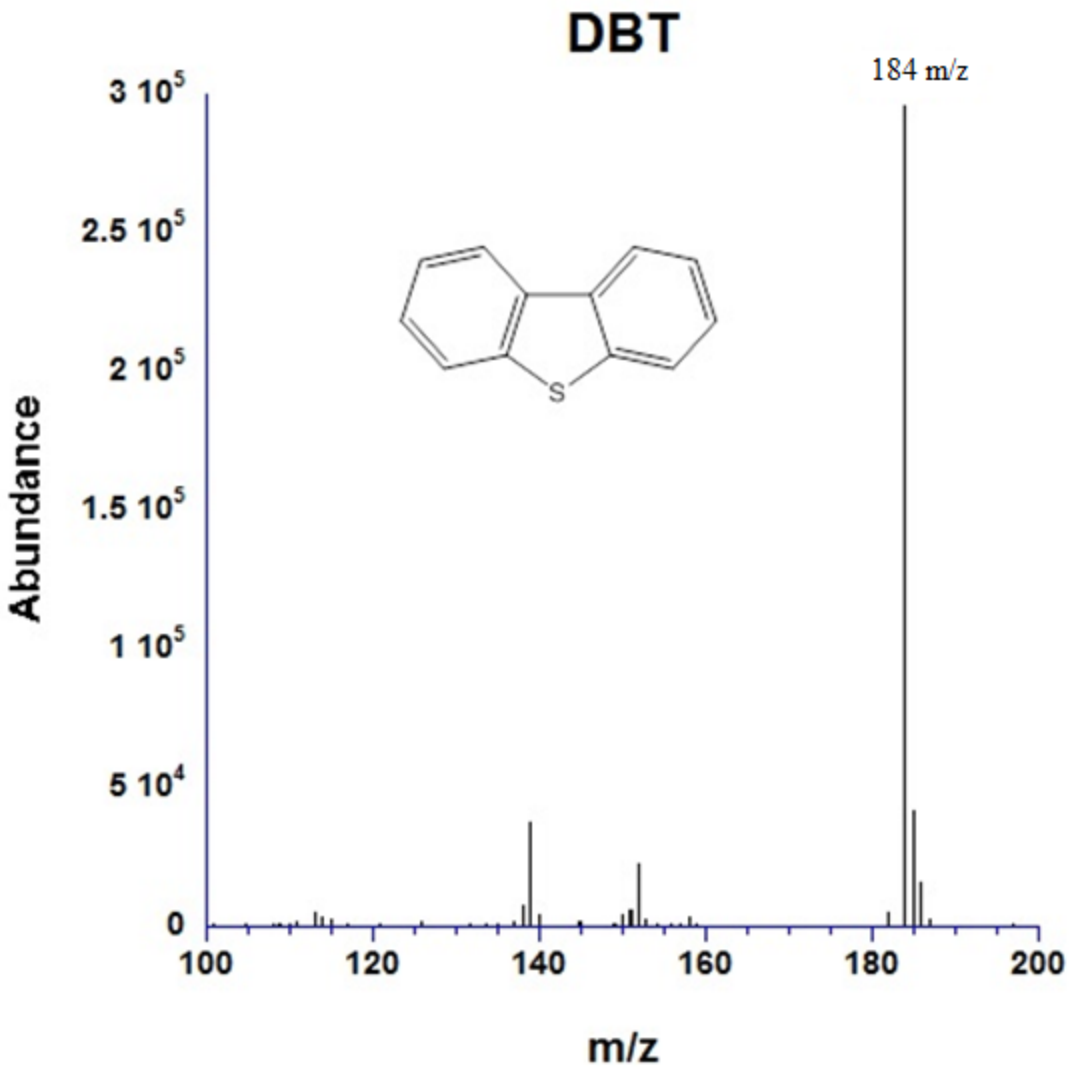

Figure 50: Mass Spectra of DBT

Catalytic Rate Evaluation and Discussion

The reproducible effect of the U-Series catalyst is observed when plotting the DBT decay in first order reaction fashion. As can be seen by all U-series kinetic plots, the test has been broken into two sections. The first section is at the first 90 minutes of testing. The catalytic rate changes after that and a steady rate is obtained suggesting catalyst stabilization occurs after the first 90 min. In Figure 51, the catalyst seems to line out at y=17.5 after 90 min, but then increases after 120 minutes.

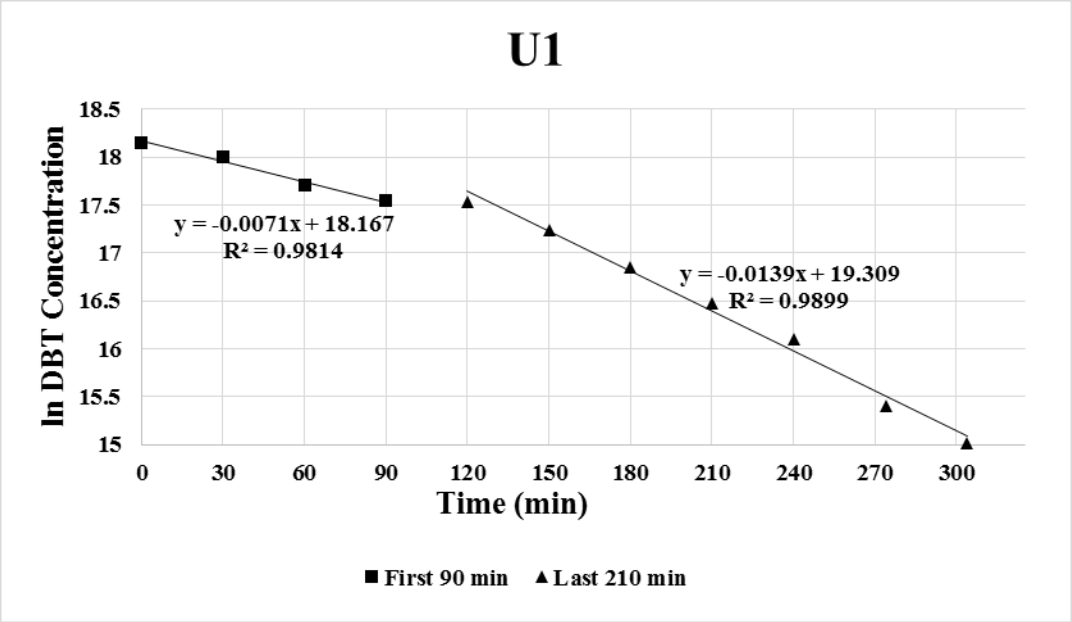

Figure 51: Kinetic plot of U1

This is because the catalyst (U-series) is synthesized at lower temperatures relative to the testing conditions unlike the BRIM catalyst, which is calcined after impregnation. The catalyst appears to be cooking still and finally stabilizes in situ. The U-series catalysts are amorphous and tend to open up in feed conditions to stabilize in optimum conditions. The surface area was also shown to increase, suggesting either the surface is reoriented in the testing conditions or it is breaking apart into smaller particles. However, the SEM or STEM data did not show smaller particles after

the DBT tests. It is important to know what the stabilized version of the catalyst is for enhancement and development of better catalysts. The kinetic plots for U2-U4, P1 and TK-578 are listed below in Figures 52-56.

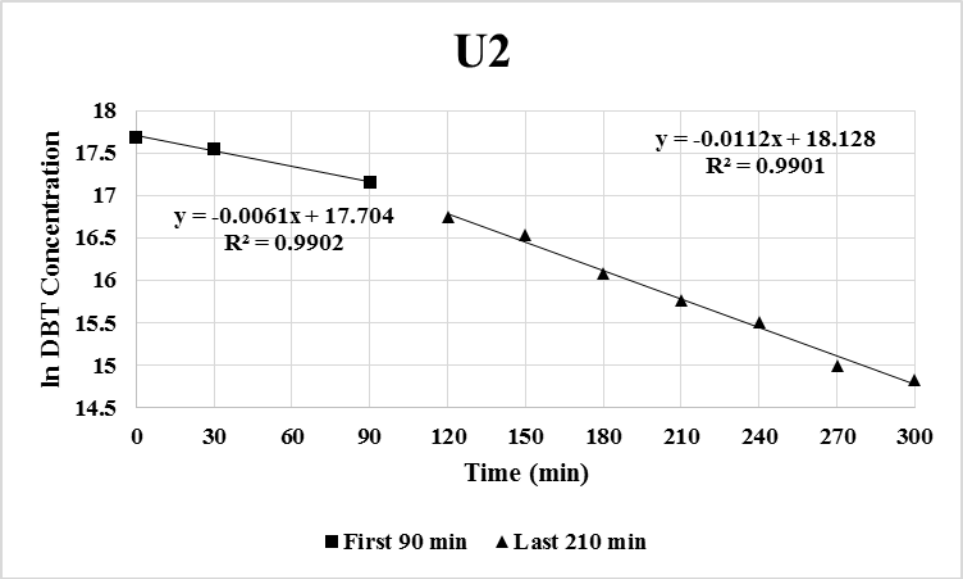

Figure 52: Kinetic plot of U2

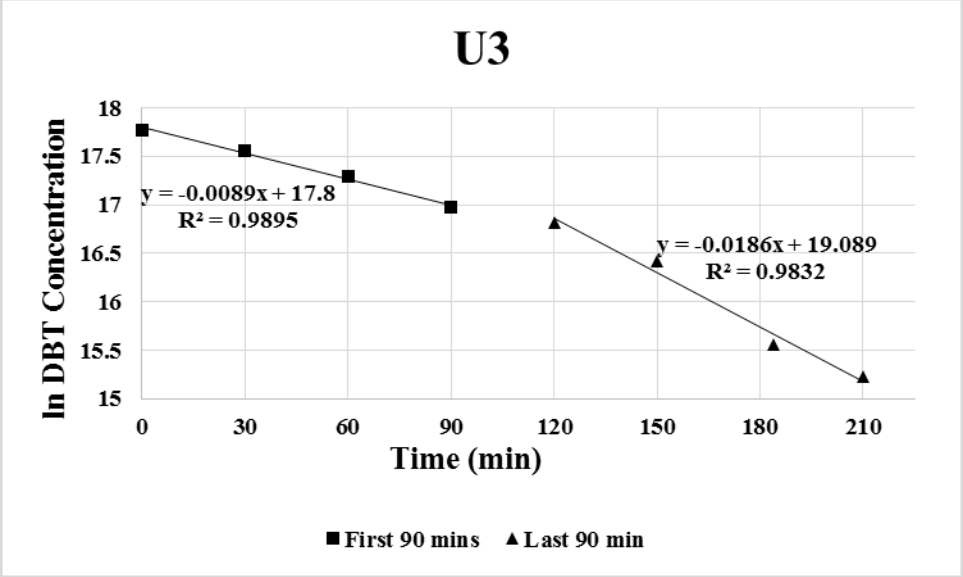

Figure 53: Kinetic plot of U3

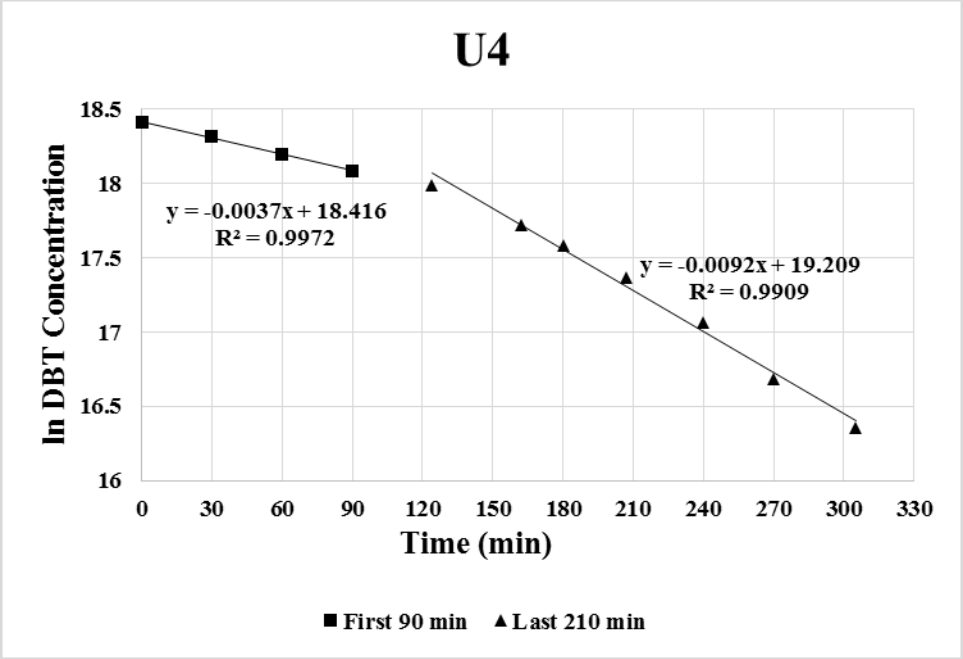

Figure 54: Kinetic plot of U4

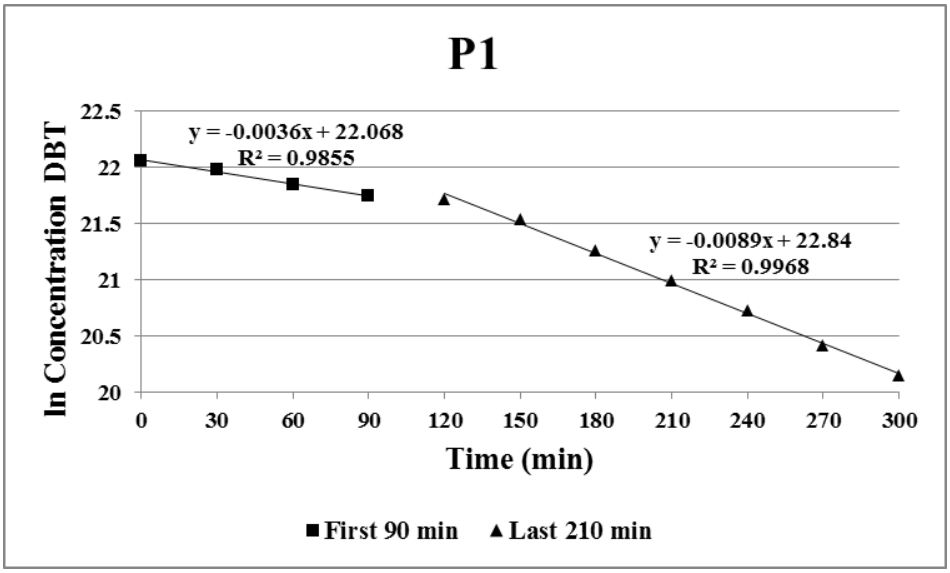

Figure 55: Kinetic plot of P1

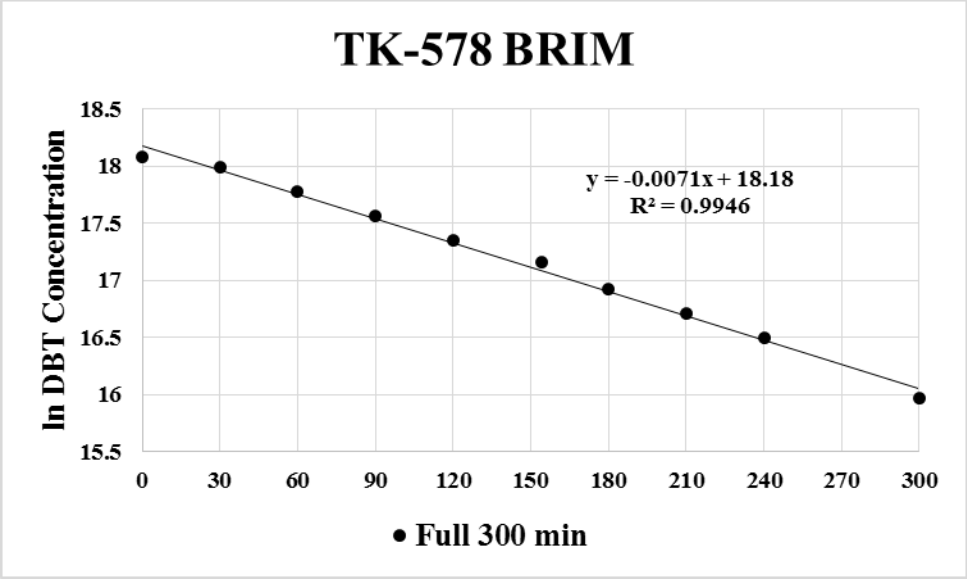

Figure 56: Kinetic plot of TK-578 BRIM

Notice Figure 56, the correlation factor is .99 for the data points plotted in first order fashion. The activity is tabulated in Table 6 and the first 90 minutes and last 210 minutes are listed for the U-series and P1 catalyst. The rates are fairly close with the exception of U4 and P1 with a slower rate than most initially. Their second half rates appear to match the first half rates of the other U-series catalysts suggesting that they might require more time to line up or stabilize. This could be to the heating issues for the larger reactor in Canada for P1. For U4, mixing all the reagents at the same time is not as good as ionizing the sulfur first. The EDA should be poured onto the sulfur and stirred to allow cleavage of the sulfur ring and ionization. The formation of sulfanes is integral to the sulfidation of MoO_3 under the suggested solvothermal conditions, i.e. relative low temperature. The data shows that catalyst activation or sulfidation can occur in a live feed however, if one looks back at the chromatogram, this catalyst is very good at hydrogenation.

Table 6: Data for calculating the rate per area of catalyst

	DBT (g/mol)	DBT mass (g)	DBT (mol)	Surface Area m^2/g first 90 min	Surface Area m^2/g last 210 min	mass of catalyst (g)	Total area (m^2)
U1	184	3.5	0.019	5	10	0.5	2.5
U2	184	3.5	0.019	8	14	0.5	4
U3	184	3.5	0.019	5	30	0.5	2.5
U4	184	3.5	0.019	3	8	0.5	1.5
P1	184	3.5	0.019	6	8	0.5	3
TK-578 BRIM	184	3.5	0.019	150	150	0.5	75

Table 6 shows all the data for the calculations involved in the rate determination. BRIM catalyst has much surface area and the others vary as well. In an attempt to remove such factors such as surface area on catalytic rate, we included the area in the conversion of DBT moles per second. Total area was tabulated but not needed for the calculations.

Table 7: Percent of Dibenzothiophene Remaining After 300 Minutes

% DBT Remaining	
TK-578 BRIM	12
U1	4
U2	6
U3	0
U4	13
P1	15

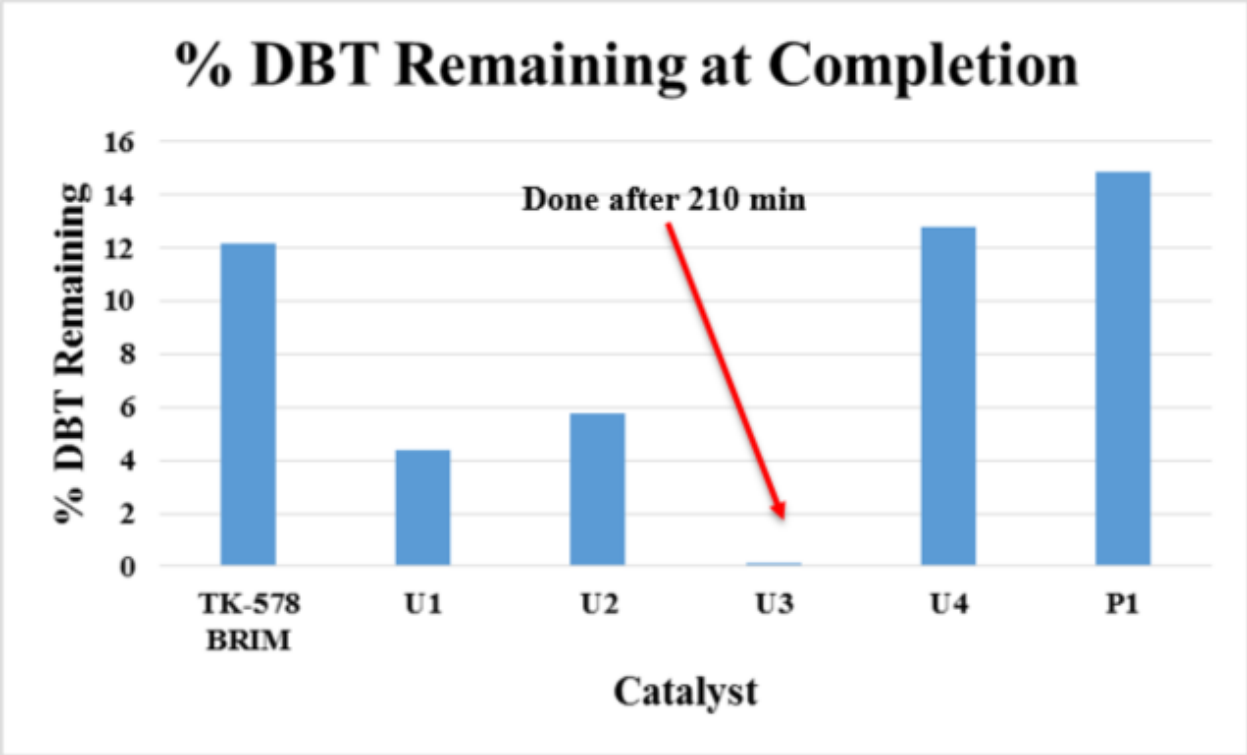

Figure 57: Bar Graph Illustrating Results of DBT Test

Figure 57 shows the remaining DBT after five hours. U3 was the only catalyst to convert all DBT in under 300 minutes.

Table 8: Calculated rate per area of catalyst for first 90 minutes and last 210 minutes

	First 90 min rate (k) s^{-1}	Last 210 min rate (k) s^{-1}	First 90 min $mol/m^2 \cdot s$	Last 210 min $mol/m^2 \cdot s$
U1	-1.2E-04	-2.3E-04	-9.0E-08	-1.8E-07
U2	-1.0E-04	-1.9E-04	-4.8E-08	-8.9E-08
U3	-1.5E-04	-3.1E-04	-1.1E-07	-2.4E-07
U4	-6.2E-05	-1.5E-04	-7.8E-08	-1.9E-07
P1	-6.0E-05	-1.5E-04	-3.8E-08	-9.4E-08
TK-578 BRIM	-1.2E-04		-3.0E-09	

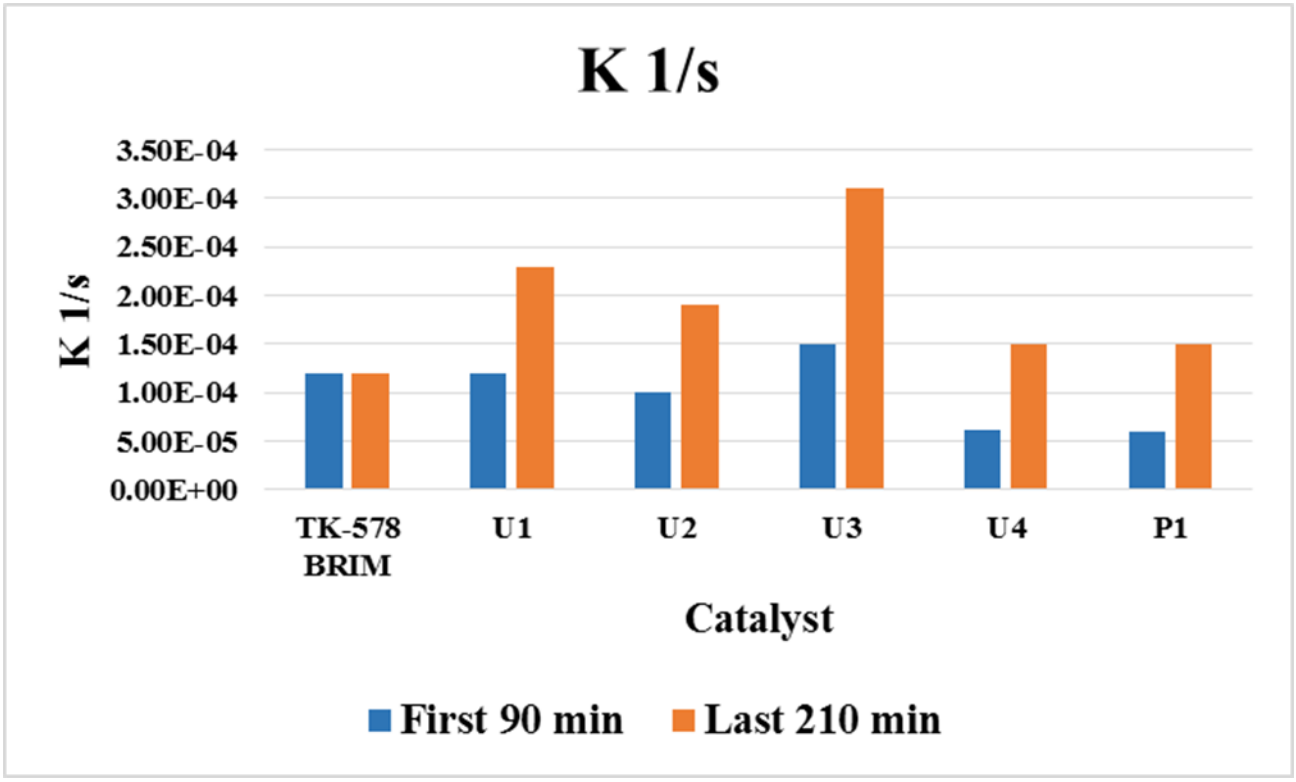

Figure 58: Rate Constant Independent of Surface Area

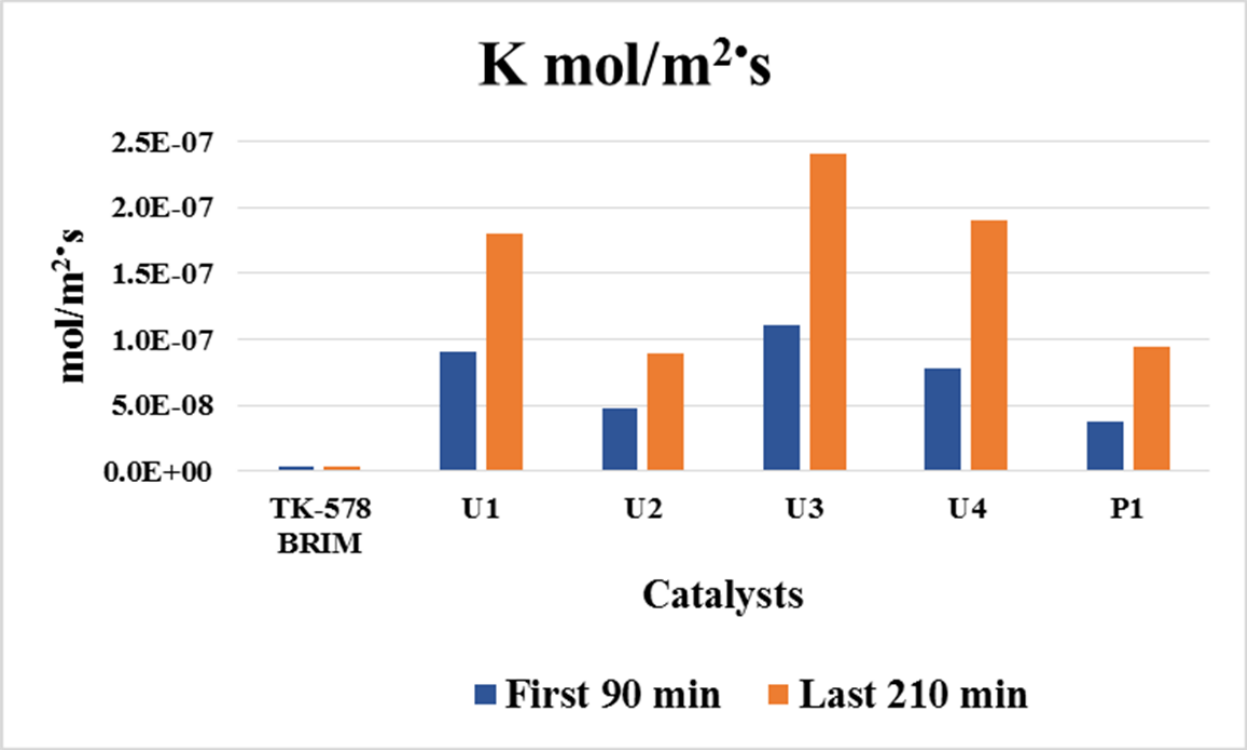

Figure 59: Rate Constant Including Surface Area

In Table 8, the calculated data is presented in pure rate as 1/s and then as a function of surface area of the material. The largest k values initially belong to U3 and U1, while U2 last 210 minutes competitive as well. BRIM rate is in the same order of magnitude, but the real change is observed when incorporating the surface area. By using surface area measurements in the calculations, rate is purely dependent on the properties of the catalyst not the amount. Granted, the unsupported catalysts have no alumina to dilute the metals, but that is not relevant to this reaction. The surface area and adsorption are what is important. When calculating with surface areas, the rate for BRIM is 2 order of magnitude lower than U3 which is UTEP's best catalyst.

CHAPTER 5: CONCLUSION

Catalysts synthesized here at UTEP exhibit competitive catalytic rates when compared to an industry leading catalyst in hydrodesulfurization. When taking surface area into account, the U-series unsupported catalysts actually outperformed the TK-578 BRIM catalyst. The reaction order for the CoMo type catalyst was determined experimentally to be first order. After the evaluation of U-series kinetic plots, it was demonstrated that the catalyst arranges into its stable form after 90 minutes in refinery like conditions. The U-series catalysts including P1 appear to adapt to the chemical environment and perform extremely well as a result despite their low surface area. The catalysts used in industry do not have the advantage as they are calcined at higher temperatures than they are exposed to in the refinery after impregnation. Calcining at higher temperatures than the refinery conditions lock in the phase of the catalyst, or "stabilize" it. Synthesizing the catalyst at lower temperatures results in an amorphous natured material and could possibly extend the life of the catalyst. It has been observed that catalysts in refineries tend to further crystallize over time and this is suspected to lower their activity along with excessive carbon capping (hard carbon). It was discussed that the stable form of the catalyst has been shown to contain a carbide surface, if that is the case it would be beneficial to synthesize the catalyst in the presence of a hydrocarbon such as DEG. Furthermore, this method has demonstrated to be a viable option for industrial commercialization.

Certainly, there are further modifications and studies to be conducted to continue the scale up, but the P1 efficacy has demonstrated that it is more than possible to succeed in commercialization. Future work would include increasing the surface area of the material by growing the catalyst on a zeolite or alumina using the same method. Other diluents can be used to modify the procedure and would possibly lower the time, temperature and pressure currently experienced. This catalyst has yet to be tested in a live feed—live feed testing is the next logical step for this catalyst. P1 had some sulfidation problems, but the catalyst performed well and was

fully sulfided after the five hour DBT test. The low pressures for this method make it possible to load the reactor to maximum without a drop in activity of the final product.

As of lately, Porocel has placed the project on hold due to the recent price drop in Mo and Co. The main source of revenue for Porocel is based on the regeneration or rejuvenation of catalysts. When the prices of Co and Mo decreased, their customers began to purchase new catalysts instead of opting to purchase refurbished catalysts. Porocel Industries LLC is in the process of licensing negotiations with the university in hopes of continuing the project when their situation improves.

REFERENCES

1. Shojai, Siamack. The New Global Oil Market: Understanding Energy Issues in the World Economy. Westport, CT: Praeger, 1995. Print.
2. Walter Licht, Thomas Dublin (2005). The Face of Decline: The Pennsylvania Anthracite Region in the Twentieth Century. Cornell University Press.
3. Edwards, John D. "Crude oil and alternate energy production forecasts for the twenty-first century: The end of the hydrocarbon era." AAPG bulletin 81.8 (1997): 1292-1305.
4. "International Energy Statistics - EIA." International Energy Statistics - EIA. N.p., n.d. Web. 18 Apr. 2016.
5. Speight, James G. The chemistry and technology of petroleum. CRC press, 2014. "Regulations and Standards." Regulations & Standards. N.p., n.d. Web. 18 Apr. 2016.
6. Forbes, R.J. More Studies in Early Petroleum History: 1860-1880. Leiden: E.J. Brill, 1959. Print.
7. Tissot, Bernard P., and Dietrich H. Welte. "Composition of Crude Oils." Petroleum Formation and Occurrence (1978): 333-68. Print.
8. Hinkle, Amy, et al. "Correlating the chemical and physical properties of a set of heavy oils from around the world." Fuel 87.13 (2008): 3065-3070.
9. Raheem, Momoh Omuya. Enhancing Light-Ends Recovery Through Joint Atmospheric Distilliation of Heavy Crude and Used Engine Oil. Diss. Ahmadu Bello University, Zaria, 2011.
10. Hein, Frances J. "Heavy oil and oil (tar) sands in North America: an overview & summary of contributions." Natural Resources Research 15.2 (2006): 67-84.
11. Brooks, P. W., M. G. Fowler, and R. W. Macqueen. "Biological marker and conventional organic geochemistry of oil sands/heavy oils, Western Canada Basin." Organic Geochemistry 12.6 (1988): 519-538.

12. Tahmassebi, Hossein. "Crude oil and product differentials: historical perspective and outlook." OPEC Review 8.3 (1984): 245-276.
13. Beaton, Kendall. "Dr. Gesner's kerosene: the start of American oil refining." Business History Review 29.01 (1955): 28-53.
14. Fouquet, Roger, and Peter JG Pearson. "Seven centuries of energy services: The price and use of light in the United Kingdom (1300-2000)." The Energy Journal (2006): 139-177.
15. Singh, A., et al. "Model-based real-time optimization of automotive gasoline blending operations." Journal of process control 10.1 (2000): 43-58.
16. Larson, Henrietta Melia, and Kenneth Wiggins Porter. History of Humble Oil & Refining Company: A Study in Industrial Growth. Harper, 1959.
17. "How an Oil Refinery Works." API. N.p., n.d. Web. 18 Apr. 2016.
18. "Heavy Fuel Refinery Process." What Happens to Crude Oil in the Refinery? N.p., n.d. Web. 18 Apr. 2016.
19. "United States Department of Labor." OSHA Technical Manual (OTM). N.p., n.d. Web. 18 Apr. 2016.
20. Gissy H., Bartsch R., Tanielian C., Hydrodesulfurization, Journal of Catalysis, Volume 65, Issue 1, 1980, Pages 150-157.
21. Acres, G. J. K., and Harrison, B., "The development of catalysts for emission control from motor vehicles: early research at Johnson Matthey." Topics in Catalysis 28.1-4 (2004): 3-11.
22. Angelici, Robert J. Polyhedron Vol. 16, No. 18, pp. 3073-3088, 1997.
23. Weisser O., and Landa S., Sulfide Catalysts: Their Properties and Applications
24. Duchet, J. C., et al. "Carbon-supported sulfide catalysts." Journal of Catalysis 80.2 (1983): 386-402.
25. Luck, F. "A review of support effects on the activity and selectivity of hydrotreating catalysts." Bulletin des Sociétés Chimiques Belges 100.11-12 (1991): 781-800.

26. Burch, R., and A. Collins. "Metal sulfide-support interactions." Journal of Catalysis 97.2 (1986): 385-389.
27. Maity, S. K., J. Ancheyta, and Mohan S. Rana. "Support effects on hydroprocessing of Maya heavy crude." Energy & fuels 19.2 (2005): 343-347.
28. "United States Department of Labor." OSHA Technical Manual (OTM). N.p., n.d. Web. 18 Apr. 2016.
29. Ho, T. C., and Sobel J. E., "Kinetics of dibenzothiophene hydrodesulfurization." Journal of Catalysis 128.2 (1991): 581-584.
30. Daage, M., and R. R. Chianelli. "Structure-function relations in molybdenum sulfide catalysts: the" rim-edge" model." Journal of Catalysis 149.2 (1994): 414-427.
31. Liu, Shuzhi, et al. "Deep desulfurization of diesel oil oxidized by Fe (VI) systems." Fuel 87.3 (2008): 422-428.
32. Bataille, Frédéric, et al. "Alkyldibenzothiophenes hydrodesulfurization-promoter effect, reactivity, and reaction mechanism." Journal of catalysis 191.2 (2000): 409-422.
33. Kwart, H., G. C. A. Schuit, and B. C. Gates. "Hydrodesulfurization of thiophenic compounds: the reaction mechanism." Journal of Catalysis 61.1 (1980): 128-134.
34. Sánchez-Delgado, Roberto A. "Breaking C-S bonds with transition metal complexes. A review of molecular approaches to the study of the mechanisms of the hydrodesulfurization reaction." Journal of molecular catalysis 86.1 (1994): 287-307.
35. Angelici, Robert J. "Heterogeneous catalysis of the hydrodesulfurization of thiophenes in petroleum: an organometallic perspective of the mechanism." Accounts of Chemical Research 21.11 (1988): 387-394.
36. Pecoraro T.A., Chianelli R.R., J. Catal., 67, 430, 1981.
37. Chianelli, Russell R., Mohammad H. Siadati, Myriam Perez De La Rosa, Gilles Berhault, Jess P. Wilcoxon, Roby Bearden, and Billie L. Abrams. "Catalytic Properties of Single

Layers of Transition Metal Sulfide Catalytic Materials." Catalysis Reviews 48.1 (2006): 1-41. Print.

38. Lindner, J. M.A. Villa Garcia, A. Sachdev, J. Schwank, J. Catal. 120 (1989) 487.
39. Sanders, J.V. K.C. Pratt, J. Catal. 67 (1981) 331.
40. Harris, S., and Chianelli, R. R., J. Catal. 86, 400 (1984).
41. Yuanyuan Zhu, Quentin M. Ramasse, Michael Brorson, Poul G. Moses, Lars P. Hansen, Henrik Topsøe, Christian F. Kisielowski, Stig Helveg, Location of Co and Ni promoter atoms in multi-layer MoS2 nanocrystals for hydrotreating catalysis, Catalysis Today, Volume 261, 1 March 2016, Pages 75-81.
42. Karroua M., Ladriere L., Matralis H., Grange P., Delmon B., J. Catal. 138 (1992) 640.
43. Koranyi T.I., de Vries G., Lun X. , Paal Z., Catal. Today 5 (1989) 185.
44. Vartuli, Beck Roth, American Chemical Society 114 (1992) 10834.
45. Delarosa, M. "Structural Studies of Catalytically Stabilized Model and Industrial-supported Hydrodesulfurization Catalysts." Journal of Catalysis (2004): n. pag. Web.
46. Xiao-Dong Wen, Zhi Cao, Yong-Wang Li, Jianguo Wang, and Haijun JiaoJ. Phys. Chem. B 2006, 110, 23860-23869.
47. Brenda Torres Escobar, "Transition metal catalysts for hydrodesulphurization reactions applied to petroleum industry" (January 1, 2009). ETD Collection for University of Texas, El Paso. Paper AAI3358898.
48. Putnam, Garth L., and Kenneth A. Kobe. "Ethylene Diamine as an Ionizing Solvent." Trans. Electrochem. Soc. Transactions of The Electrochemical Society 74.1 (1938): 609. Print.
49. Davis, Robert Earl, and Hisham F. Nakshbendi. "Sulfur in Amine Solvents." Journal of The American Chemical Society (n.d.): n. pag. ResearchGate. Web. 17 Apr. 2016.

50. Fahim, M. A., Taher A. Alsahhaf, and Amal Sayed. Elkilani. "Refining Processes." Introduction. Fundamentals of Petroleum Refining. Amsterdam: Elsevier, 2010. N. pag. Print.
51. Rui Wang, Kevin J. Smith, Hydrodesulfurization of 4,6-dimethyldibenzothiophene over high surface area metal phosphides, Applied Catalysis A: General, Volume 361, Issues 1–2, 20 June 2009, Pages 18-25.
52. Lauritsen J.V., Nyberg M., Nørskov, J.K., Clausen B.S., Topsøe H., Lægsgaard E., Besenbacher F., Hydrodesulfurization reaction pathways on MoS2 nanoclusters revealed by scanning tunneling microscopy, Journal of Catalysis, Volume 224, Issue 1, 15 May 2004, Pages 94-106.
53. Sing, K. S. W. "Reporting physisorption data for gas/solid systems with special reference to the determination of surface area and porosity (Recommendations 1984)" Pure and Applied Chemistry, 57.4 (2009): 603-619

APPENDIX

Fitted XRD Patterns of Starting Material

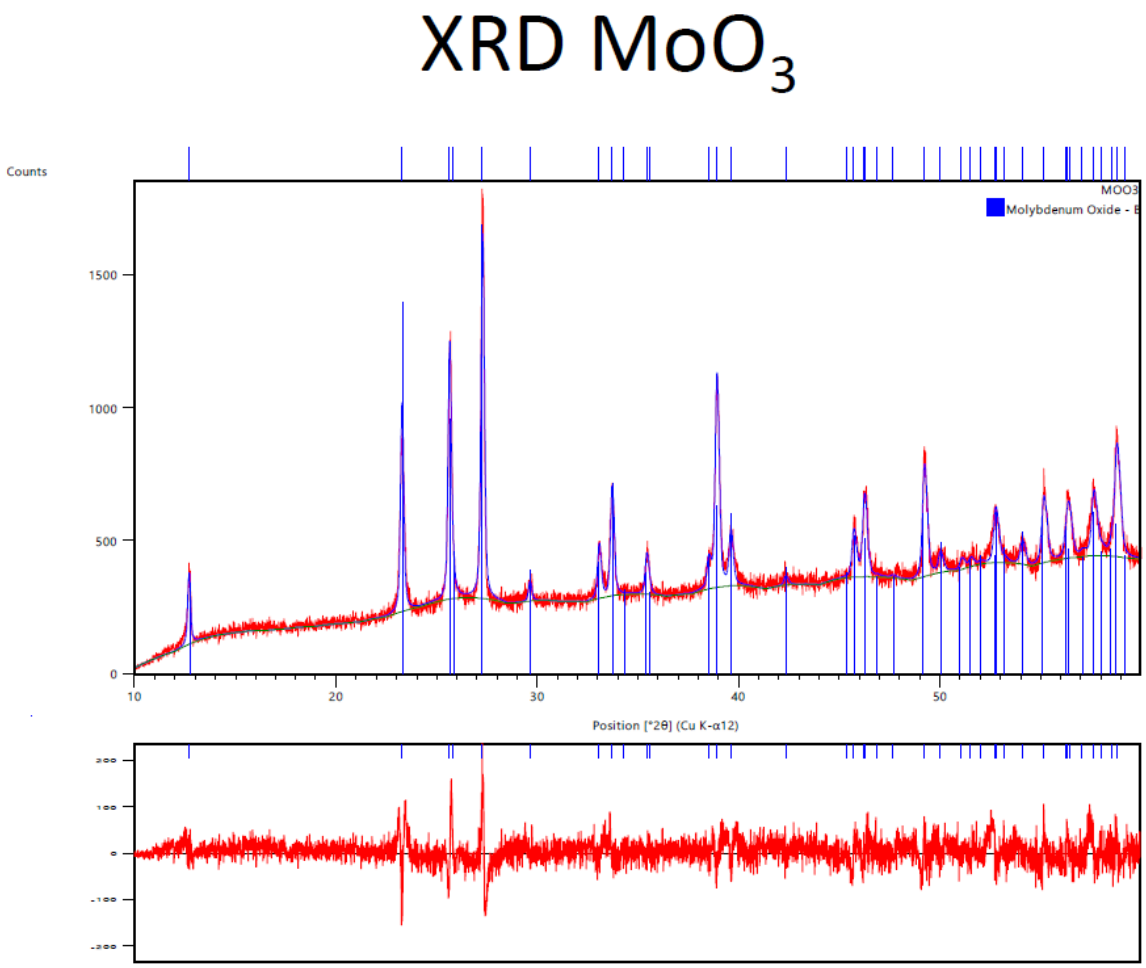

Figure 60: Fitted XRD of MoO_3

XRD $Co(NO_3)_2 \cdot 6H_2O$

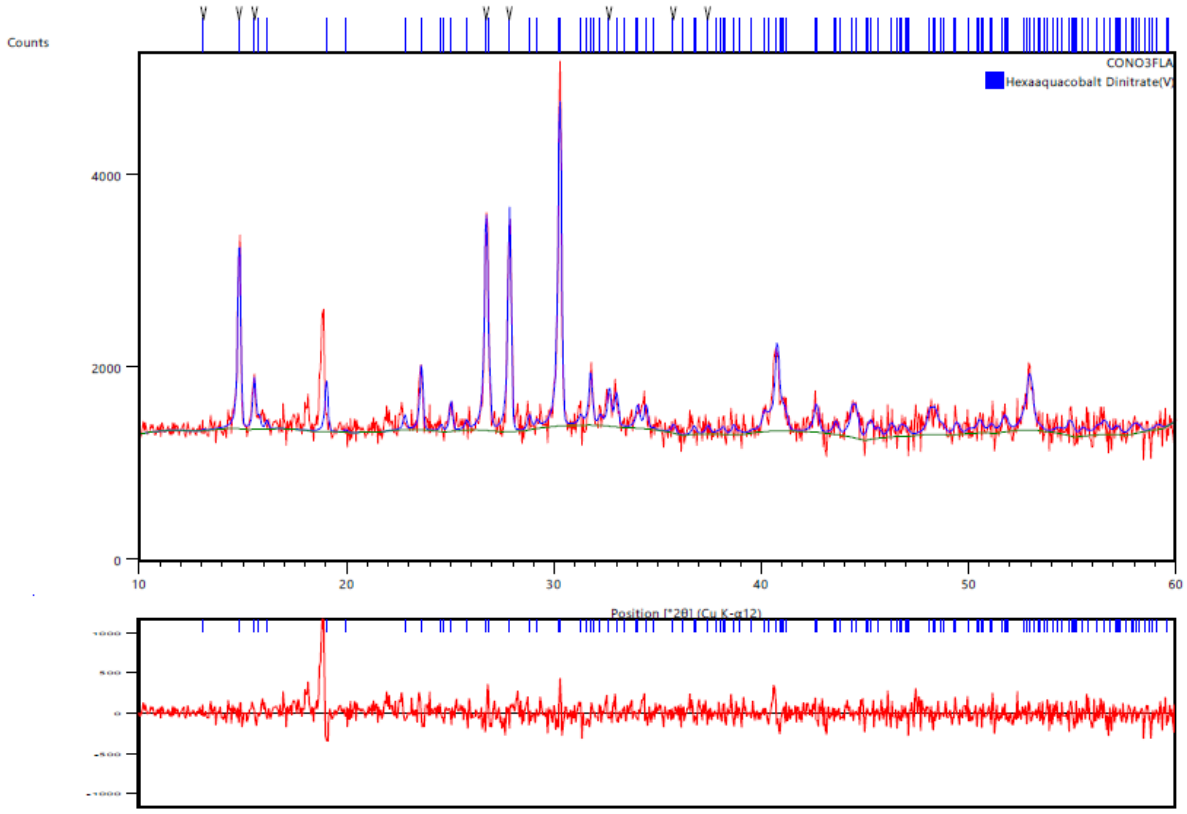

Figure 61: Fitted XRD of Cobalt Nitrate Hexahydrate

XRD S^8

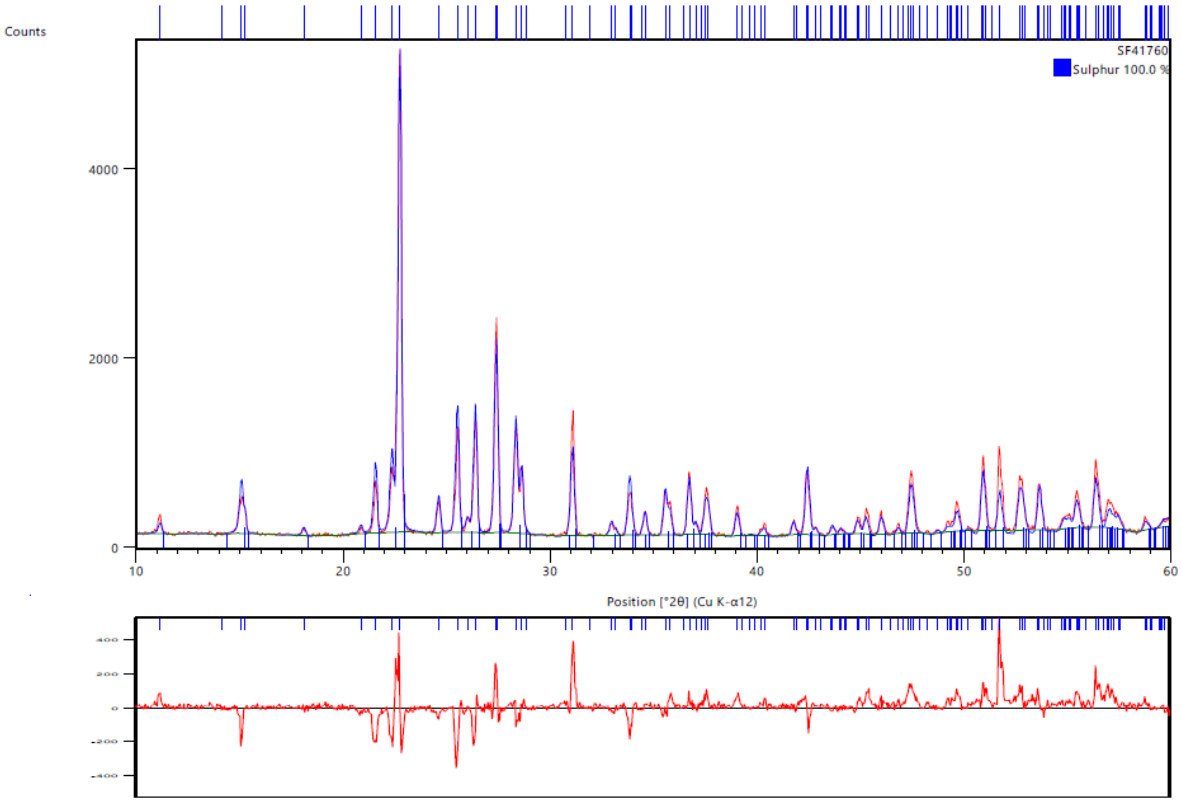

Figure 62: Fitted XRD of Sulfur Zero

Isotherms Discussed in Chapter 4

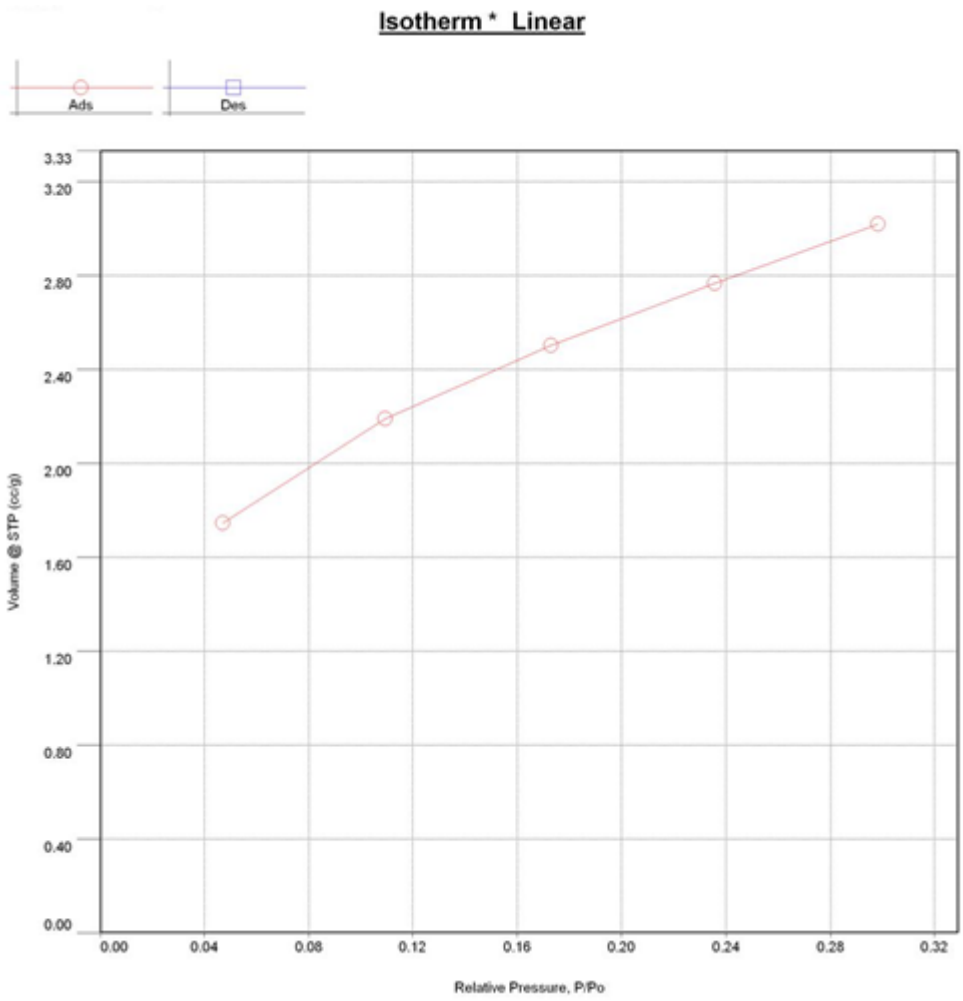

Figure 63:Isotherm for U1 spent catalyst

Figure 56 shows nitrogen adsorption for U1 spent catalyst and the surface area was calculated to be 9.612 m^2/g. The correlation coefficient, r, was 0.999. Surface area almost doubled after the five hour HDS test. The surface area is rather low when compared to commercial catalysts. Commercial catalysts have surface area values above 100 m^2/g. Hydrothermal/solvothermal synthesis is correlated with producing high surface area materials, so these surface areas were unexpectedly low.

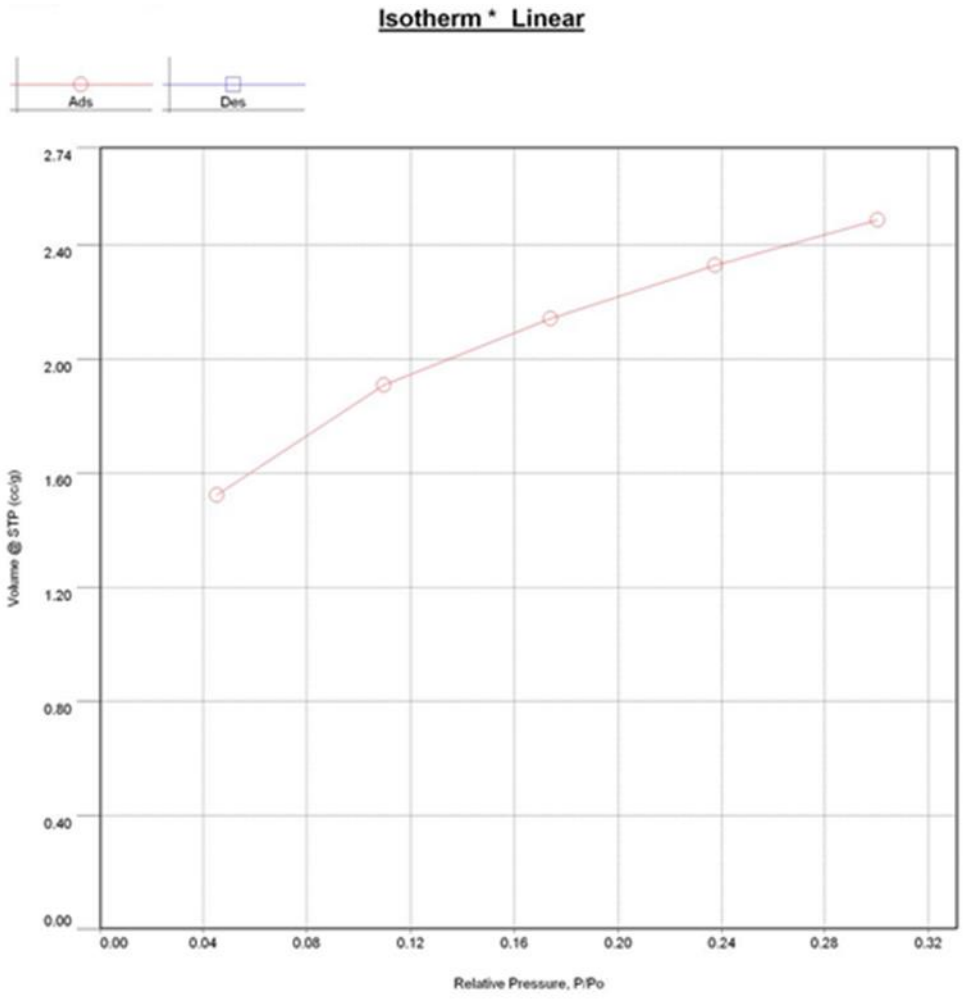

Figure 64: Isotherm for U2 fresh catalyst

The isotherm on figure 57 shows nitrogen adsorption for the U2 fresh catalyst and the surface area was calculated to be 7.817 m^2/g. Correlation coefficient was 0.998.

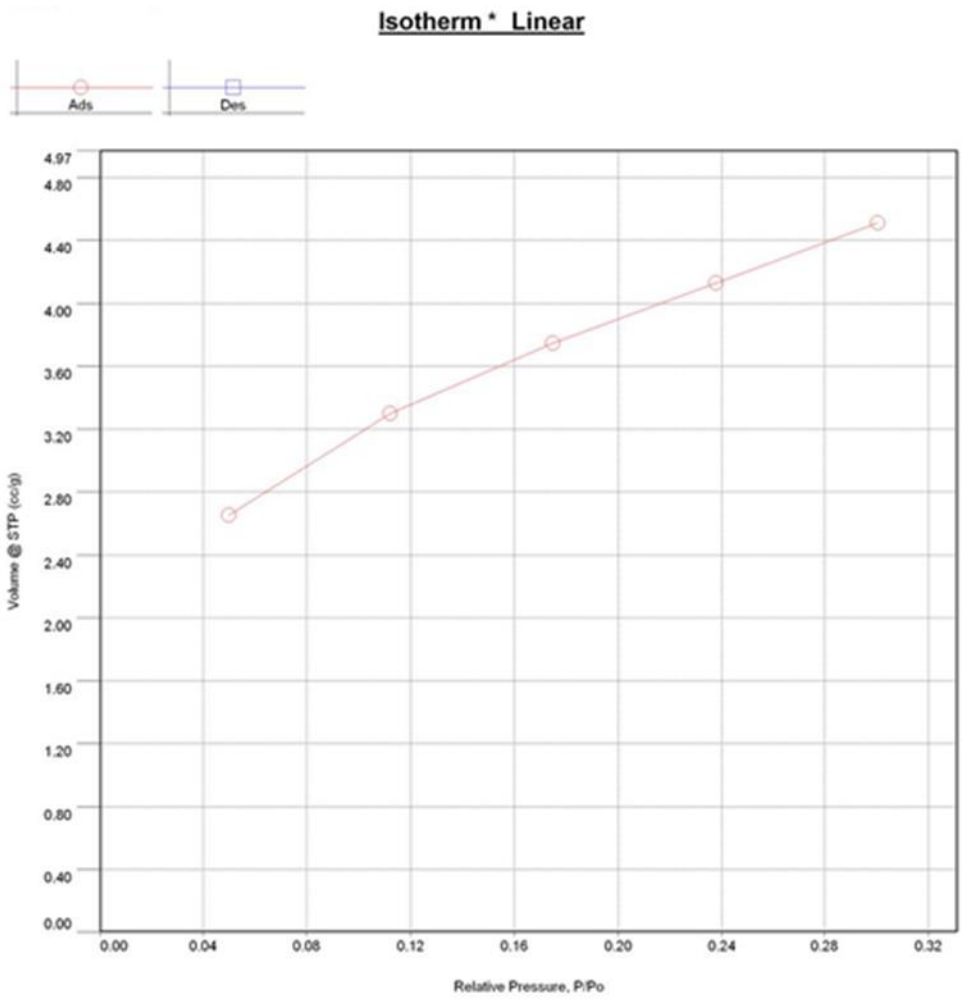

Figure 65: Isotherm for U2 spent catalyst

The isotherm on figure 58 shows nitrogen adsorption for the U2 spent catalyst and the surface area was calculated to be 14.293 m^2/g. Correlation coefficient was 0.989. Surface area nearly doubled again although overall the surface area was poor relative to industry expectations.

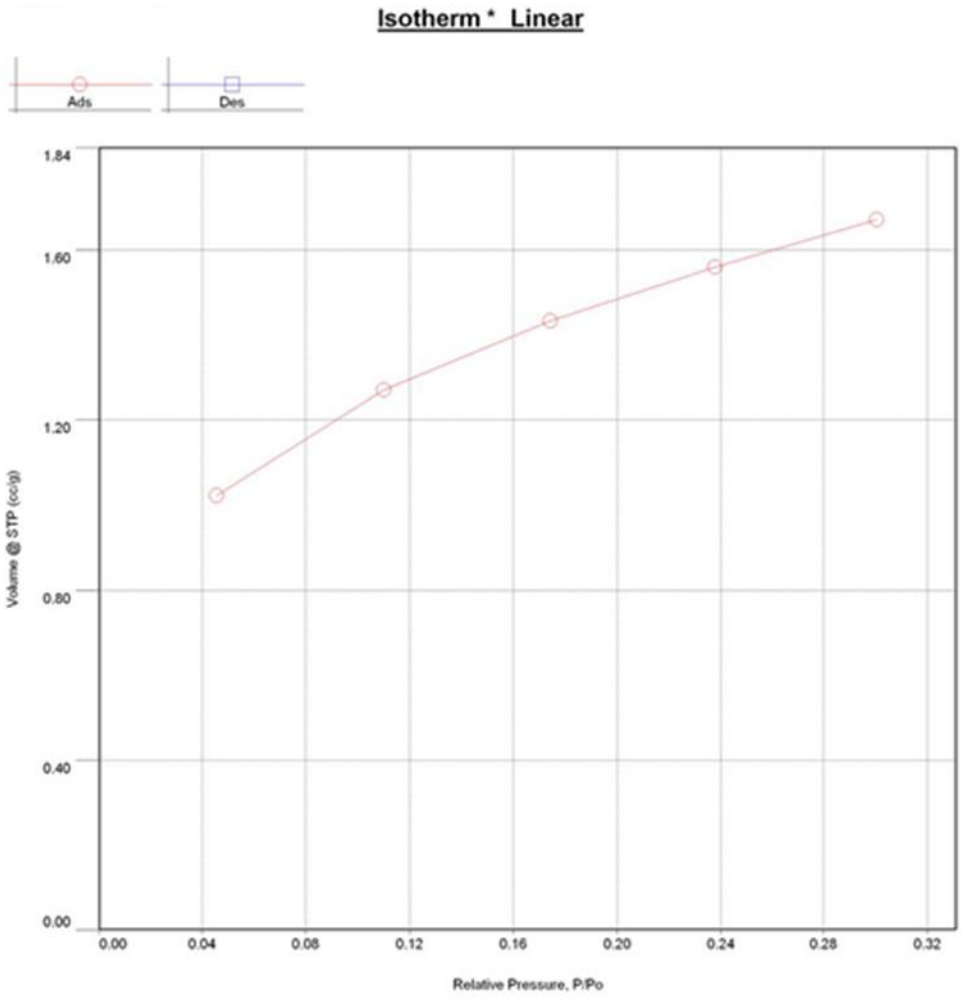

Figure 66: Isotherm for U3 fresh catalyst

The isotherm on figure 59 shows nitrogen adsorption for the U3 fresh catalyst and the surface area was calculated to be 5.259 m^2/g. The correlation coefficient was 0.996.

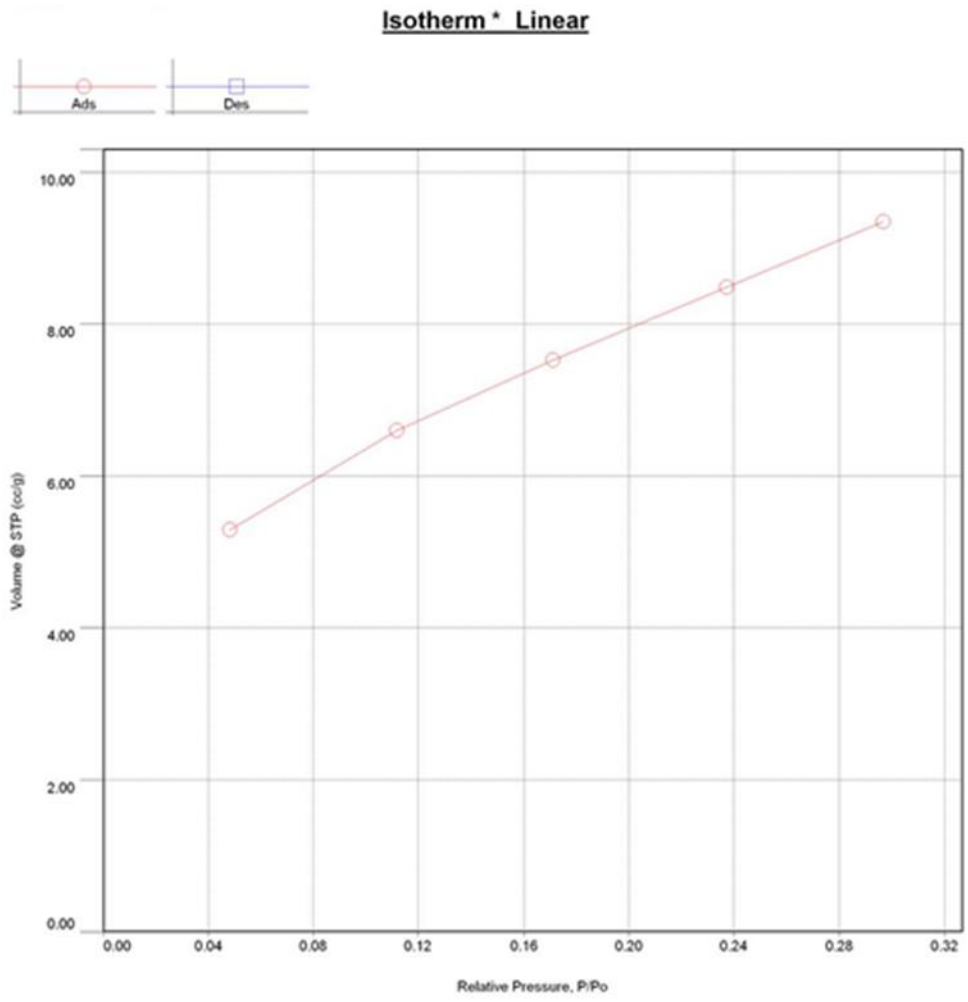

Figure 67: Isotherm for U3 spent catalyst

The isotherm on figure 60 shows nitrogen adsorption for the U3 spent catalyst and the surface area was calculated to be 29.914 m^2/g. The improvement in surface area for the amorphous U3 catalyst was nearly a 6x increase. The correlation coefficient was 0.996.

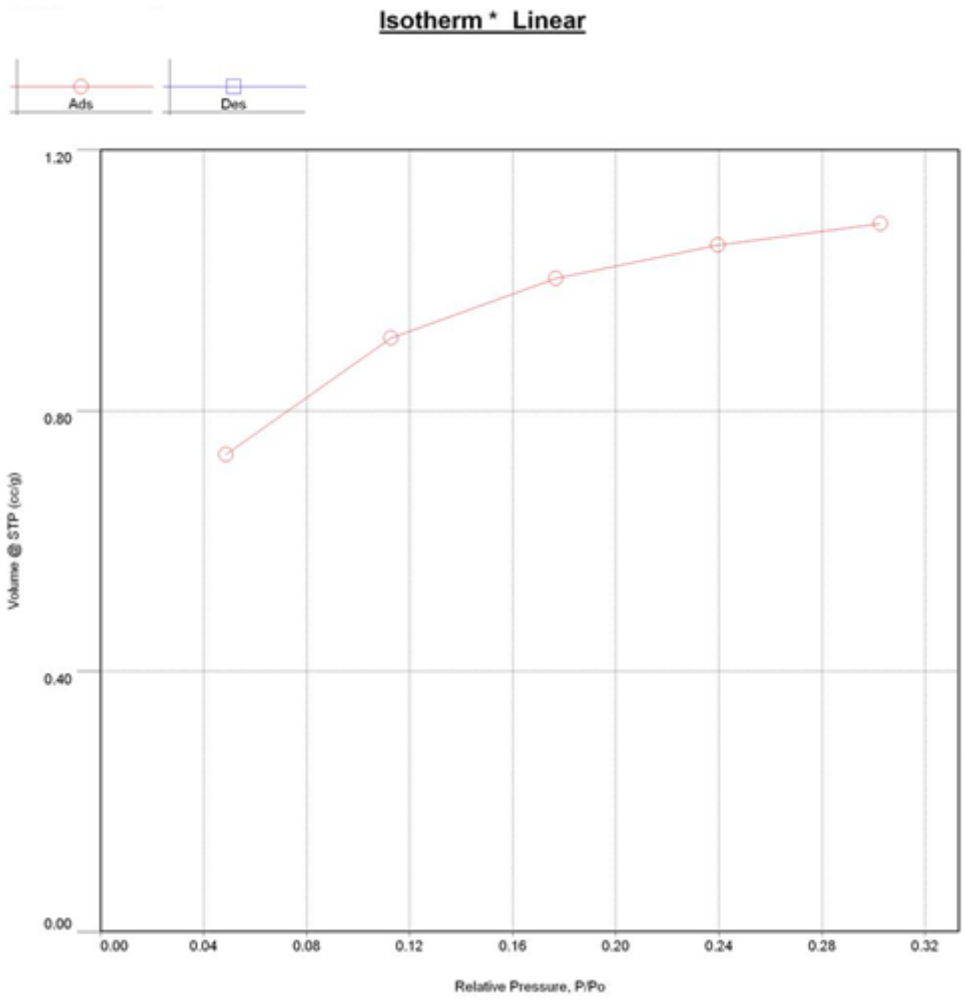

Figure 68: Isotherm for U4 fresh catalyst

Figure 61 shows nitrogen adsorption for the U4 fresh catalyst with a plotted isotherm and the surface area was calculated to be 3.385 m2/g. The correlation coefficient, r, was 0.997.

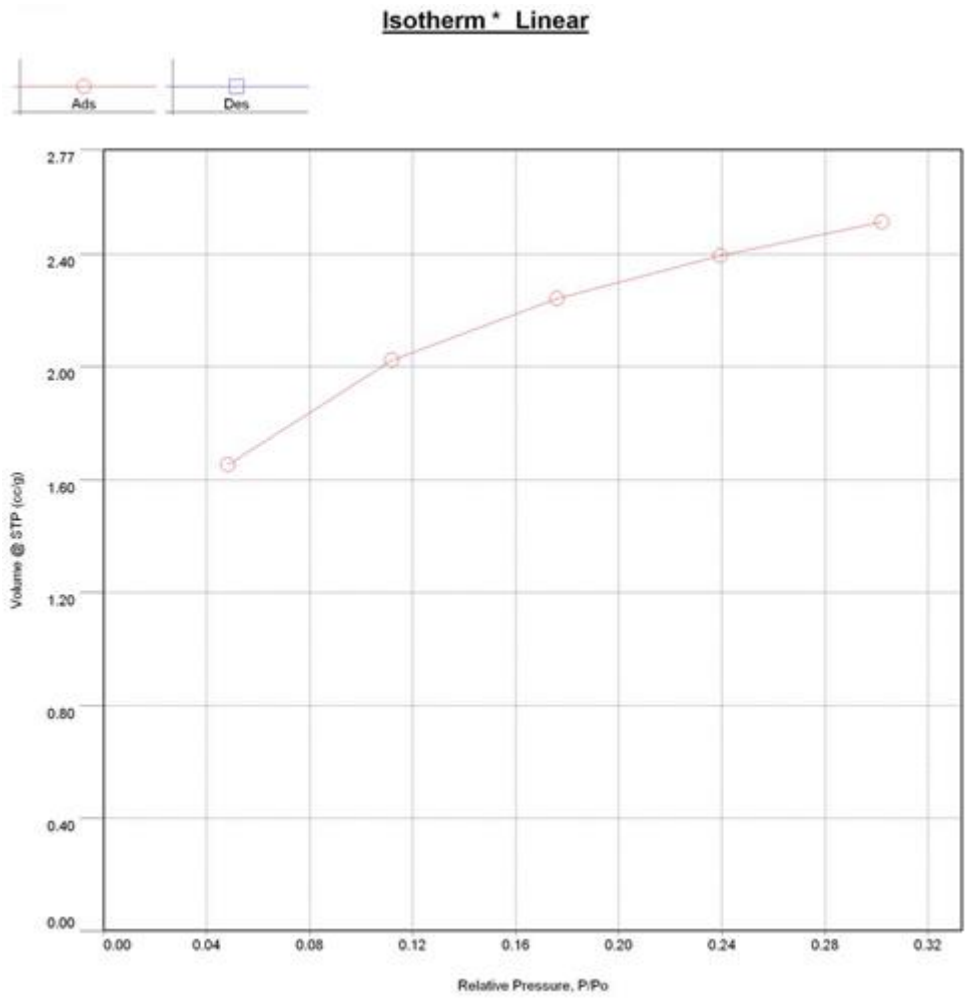

Figure 69: Isotherm for U4 spent catalyst

The isotherm on figure 62 shows nitrogen adsorption for the U4 spent catalyst—the surface area was calculated to be 7.839 m^2/g. The improvement in surface area for the amorphous U3 catalyst was more than doubled during the catalytic test. The correlation coefficient was 0.999.

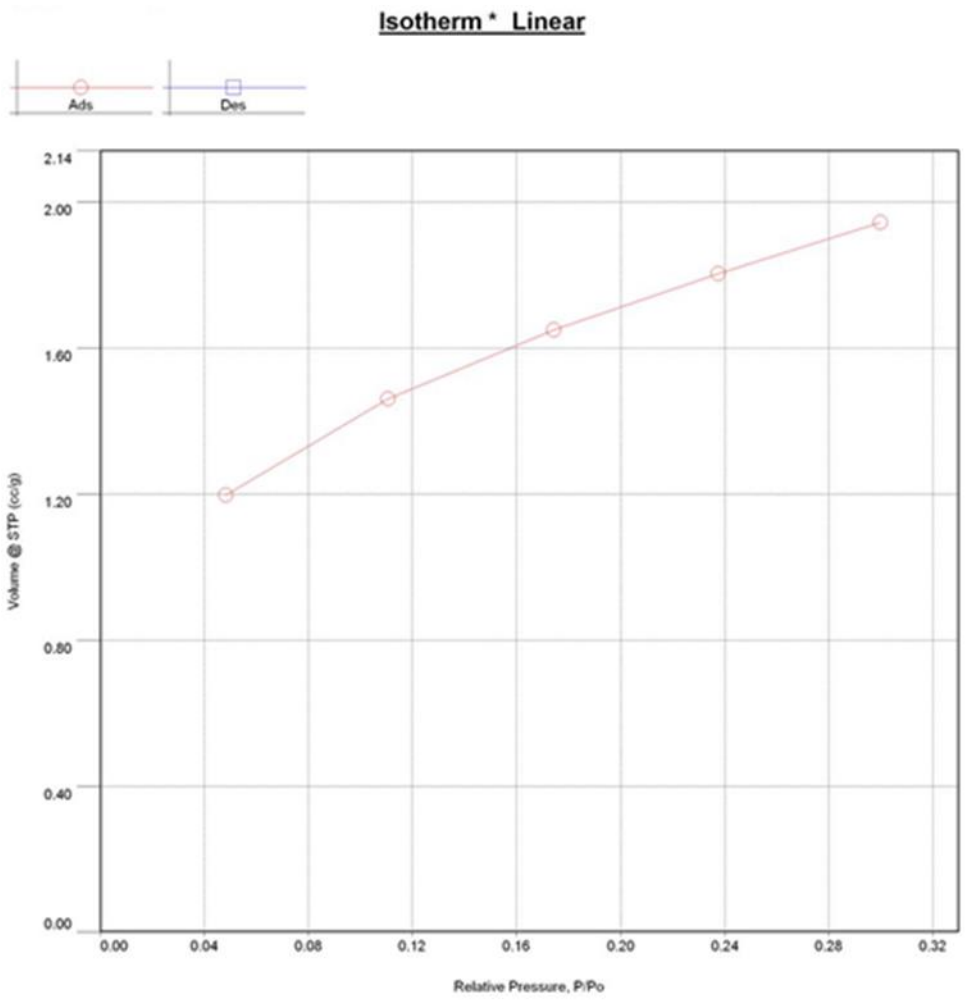

Figure 70: Isotherm for P1 fresh catalyst

The isotherm on figure 63 shows nitrogen adsorption for the Porocel made (P1) fresh catalyst—the surface area was calculated to be 6.123 m^2/g. The correlation coefficient was 0.999.

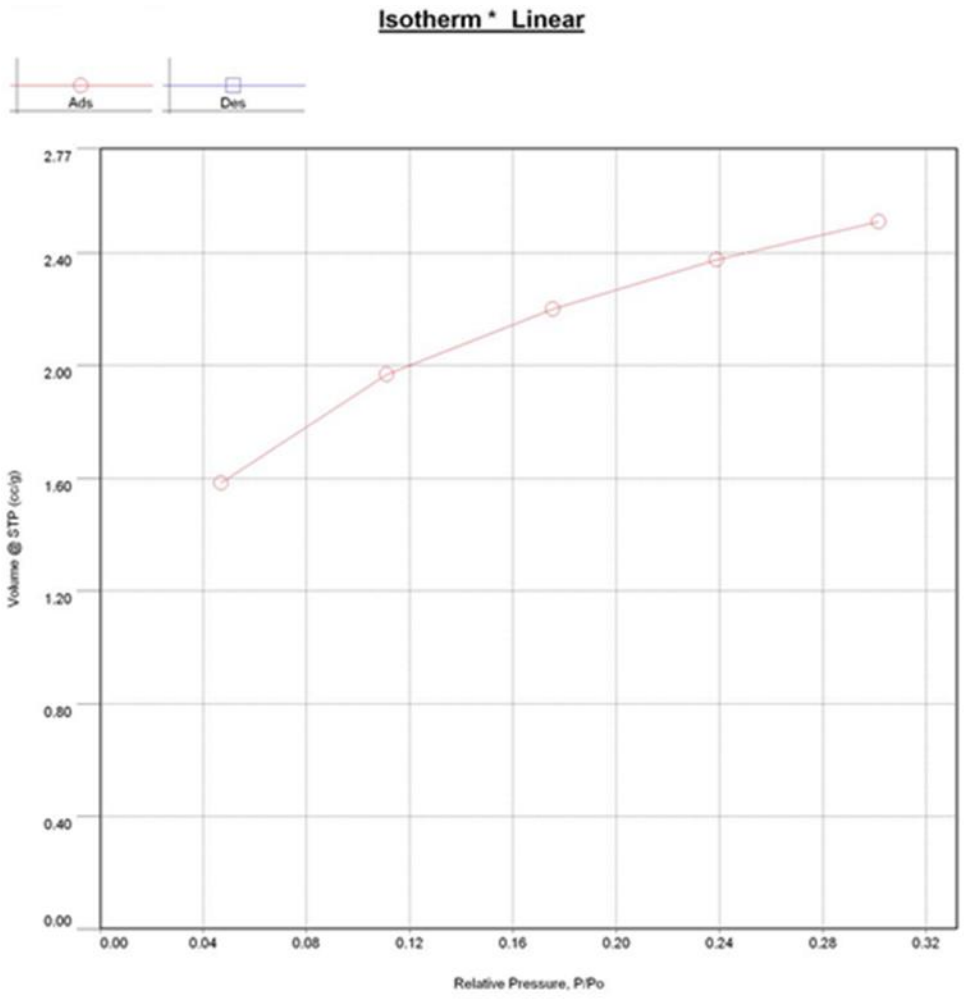

Figure 71: Isotherm for P1 spent catalyst

The isotherm on figure 64 shows nitrogen adsorption for the Porocel made (P1) spent catalyst—the surface area was calculated to be 7.871 m^2/g. There was not much increase in surface area for P1, and the inconsistencies and low surface areas prompt further evaluation in chemisorption or perhaps another method of surface area determination to corroborate results. The correlation coefficient was 0.999.

Mass Spectra for all Peaks in Figure 54

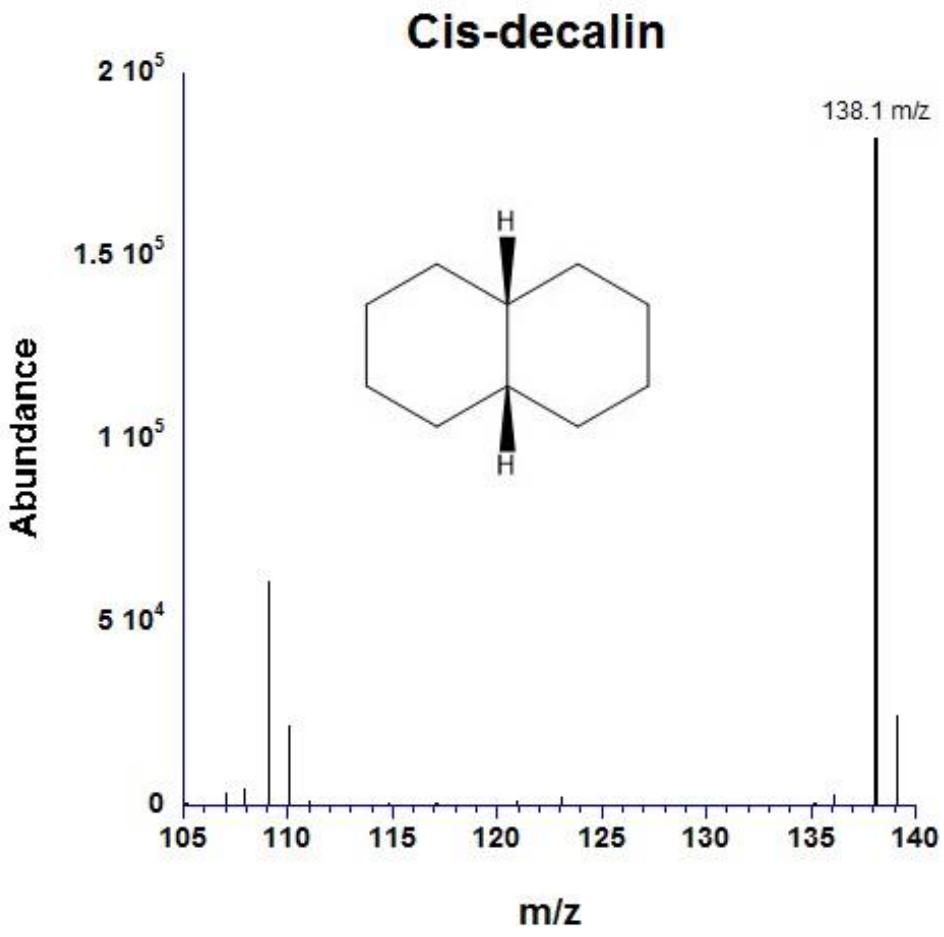

Figure 72: Mass spectra of cis-decalin

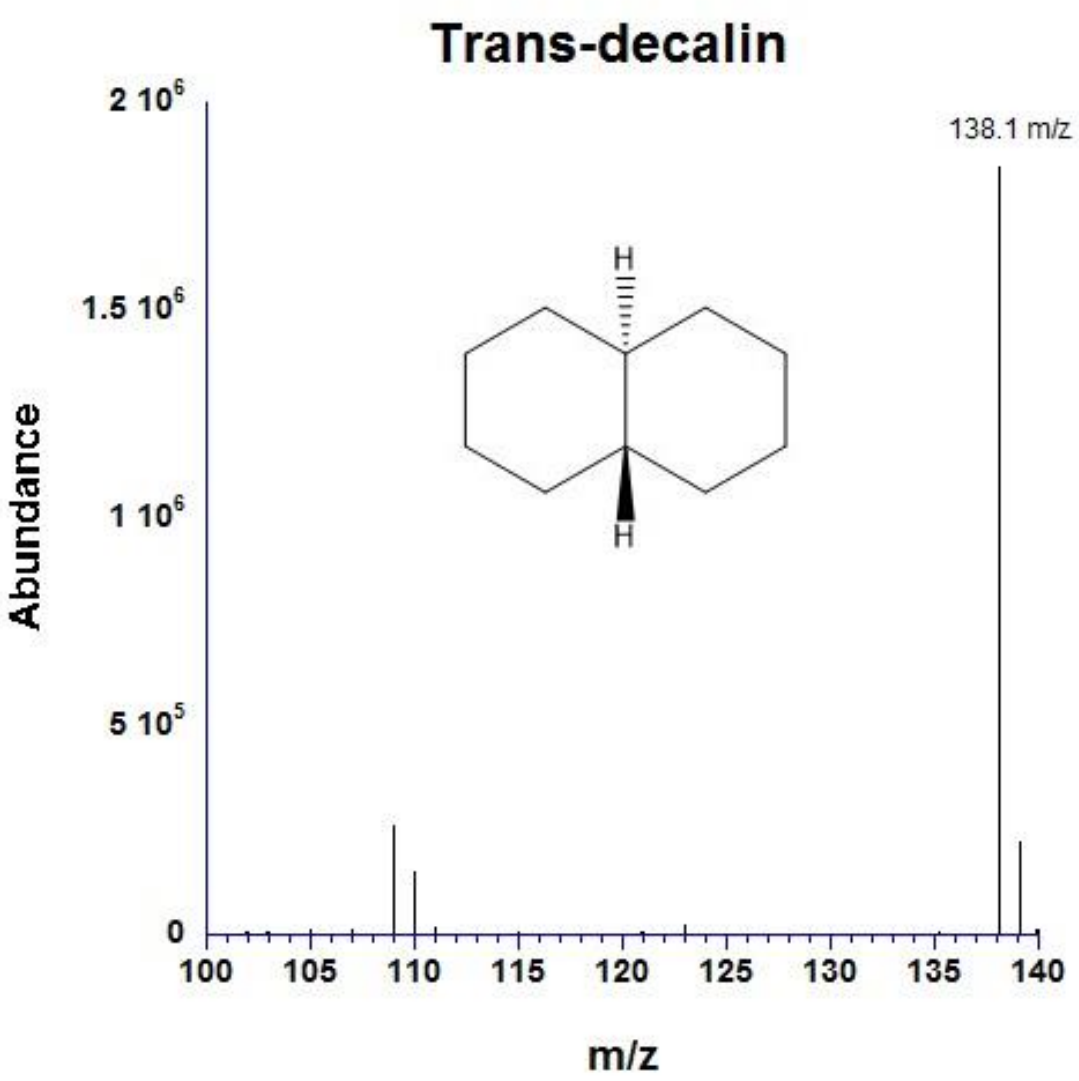

Figure 73: Mass spectra of trans-decalin

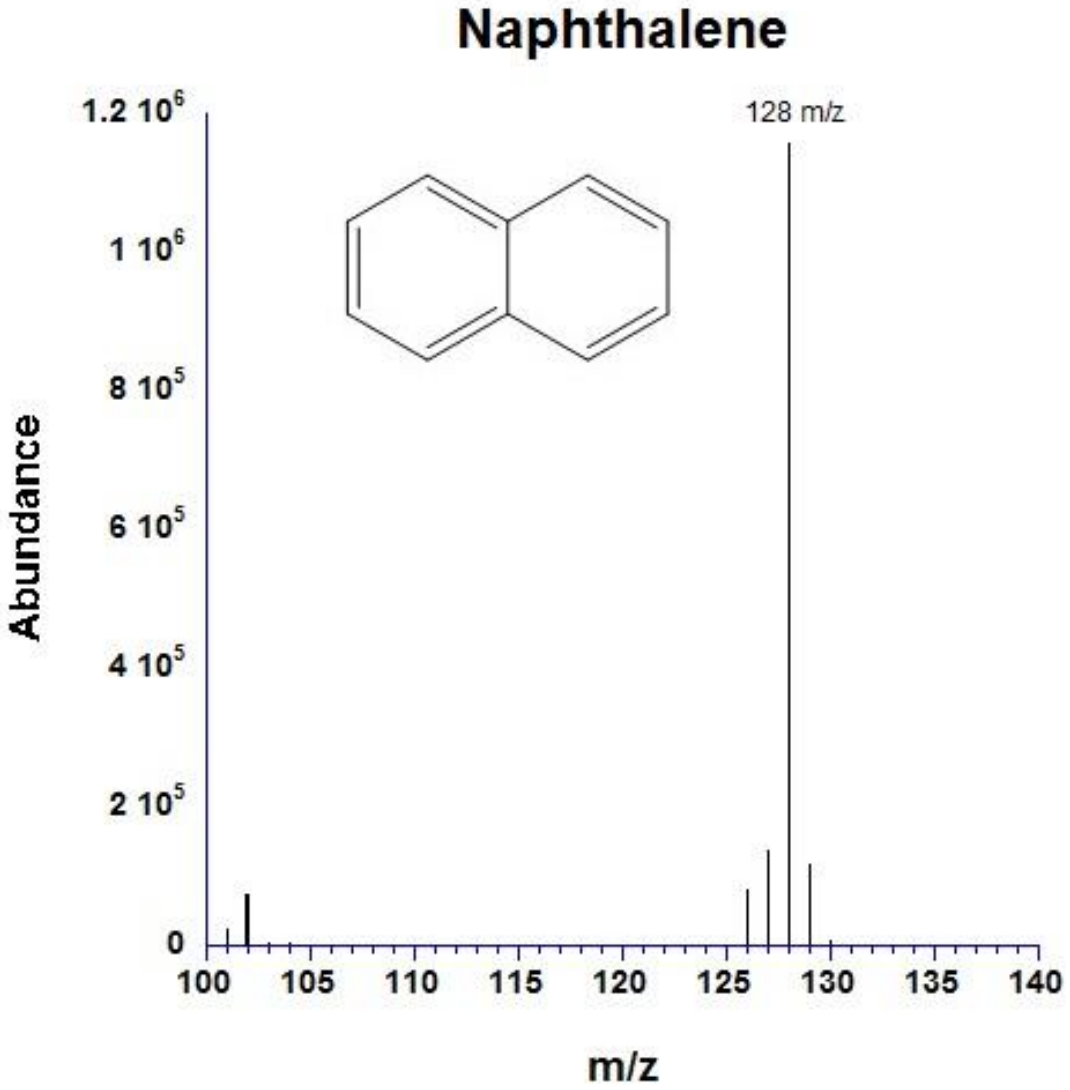

Figure 74: Mass spectra of naphphtalene

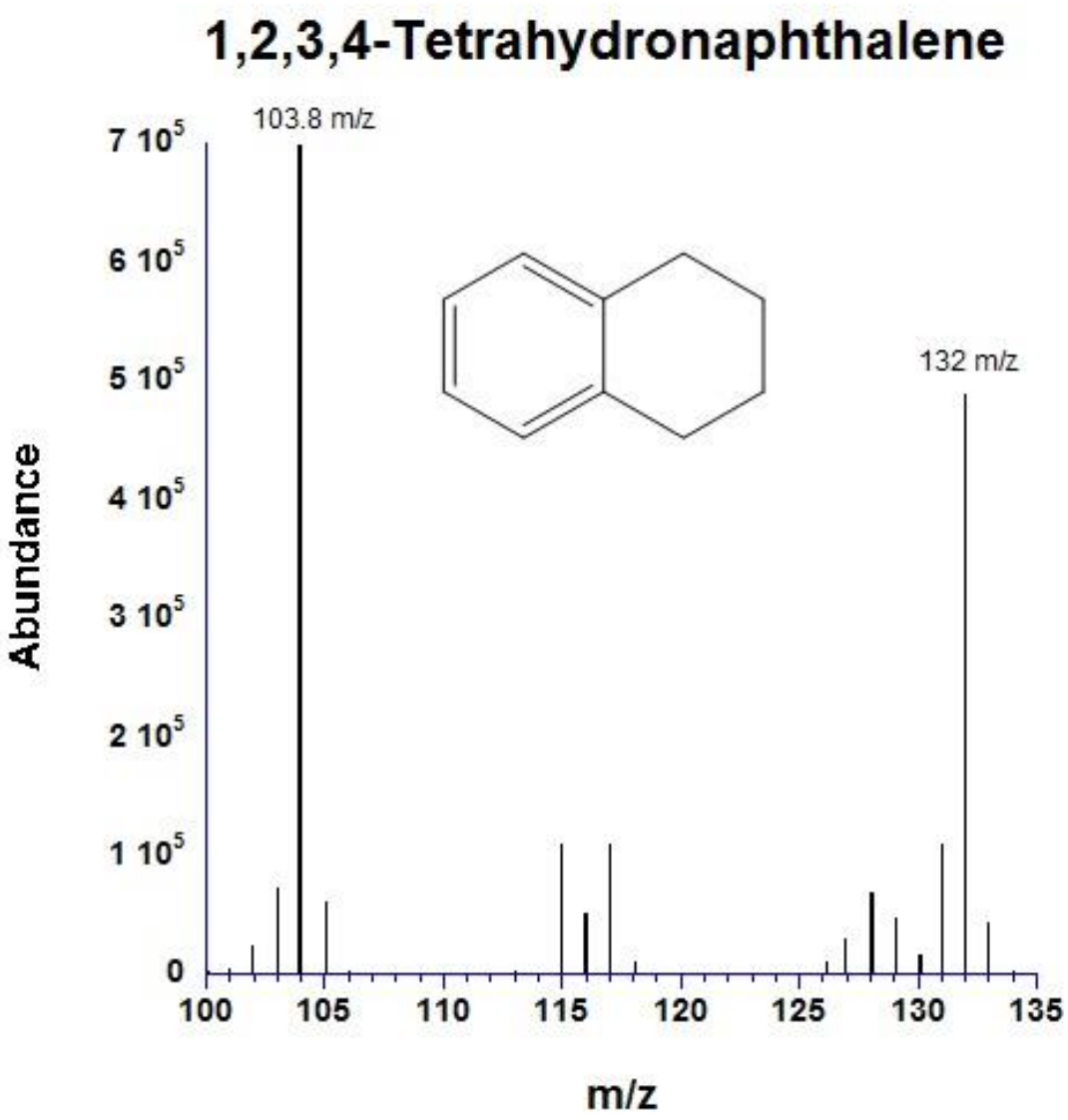

Figure 75: Mass spectra of 1,2,3,4-Tetrahydronaphthalene

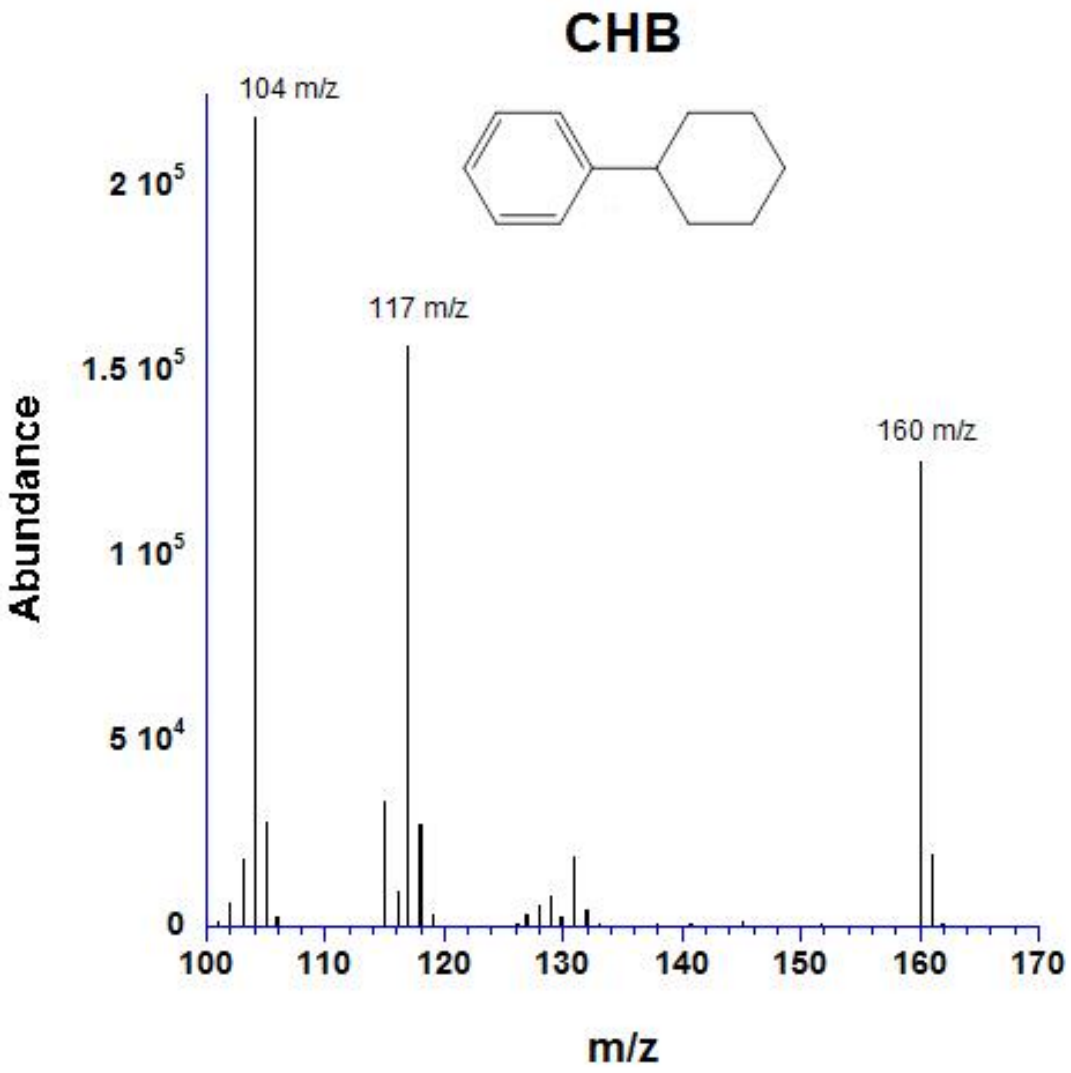

Figure 76: Mass spectra of cyclohexylbenzene

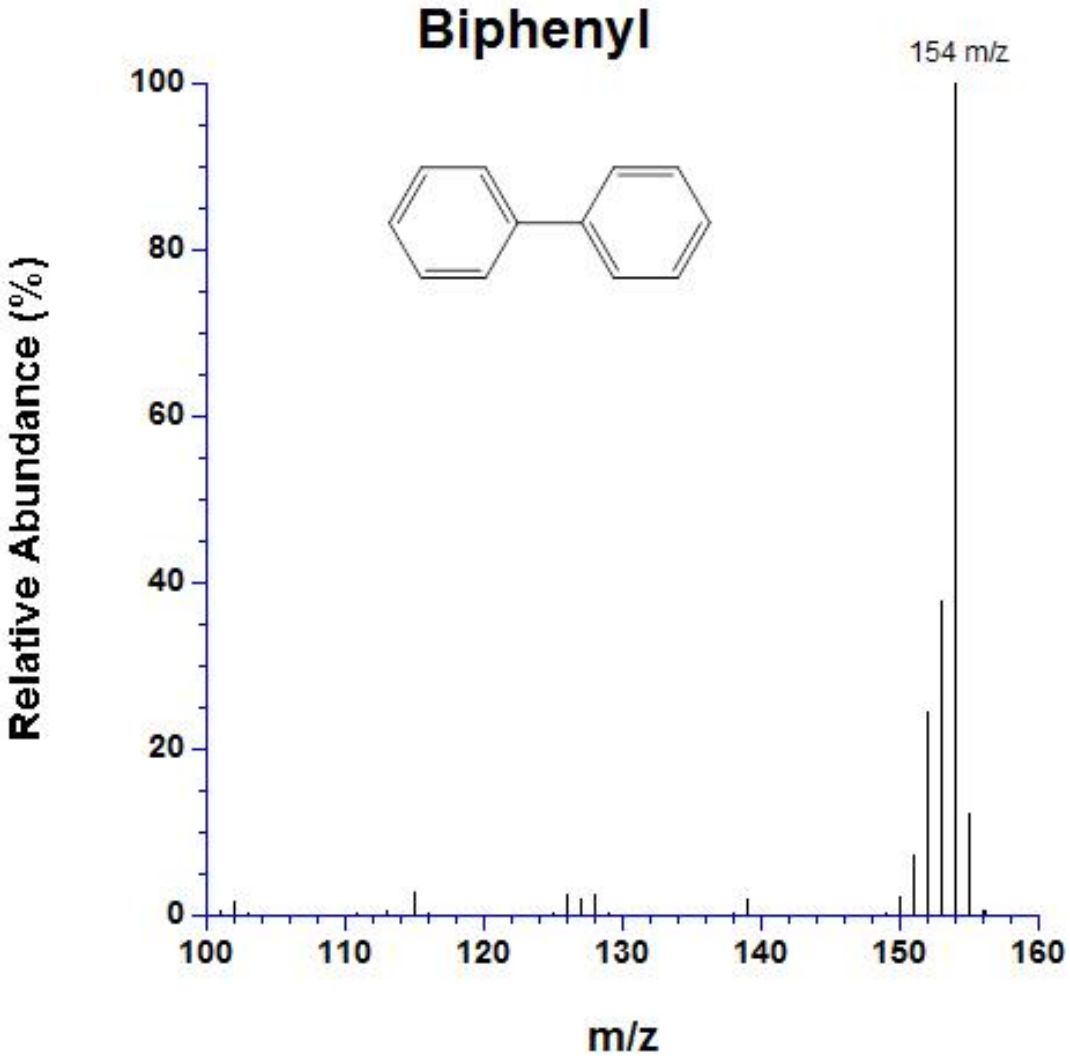

Figure 77: Mass spectra of biphenyl

VITA

Juan Hilario Leal attended the University of Texas Pan American and earned a bachelor's of science in Biology with a minor in Chemistry in 2009. Mr. Leal taught high school physics and chemistry until 2011 when he began the M.S. in chemistry program. Mr. Leal graduated with his M.S. chemistry degree in December of 2013 with a focus on polymer synthesis, inorganic synthesis and characterization. During the spring of 2014, Juan enrolled in the Ph.D. program in Material Science and Engineering at the University of Texas at El Paso.

During his time as a Ph.D. candidate, Juan joined the research group at Materials Research and Technology Institute (MRTI) at UTEP where his focus was primarily on heterogeneous catalyst development. Juan primarily assisted with the project's main goal of scale up and commercialization of a cobalt supported molybdenum disulfide catalyst for Porocel Industries, LLC. Mr. Leal is currently working on two patents related to his doctoral project. Juan's work includes the synthesis and characterization of novel nano-structured catalysts. Juan also worked as an adjunct professor at El Paso Community College where he taught chemistry courses.

Dr. Leal's dissertation titled, "Commercialization of Cobalt Promoted Molybdenum Disulfide Hydrodesulfurization Unsupported Catalyst", was supervised by Dr. Russell R. Chianelli. Dr. Leal has accepted a post-doctoral position with the physics department at UTEP.

Permanent address: 303 East 9th St.
Elsa, Texas 78543

This dissertation was typed by Juan Hilario Leal